Aspects of chiral symmetry breaking in holographic QCD

Partha Nag

Department of Theoretical Physics,

Tata Institute of Fundamental Research,

Mumbai, India

A thesis submitted for the degree of

Doctor of Philosophy
in
Physics

Declaration

I state that the work embodied in the thesis forms my own contribution to the research work carried out under the guidance of Prof. Avinash Dhar. This work has not been submitted for any other degree to this or any other university or body. Whenever references have been made to previous works of others, it has been indicated.

Prof. Avinash Dhar
(Thesis supervisor)

Partha Nag
(Candidate)

Acknowledgments

I would like to thank my thesis supervisor Prof. Avinash Dhar whose constant guidance has made this thesis possible. I thank Dr Gautam Mandal for the insightful discussions carried out with him during one of the projects in this thesis and at various other stages. I may not also forget the contribution of my friends and other members of the Department of Theoretical Physics for the fruitful discussions which have added to my learning to a great extent. Last but not the least, I wish to thank my family, particularly, my mother and my wife whose patient support has been one of the key ingredients of this thesis.

Contents

Synopsis

In the last forty years, Quantum Chromodynamics (QCD) has successfully emerged as the microscopic theory of strong force, the force that binds neutrons and protons inside the nucleus of an atom. The basic degrees of freedom in QCD are given by six flavors of quarks interacting through the exchange of gluons, gauge fields sourced by color charge (hence the name *chromodynamics*). With three kinds of colors, the gauge theory is an SU(3) non-abelian gauge theory. The full QCD action is given by

$$S = \int d^4x \left\{ -\frac{1}{4} F^a_{\mu\nu} F^{a\,\mu\nu} + \overline{q}_{fi} \left(i\gamma^\mu (\partial_\mu \delta i j - g A^a_\mu t^a_{ij}) - m_f \delta^{ij} \right) q_{fj} \right\}$$
$$\text{where} \quad F^a_{\mu\nu} = \partial_\mu A^a_\nu - \partial_\nu A^a_\mu + g\epsilon^{abc} A^b_\mu A^c_\nu, \tag{1}$$

where g is the coupling strength, the indices $a, b, c = 1, ..., 8$ run over the eight generators t^a of the SU(3) color group and $i, j = 1, 2, 3$ run over the three colors. The quarks transform as fundamental under the color gauge transformation and the gauge fields as adjoint. Therefore, the generators t^a appearing in the action are in the fundamental representation of the color group. The index $f = 1, ..., 6$ runs over the six flavors of quarks which are found to occur in a broad hierarchy of masses. Of these, the light quarks u and d can be approximated to have nearly the same mass leading to an approximate SU(2) global flavor symmetry.

In 1963, Gell-Mann and Zweig proposed the quark model. This composite model of hadrons had great successes in predicting new states and in explaining the strengths of transitions between different hadrons through electromagnetic and weak interactions. However, the birth of QCD in the present form was largely due to the works of Greenberg and Han and Nambu which lead to the concept of color gauge fields. The success of QCD as the theory of strong interaction is backed by a number of experimental data matching predictions from QCD. Most of these tests are provided by scattering experiments involving large momentum transfer in which the inside of a hadron can be probed. A few examples are deep inelastic scattering, Drell-Yan process in colliders, heavy quark production in hadron-hadron collisions etc. The predictions made in these processes are based on the application of perturbative QCD. Such an approach is reasonable for scattering experiments involving

large momentum transfer due to *asymptotic freedom* in the theory. Perturbative calculations in QCD show that the coupling strength decreases with energy and this phenomenon is known as *asymptotic freedom* [see Figure 1]. This property was discovered by Politzer [8] and independently by Gross and Wilczek[7].

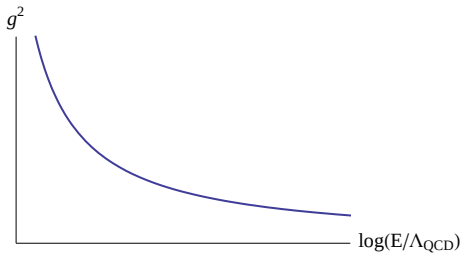

Figure 1: Flow of coupling squared with log of energy. The scale M is generated through dimensional transmutation and may be taken to be the confinement scale in QCD.

Looking at the flow of coupling depicted in figure 1, it may be naively expected that it keeps growing with decreasing energy giving a qualitative explanation of the phenomenon called *confinement*. (it is only a 'naive' expectation, because perturbative arguments fail when the coupling is order one.) Confinement prevents liberation of free quarks and gluons from hadrons. This is in conformity with our observation that the physical states are always found to be in hadronic states. At very high energies, RHIC experiments have shown evidence for the existence of a deconfined phase of quark-gluon plasma (QGP), but the final states one observes are only hadrons. An analytic treatment of confinement in QCD requires a non-perturbative treatment which, however, is not available to us.

Another property of our interest in QCD (and in this thesis) is *chiral symmetry breaking* (χSB). It is known that the masses of u and d quarks are extremely small compared to other scales in QCD. In fact, even s quark is pretty light from this point of view. Therefore one often considers the three to constitute a massless flavor triplet. Under this approximation, QCD has a global symmetry given by

$$Q_L \to e^{i\alpha_L^p \tau^p} Q_L \qquad Q_R \to e^{i\alpha_R^p \tau^p} Q_R, \tag{2}$$

where Q_L and Q_R are the left-handed and right-handed triplets respectively. $p = 1, ..., 8$ runs over the eight generators τ^p of SU(3) flavor group in the fundamental representation. Thus, the action is invariant under separate flavor group transformations in the left-handed and right-handed sectors. This approximate global symmetry in QCD is referred to as an $SU(3)_L \times SU(3)_R$ chiral symmetry. If the quarks were not massless but only had equal masses the symmetry would be only a subgroup of the above given by $\alpha_L^p = \alpha_R^p$, referred to as vector symmetry as opposed to axial symmetry corresponding to $\alpha_L^p = -\alpha_R^p$. One should note that even though the action has chiral symmetry the vacuum may not have it, leading to spontaneous breaking. For instance, due to interactions, the vacuum may grow a finite chiral condensate $\langle Q_L^\dagger Q_R \rangle$ leaving behind only the vector subgroup of chiral symmetry. Once it

is known that spontaneous χSB has occurred, the low energy dynamics can be expressed in terms of meson fields. It turns out that the low energy action is completely fixed by just the symmetries of the QCD action (1) independent of its microscopic details.

Though large number of arguments indicate that QCD has both confinement and χSB, a derivation is still missing. This is because, the scales of χSB and confinement are nearly the same in QCD and hence both require a non-perturbative treatment. However, these phenomena have been demonstrated in other alternate QCD-like theories. A prime example is provided by $\mathcal{N}$=2 SU(2) super Yang-Mills theories considered by Seiberg and Witten. Because of an electric-magnetic duality, the strongly coupled vacuum can be expressed as a weakly coupled theory of monopoles. Confinement can be described perturbatively in the dual theory as monopole condensation [36]. Further, with additional matter multiplet given by $\mathcal{N}$=1 chiral and anti-chiral superfields, it is found to show χSB driven by monopole condensation [37].

χSB has been studied in some other effective theories of QCD like sigma models and Nambu−Jona-Lasinio model (NJL). The low energy and static properties of mesons are well described by a non-linear sigma model. One can calculate the fermion determinant as a derivative expansion of meson field. Terminating at the quadratic level, a sigma model is generated. The gauged sigma model includes vector meson and axial-vector meson couplings also. A matching between the meson masses and decay constants calculated from this model with the experimental values can be found in [40]. Similarly, NJL model is a non-gauge theory involving chiral fermions interacting with each other through a four-fermi interaction [41]. It can be thought of as a low energy effective theory of QCD obtained after integrating out the gluons. Even though gluons are massless, an infrared cutoff is provided due to confinement allowing us to integrate them leading to an effective four-fermi interaction. The attractive interaction between the left-handed and the right-handed fermions leads to a dynamical breaking of chiral symmetry.

In spite of developments in some special models, it still remains a challenge to present a derivation of confinement and χSB in QCD because of the non-perturbative regime involved. An analytic tool to study field theories non-perturbatively is provided by the large N technique. One may wish to study qualitative features of QCD non-perturbatively using this method. It involves defining a new coupling constant λ ('t Hooft coupling) in terms of the Yang-Mills coupling as $\lambda = g^2N$ and looking at the theory at a fixed λ. The perturbation series has two parameters given by λ and $1/N$. For a large value of N, it suffices to look at just the diagrams occurring with the leading power of $1/N$, often referred to as planar diagrams because of the associated topology. However, it still turns out to be difficult to sum up all the planar diagrams as would be required for λ that is not small enough.

A powerful non-perturbative method is Wilson's formulation of QCD on a space-time lattice. This formulation, known as Lattice Gauge Theory (LGT), may be studied on a computer eventually

taking the continuum limit. Significant progress has been made in calculating hadron masses and decay constants in recent years [47]. The calculated values of decay constants of many of the light mesons are found to lie within the experimental error though in some cases the combined statistical and systematic error is as high as seven percent. Masses of hadrons have been calculated taking into account the electromagnetic effects and the ground state values for many of them are found to be within the experimental errors. A longstanding challenge before LGT methods has been to take into account the dynamics of quarks. Many of the algorithms are based on quenched approximation where the quarks are made infinitely massive. In the last few years, however, with improved algorithms and better computers many of the works carried out in LGT have incorporated finite quark masses. But, computation of various quantities still requires extrapolation to physical values of quark masses.

In the last decade, non-perturbative studies in QCD-like theories has taken a new turn. The seminal work by Maldacena in 1998 [48] gave birth to what we today call AdS/CFT correspondence or more generally, gauge/gravity correspondence or holography. It provides a duality between a gauge theory and a string theory. Even though, it may be too difficult to solve the full string theory, when the value of 't Hooft coupling of the gauge theory is large, the string theory can be approximated at low energies with a theory of gravity. The duality then goes between a quantum theory of gravity and a strongly coupled gauge theory that lives in one lower dimension in the boundary of the space-time the gravity theory lives in. This is precisely the region where non-perturbative methods become essential in the gauge theory. Further, in the limit of large N, the quantum corrections in the bulk theory are suppressed giving rise to a classical theory of gravity as the dual. Thus, in the limit of large N and strong coupling, AdS/CFT becomes a very useful tool to study gauge theories as computations in the classical theory of gravity are often quite simple to carry out.

This technique has been applied to many brane models whose low energy limits have QCD-like features to varying degrees. The first attempt in this direction was due to Maldacena whose work lead to a gauge/gravity correspondence for strongly coupled $\mathcal{N} = 4$ super Yang-Mills theory obtained in a setup of large number of overlapping $D3$ branes. Another example of the correspondence can be found in the context of a large N non-supersymmetric gauge theory as proposed by Witten using overlapping $D4$ branes. Confinement in such gauge theories finds a gravity description in the form of a blackhole geometry. Chiral symmetry and its breaking can be described by introducing flavors to these gauge theories. This is done by introducing additional branes, often referred to as flavor branes, to the setup. Karch and Katz proposed the $D3 - D7$ embedding introducing fundamental hypermultiplets to $\mathcal{N} = 4$ super Yang-Mills. The system breaks chiral symmetry and leads to a rich spectrum of mesons. Meson spectrum has been obtained in other string embeddings like the $D4 - D6$ system in the context of non-supersymmetric gauge theory.

Another such model that has found a considerable mention in literature, is Sakai-Sugimoto model

(SS model) [67]. SS model (and its variations) has been one of the closest one has been able to get to QCD using simple string embeddings. It gives an elegant description of confinement and non-abelian χSB using gauge/gravity duality. It consists of large number N_c of overlapping $D4$ branes wrapped on a circle of radius R_k providing the color degrees of freedom. Intersecting them are N_f $D8$ branes and N_f anti-$D8$ ($\overline{D8}$) branes separated from each other along the compact direction x^4 by a distance L and providing the flavor degrees of freedom. This is shown in the first of Figure 2. At low energies, this model gives rise to an effective QCD-like theory. Holographic calculations have been used to obtain hadron spectra and decay rates which have often been found to be surprisingly close to the experimental values. Studies of the model at finite temperature and finite baryon chemical potential have also been made to obtain the phase diagram.

Unlike QCD, SS model provides a good handle to study χSB both in the weak and strong coupling limits. The weakly coupled model is actually a one parameter deformation of QCD, with the extra parameter provided by the ratio of the separation L to the radius of the circle R_k. It turns out that by tuning the parameter to smaller and smaller values one can tune χSB energy scale to be much larger than the confinement scale. This allows a perturbative treatment of the phenomenon.

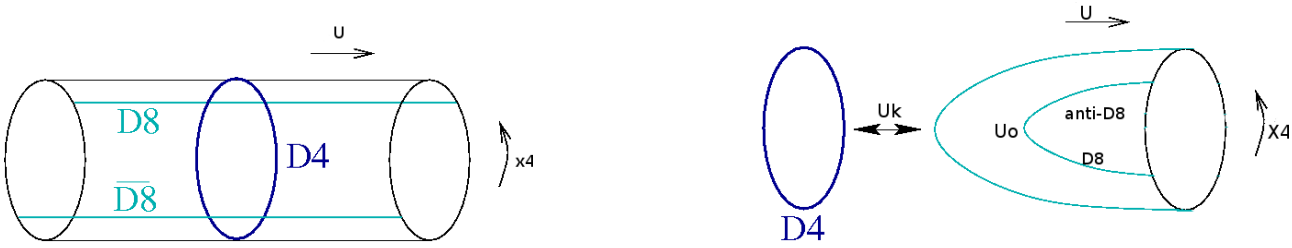

Figure 2: Flavor brane embeddings in the U, x^4-plane both in the weak coupling and strong coupling limits. U is the direction perpendicular to $D4$ branes and U_k is the value of U at the horizon.

In the strong coupling limit, the $D4$ branes can be replaced by the near horizon geometry and one can study the $D8$, $\overline{D8}$ branes as probes in the supergravity background. In the work carried out in [67], Sakai and Sugimoto showed that χSB acquires a geometric meaning in the form of the meeting of separated flavor branes close to the horizon of the $D4$ geometry. This is shown in the second of Figure 2. They also studied the meson spectra arising from flavor brane gauge fields and obtained an infinite tower of Kaluza-Klein states of mesons with the Kaluza-Klein scale of the order of confinement scale. In particular, the analog of a massless pion was obtained in the model. With infinitely more states of mesons than in QCD and no state higher than spin 2, the holographic description of SS model is different from a large N_c QCD. But the hope is that many qualitative properties may be similar in the two. This is based on the expectation that such properties may survive the tuning of coupling from weak to strong. The model, however, does not have any parameter for quark masses. For phenomenological reasons, it is important to incorporate it as observed quantities like hadron masses

depend on it.

In this thesis, we mainly intend to study various aspects of chiral symmetry breaking in holographic QCD. As mentioned above, SS model presents a good arena to study the phenomenon in a holographic setup that resembles QCD to a good extent. With this motivation, we take up two major problems in this direction which can be classified as:

- study of χSB in weakly coupled SS model and

- introducing a quark mass deformation to strongly coupled SS model.

In our study of the weakly coupled model reported in [70], we obtain the effective interaction between the left-handed and right-handed quarks at low energies in a suitable hierarchy of scales. In order to do this we take advantage of the fact that the model provides a parameter to tune χSB energy scale to be much larger than confinement scale, allowing a perturbative treatment. The effective action of the quarks can be written in the form of a non-local NJL action. We obtain numerical solutions to the gap equation and inspect the conditions for χSB. We also study the model in the non-compact limit and find that it does not admit any consistent χSB solution.

In the second work reported in [121, 122], we propose a quark mass deformation of strongly coupled SS model by incorporating the $8-\overline{8}$ open string tachyon in the holographic setup. In string theory, all the physical parameters of a low energy effective theory should eventually come from the condensation of some field. The tachyon field transforms as a bifundamental under the flavor group and would couple to a bilinear of a left-handed and a right-handed quarks. This makes it a good candidate to provide the quark mass parameter on condensation. It turns out that the field also provides an order parameter for χSB in the model, something that was lacking in the original SS model. Using the tachyon DBI action of the flavor branes in the $D4$ background, it is found that the tachyon condenses and the UV behaviour has two modes. The non-normalisable mode provides the quark mass parameter and the normalisable mode gives chiral condensate. We also obtain the meson spectra from the flavor brane gauge field fluctuations. In particular, the analog of a massive pion appears with its mass satisfying the well known Gell-Mann−Oakes−Renner relation.

In the following, we present a more detailed exposition to these works.

1. χSB in the weakly coupled SS model

In the weak coupling limit of the model, the brane configuration is given by the first of Figure 2. It may also be summarised as below (the small circles denote the world volume of the branes)

$$\begin{array}{lcccccccccc} & 0 & 1 & 2 & 3 & (4) & 5 & 6 & 7 & 8 & 9 \\ \text{D4} & \circ & \circ & \circ & \circ & \circ & & & & & \\ \text{D8-}\overline{D8} & \circ & \circ & \circ & \circ & & \circ & \circ & \circ & \circ & \circ \end{array} \tag{3}$$

where the direction x^4 is compact and the common world volume of the flavor and color branes, x^μ, $\mu = 0, .., 3$ give the physical 3 + 1-dim space-time. Antiperiodic boundary conditions are applied on the $D4$ brane adjoint fermions along the compact direction, x^4. This leaves the model with SUSY completely broken. After a GSO projection, the low energy spectrum consists of left-handed and right-handed quarks in 3 + 1 dimensions interacting through the exchange of $D4$-brane gauge fields. These gauge fields lead to a five dimensional $U(N_c)$ Yang-Mills theory with coupling $g_5^2 = (2\pi)^2 g_s l_s$ of length dimension. In our analysis, the scales of the model are assumed to be in the hierarchy $g_5^2 N_c \ll l_s \ll L \ll \pi R_k$. $g_5^2 N_c \ll l_s$ ensures that string loop corrections are small. $l_s \ll L$ allows us to neglect non-trivial dilaton and RR ten-form field created by $D8$ branes. $L \ll \pi R_k$ allows us to study χSB perturbatively by tuning χSB length scale to be much below confinement scale as explained later in this section.

The theory can be expressed in 3 + 1 dimensions by expanding the $D4$ gauge field in harmonic functions of x^4. One is, thus, left with an infinite tower of KK modes of 3 + 1-dim fields. The massive modes can be integrated out to give an effective non-local four fermi interaction between the left-handed and right-handed quarks. Rest of the action, involving the zero mode of the $D4$ gauge field, is given by QCD action. In general, it is not easy to integrate out the massless gauge field. However, asymptotic freedom in QCD action allows computation of the high energy behaviour of the effective interaction that would result from such an integration. Further, confinement provides an IR cutoff of the order of glueball mass scale (confinement scale) on the interaction. This allows us to write a qualitative form for the effective interaction even at low energies. Note that for χSB length scale much smaller than confinement scale, the nature of interaction only at high energies is important which we know quite accurately.

Summing up the effects of both the zero mode and the non-zero modes, we arrive at the effective action given by

$$\begin{aligned} S_{\text{eff}} &= i \int d^4x \Big(q_L^{\dagger\alpha}(x) \bar{\sigma}^\mu \partial_\mu q_L^\alpha(x) + q_R^{\dagger\alpha}(x) \sigma^\mu \partial_\mu q_R^\alpha(x) \Big) \\ &\quad + g_4^2 \int d^4x \, d^4y \, G(x-y) [q_L^{\dagger\alpha}(x) q_R^\beta(y)] [q_R^{\dagger\beta}(y) q_L^\alpha(x)], \end{aligned} \tag{4}$$

where α, β are flavor indices. The Fourier transform of the Green's function, $\tilde{G}(k)$ has a qualitative form given by $\tilde{G}(k) = \left(\frac{1+\pi R_k \bar{k}}{k^2+\Lambda^2}\right) e^{-\bar{k}L}$ in Euclidean momentum $\bar{k}$. The form is based on the following qualitative features that the Green's function would have in various limits. For $\bar{k} \sim \Lambda$, $\tilde{G}(k) \sim 1/(\bar{k}^2 + \Lambda^2)$ connected to the fact that the range of the four fermi coupling is set by the glueball mass of the order of Λ. For $\Lambda \ll \bar{k} \ll 1/\pi R_k$, $\tilde{G}(k) \sim 1/\bar{k}^2$ as the 3+1- dimensional description remains valid in this region. For $\bar{k} \gg 1/\pi R_k$, $\tilde{G}(k) \sim \pi R_k e^{-\bar{k}L}/\bar{k}$ where we have used $L \ll \pi R_k$. This reflects the necessity of the 4 + 1-dimensional description. The exponential behaviour indicates a short-distance cutoff on the four fermi interaction.

For studies of χSB we are interested in the dynamics of the chiral bilinear $q_L^{\dagger\alpha}(x) q_R^{\alpha}(y)$. Hence, it is useful to introduce a bilocal auxiliary scalar field coupling with the bilinear field. One can then integrate out the fermions to obtain an action for the scalar field and its equation of motion, also called the gap equation. For χSB, it has to admit a non-trivial solution. The gap equation obtained for the chiral condensate can be written as follows. Let us denote the chiral condensate as $\frac{1}{N_c}\langle q_L^{\dagger\alpha}(x) q_R^{\alpha}(0)\rangle = \phi(x) \equiv \frac{\phi_0}{4\pi^2 l^3}\varphi(|x|/l)$ where the parameter l of length dimension gives the correct dimensions to the condensate so that ϕ_0 and φ can be assumed to be dimensionless. Notice that in writing it in the above form we have used Poincare invariance of the vacuum. Further, it is convenient to use the notation, $T(x) \equiv \frac{4\pi^2\lambda}{N_c} G^E(x)\langle q_L^{\dagger\alpha}(x) q_R^{\alpha}(0)\rangle$ where $\lambda = g_5^2 N_c/8\pi^3 R_k$. Defining dimensionless functions $f(kl) = \tilde{\phi}(k)/l\phi_0$ and $t(kl) = \tilde{T}(k)/(\lambda l \phi_0)$ where l is a parameter of length dimension, the gap equation can be expressed as

$$f(p) = \frac{\bar{\lambda} t(p)}{p^2 + \bar{\lambda}^2 \phi_0^2 t^2(p)}, \qquad \bar{\lambda} \equiv \lambda l_\Lambda. \tag{5}$$

We often refer to the *rhs* of the equation as $f_t(p)$. In the above expression we use the subscript Λ on l to indicate that the quantity is expressed in dimensionless units of Λ^{-1}. We adopt a similar notation for the other scales in the model too.

Gap equation (5) can now be solved numerically. From the expected physical properties of the order parameter $\phi(x)$ associated with a nontrivial solution, we make an ansatz:

$$\varphi(x) = \frac{e^{-x}}{(c^2 x^2 + 1)^{\sigma}}. \tag{6}$$

From the form of the ansatz it may be noticed that the parameter l in the solution gives the length scale of χSB. The shorter the scale, the narrower the bilocal chiral condensate is. We seek a solution of this form using Mathematica. In particular, we adopt the following procedure. We choose a certain brane configuration by making a choice for the parameters R_Λ and L_Λ. With this, for each value of λ we should now look for a solution i.e., a set of values of the parameters l_Λ, ϕ_0, σ and c that would solve the equation. It turns out that it is easier to fix l_Λ to a given value and then look for the set of values

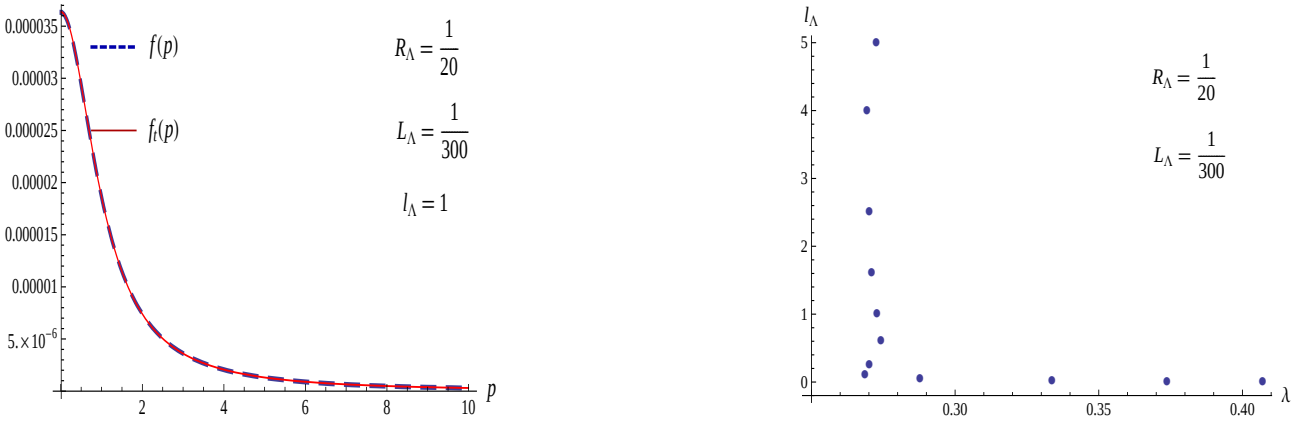

Figure 3: Left: Fit between $f(p)$ and $f_t(p)$ with l_Λ=1. Right: Variation of l_Λ with λ. For both, R_Λ=1/20, L_Λ=1/300.

of $\bar{\lambda}$, ϕ_0, σ and c that would solve the equation. This exercise is repeated for various other values of l_Λ. We notice that the value of c required to give a good fit always turns out to be $\frac{l_\Lambda}{L_\Lambda}$. The first of Figure 3 indicates the matching between the *lhs* and the *rhs* of the gap equation for a typical numerical solution. In the second of Figure 3, we have plotted the variation of the χSB length scale with the coupling. Notice that the model indicates a critical value of the coupling below which there is no χSB. Also note that as we increase λ we can have a wide range of solutions where $l_\Lambda \ll 1$ for which χSB can be described perturbatively. Further, it is found that there is no solution with $\lambda_\Lambda < L_\Lambda$. This implies, the smaller the value of L_Λ, the better it is from the point of view of applying perturbation theory to χSB .

We also try to study the non-compact limit of the model maintaining the hierarchy $L \ll \pi R_k \ll \Lambda^{-1}$. However, we do not find any consistent χSB solution in this limit. This may indicate that the weakly coupled non-compact SS model which does not confine also does not have χSB.

2. Quark mass deformation to strongly coupled SS model

Like the weakly coupled model, the strong coupling version also displays various features associated with χSB. In this limit, as worked on by Sakai and Sugimoto, the $D4$ branes are replaced by the near horizon geometry and the flavor branes are treated as probes in this background. We modify their model by incorporating the $8-\overline{8}$ open string tachyon. The tachyon DBI action of a brane-antibrane system in flat background was proposed by Ashok Sen [99]. Mohammed Garousi proposed a simple extension of the action to curved background in non-compact space [110].

With the assumption that the $8-\overline{8}$ separation, L, is much smaller than the KK radius R_k, this formula may also be applied to our system with compact x^4. The fields involved are given by L, the tachyon τ and the flavor brane gauge fields. The gauge fields are assumed to have dependence on and components along the physical directions x^μ and the holographic coordinate U. Treating them as

fluctuations, one can solve for the brane profile $L(U)$ and the tachyon magnitude $T(U)$ from the DBI action,

$$S = -V_4 \int d^4x \int dU\, V(T) \left(\frac{U}{R}\right)^{-3/4} U^4 \left(\sqrt{D_{L,T}} + \sqrt{D_{R,T}} \right), \tag{7}$$

where $D_{L,T} = D_{R,T} \equiv D_T$ and $D_T = f(U)^{-1} \left(\frac{U}{R}\right)^{-3/2} + f(U) \left(\frac{U}{R}\right)^{3/2} \frac{L'(U)^2}{4} + T'(U)^2 + T(U)^2 L(U)^2$. The potential $V(\tau)$ depends only on the modulus T of the complex tachyon τ. In particular, we use the tachyon potential used in [114, 115, 116] for calculation of decay of unstable D-branes in two-dimensional string theory, $V(T) = \mathcal{T}_8 \operatorname{sech} \sqrt{\pi} T$. The equations of motion for the tachyon and the brane profile are non-linear coupled equations and are difficult to solve exactly. However, one can solve for the UV and the IR behaviour analytically and find a numerical solution matching the two. In the UV, we seek a solution such that the $8 - \overline{8}$ separation approaches a constant and the tachyon becomes small. The general solution with such a form is given by $T(u) = \frac{1}{u^2}(T_+ e^{-h_0 u} + T_- e^{h_0 u})$, $h(u) = h_0 - h_1 u^{-9/2}$ where we have defined $U = u/R^3$, $L(U) = R^3 h(u)$. This behaviour, however, holds only if the growing part of the tachyon is small enough which requires us to put an upper cutoff on u given by $T_+^2 e^{-2h_0 u_{\max}} + T_-^2 e^{2h_0 u_{\max}} << \frac{u_{\max}^{5/2}}{2h_0^2}$. The parameter T_-, associated with the non-normalisable mode of the tachyon, is interpreted as the quark mass parameter.

One can also solve for the IR behaviour. For a smooth joining of the brane and antibrane at u_0, the derivative of h must diverge at this point, and the solution works out to $h(u) = \sqrt{\frac{26}{\pi u_0 f_0}} u_0^{-3/4} (u - u_0)^{1/2} + \cdots$, $T(u) = \frac{\sqrt{\pi}}{4} f_0 u_0^{3/2} (u - u_0)^{-2} + \cdots$. An important feature of the above solution is that it depends only on a single parameter, namely the value of u_0. We have checked that this feature persists in the next few higher orders in a power series expansion in $(u - u_0)$. The UV behaviour of the solution, on the other hand, depends on all the four expected parameters, $T_+,\ T_-,\ h_0,\ h_1$. The solution for $u \sim u_0$ matches with only a one-parameter subspace of the four-parameter space of asymptotic solutions. This one-parameter freedom of the classical solution turns out to be analogous to the freedom to add a bare quark mass in QCD.

The IR and the UV behaviour may be matched numerically and the profiles are as shown in Figure 4. The left one of Figure 5 displays the variation of quark mass parameter T_- with u_0. We choose the region with negative T_- as the physical regime as it is consistent with the fact that driving quark mass to infinity removes the flavor branes (u_0 increases with $|T_-|$). The variation of T_+ with T_- and u_0 can also be found as plotted in the right. The chiral condensate can be obtained by performing a holographic renormalisation of the action and then taking the variation with respect to the quark mass parameter. This gives $\chi \approx \frac{4h_0 V_4 V(0)}{\mu R^9} T_+$. Thus, the right of Figure 5 gives nothing but the variation of chiral condensate with quark mass.

Finally, in order to obtain the meson spectrum, we look at the DBI action of the flavor brane gauge field fluctuations in the background configuration and tachyon profile we have found. As stated

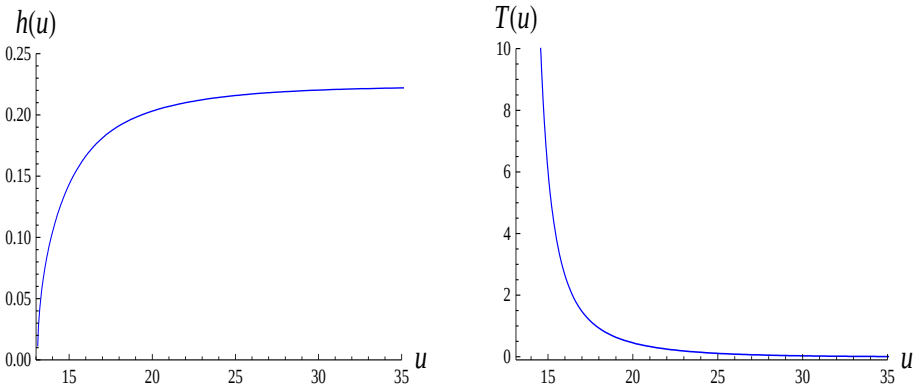

Figure 4: The brane profile and the tachyon solution for $u_0 = 12.7$.

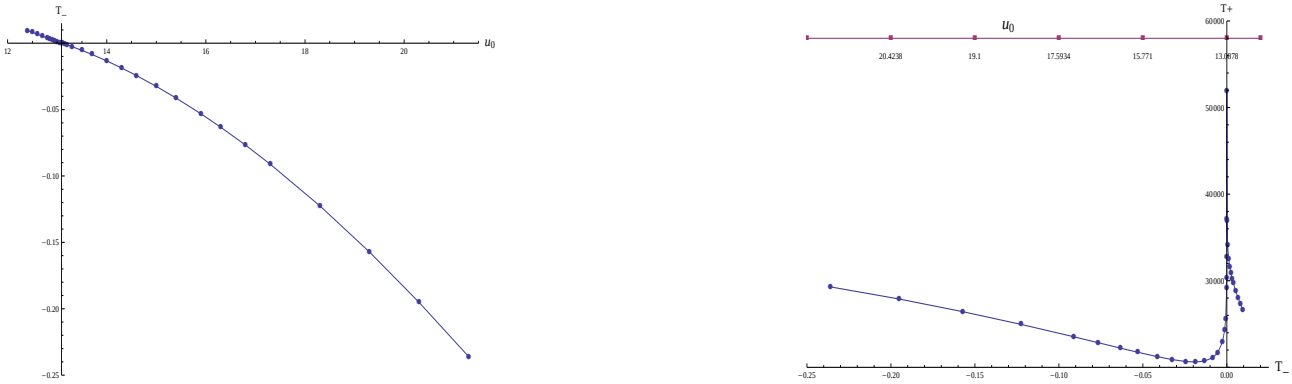

Figure 5: Variation of T_- with u_0 and T_+ with T_-.

before, the gauge fields form five dimensional vector fields along the x^μ and U directions. Expressing it in terms of vector and axial vector combinations of the gauge fields, it can be written as

Further, expanding them using a complete set of functions of U, we get KK towers of meson fields in 3 + 1-dimensions. The vector combination gives rise to the vector mesons and the axial-vector combination gives rise to the axial-vector and pseudoscalar mesons. The lowest mode of the pseudoscalar meson is found to satisfy the GOR relation

$$m_\pi^2 \approx \frac{m_q \chi}{f_\pi^2}. \tag{8}$$

This connects with the fact that there exists a massless pseudoscalar when the quark mass parameter T_- vanishes. Further, when the quark mass is small but not zero, the pseudoscalar ceases to be massless and obtains a mass precisely related through *GOR* relation, a behaviour known to occur in QCD.

Chapter 1

Introduction

There is by now impressive amount of evidence that the microscopic description of the observed strong interactions among hadrons is provided by Quantum Chromodynamics (QCD). QCD is a gauge theory which naturally emerged from the quark model of hadrons proposed by Gell-Mann and Zweig. The Gell-Mann−Zweig model [1, 2] explains the spectrum of hadronic particles but does not provide any information on the origin of strong interactions that bind the quarks inside them. It also has problems with reconciling baryons (made up of three quarks) with the Fermi-Dirac statistics of quarks. To overcome this difficulty, Greenberg [3], Gell-Mann [4] and Han and Nambu [5] introduced the concept of "color" quantum number of quarks. The discovery of scaling in deep inelastic scattering experiments [6] and that of asymptotic freedom in gauge theories [7, 8] gave a strong indication towards the idea of color gauge degrees of freedom which was first coined in [9]. These gauge fields (gluons) mediate interactions between the quarks (hence the name *chromodynamics*) constituting hadrons. By now, a large number of experimental tests of QCD have been conducted. Today, the theory is widely believed to provide the correct microscopic framework for describing strong interactions.

In order to make this thesis self-contained, we present a brief introduction to QCD in this chapter. We discuss various perturbative and non-perturbative aspects of strong interactions and briefly describe different techniques used to study them. We also give a detailed introduction to the phenomenon of *chiral symmetry breaking* in QCD, a non-perturbative phenomenon that is the main subject of this thesis. We refer the reader interested in seeking a thorough and in-depth discussion on QCD to a large number of excellent textbooks and review articles available on the subject like [10]-[22].

1.1 An overview of QCD

The basic degrees of freedom in QCD are given by six flavors of quarks and eight SU(3) gauge fields that mediate interactions between the quarks. It is described through an SU(3) non-abelian gauge theory in the presence of the six flavors of quarks. The '3' in SU(3) is referred to as three colors and hence the gauge fields are also called color gauge fields. The action can be written as

$$S = \int d^4x \left\{ -\frac{1}{4} F^a_{\mu\nu} F^{a\,\mu\nu} + \overline{q}_{i\alpha} \left(i\gamma^\mu (\partial_\mu \delta_{\alpha\beta} - g A^a_\mu t^a_{\alpha\beta}) - m_i \delta_{\alpha\beta} \right) q_{i\beta} \right\},$$
$$F^a_{\mu\nu} \equiv \partial_\mu A^a_\nu - \partial_\nu A^a_\mu + g f^{abc} A^b_\mu A^c_\nu, \tag{1.1}$$

where g is the coupling strength. The gauge fields A^a_μ represent the gluons which transform in the adjoint representation of the SU(3) color gauge group. The indices α, β = 1,2,3 denote three colors and the indices a,b,c = 1,2,...,8 indicate the eight kinds of gluons in SU(3). The quarks $q_{i\alpha}$ transform in the fundamental representation 3 of the SU(3) color gauge group where the index i is a flavor index. The generators of the gauge group are given by $t^a_{\alpha\beta}$. Also, f^{abc} is the structure constant of the SU(3) group defined by the commutation relation $[t^a\ ,\ t^b] = \mathrm{i}\ f^{abc} t^c$. Also, we use the space-time metric in the mostly negative signature given by $\eta_{\mu\nu}$ = diag(1,-1,-1,-1). $\gamma_\mu, \mu = 0, ..., 3$ represent the 4×4 Dirac matrices. In this thesis, we will be using them in Weyl representation which is given by

$$\gamma^\mu = \begin{pmatrix} 0 & \sigma^\mu \\ \overline{\sigma}^\mu & 0 \end{pmatrix}. \tag{1.2}$$

Here $\sigma^\mu = (\mathbf{1}, \sigma)$ and $\overline{\sigma}^\mu = (\mathbf{1}, -\sigma)$, $\mathbf{1}$ being 2×2 identity matrix and σ being the set of three Pauli matrices.

The index $i = 1, ..., 6$ runs over the six flavors of quarks which are found to occur in a broad hierarchy of masses. Two of these flavors, u and d quarks are very light with masses much smaller than the masses of other quarks and the confinement scale. In the approximation where these masses are neglected, the theory has an extended global symmetry, the flavor chiral symmetry. Consider just the matter terms in the QCD action. Suppressing the color indices and writing the action in terms of two-component Weyl spinors q_L and q_R [1], this can be rewritten as

$$S_{\text{quark}} = \int d^4x \left\{ q^\dagger_{Li} \overline{\sigma}_\mu (i\partial^\mu - g A^\mu) q_{Li} + q^\dagger_{Ri} \sigma_\mu (i\partial^\mu - g A^\mu) q_{Ri} - m_i (q^\dagger_{Li} q_{Ri} + q^\dagger_{Ri} q_{Li}) \right\}. \tag{1.3}$$

For N_f flavors, consider the U(N_f)×U(N_f) transformation $q_{Li} \to U_{Lij}\, q_{Lj}$ and $q_{Ri} \to U_{Rij}\, q_{Rj}$ where U_L and U_R are two separate unitary matrices in flavor space. It is easy to see that this transformation is a

[1] $q_L(x)$ and $q_R(x)$ are the two-component Weyl spinors obtained from the Dirac spinor $q(x)$ by the application of the chiral projection operators P_L and P_R, $P_L = \frac{1-\gamma^5}{2}$, $P_R = \frac{1+\gamma^5}{2}$ where $\gamma^5 = i\gamma^0\gamma^1\gamma^2\gamma^3$.

symmetry of the massless part of the action. Alternatively, these symmetry transformations can also be parametrised in terms of vector transformations which correspond to $U_L = U_R$ and axial-vector transformations, which correspond to $U_L = U_R^\dagger$. In the special case that the masses are non-zero but equal, the vector part is a symmetry but the axial part is not. If some ($n_f < N_f$) flavors are massless and the rest massive with unequal masses, then the mass terms respect the subgroup U(n_f)×U(n_f) of chiral symmetry. This is the case for QCD if we approximate the two flavors with very small masses to be nearly massless.

Even in the massless case, the quantum theory has subtleties. A U(1) part of the axial symmetry is broken due to quantum effects. Furthermore, the axial SU(N_f) undergoes spontaneous symmetry breaking, leaving behind only a vector symmetry. The Goldstone bosons associated with this symmetry breaking are identified with a triplet of pseudoscalar mesons (pions) in hadron physics corresponding to N_f=2. This is expected to hold true on neglecting the small quark masses for the *u* and *d* flavors. In reality, however, one finds that the pions are not massless but have small masses. This is because of the non-zero masses of *u* and *d* quarks [39].

1.1.1 Asymptotic freedom

There are three kinds of interaction vertices in the QCD action given in (1.1). One of these involves interaction of two quarks (straight line) with a gluon (wavy curve) while the other two give rise to interactions among three and four gluons as shown in Figure 1.1.

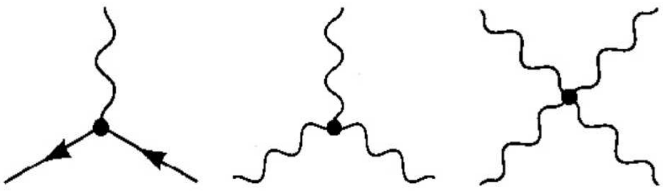

Figure 1.1: QCD interaction vertices (adapted from [10]).

In perturbation theory, these interactions lead to a renormalisation group flow of the coupling strength given by the beta function [10]

$$\beta(g) = -\frac{g^3}{(4\pi)^2}\left(\frac{11}{3}N_c - \frac{2}{3}N_f\right), \tag{1.4}$$

where N_c denotes the number of colors (for SU(N_c) colour gauge group) and N_f denotes the number of quark flavors. For $N_c/N_f > 2/11$, the beta function is negative, i.e., the coupling constant decreases with energy. In particular, for QCD we have $N_c = 3, N_f = 6$ and so it satisfies this condition. Thus, QCD has the property that at high energies it approaches a free theory. This result, called *asymptotic freedom*, is at the basis of the many successful comparisons of perturbative QCD calculations with

high energy scattering experiments involving strongly interacting particles. The key difference with an abelian gauge theory, like Quantum Electrodynamics (QED), in which the coupling grows with energy [10], is that the force carriers gluons interact among themselves. As in QED, the quark-gluon interaction leads to a coupling increasing with energy, as reflected in the second term in equation (1.4). In QCD, the self-interaction of the gluons leads to an additional opposite effect and causes the coupling to decrease with energy. The first term in (1.4) shows this. The net effect is determined by a competition between the two terms and gives rise to asymptotic freedom in QCD.

The flip side to asymptotic freedom is that at low energies the QCD coupling becomes large. This can be seen from the solution to (1.4) which is usually written in the form [2]

$$\frac{g(Q)^2}{4\pi} \equiv \alpha_s = \frac{2\pi}{b_0 \ln(Q/\Lambda_{\rm QCD})}, \qquad b_0 = (\frac{11}{3}N_c - \frac{2}{3}N_f). \tag{1.5}$$

Here, $g(Q)$ is the running coupling and $\Lambda_{\rm QCD}$ is the characteristic energy scale of QCD. We see that as Q decreases, the QCD coupling grows until at $Q = \Lambda_{\rm QCD}$, it blows up. This behaviour can be seen in the continuous curves in Figure 1.2 which have been drawn for different values of Λ_{QCD}. The striking agreement between the perturbative calculation and various experimental results can also be seen from the figure. Of course, long before the energy scale $\Lambda_{\rm QCD}$ is reached a perturbative treatment of QCD is inadequate and non-perturbative effects take over. It is believed that these non-perturbative effects lead to the confinement of quarks and gluons inside hadrons, thereby explaining their absence from the observed spectrum of strongly interacting particles. Although we still lack an analytical derivation of confinement in QCD, it has been demonstrated in very similar (supersymmetric) gauge theories [36] and also using lattice gauge theory techniques (see [38] for a review and references).

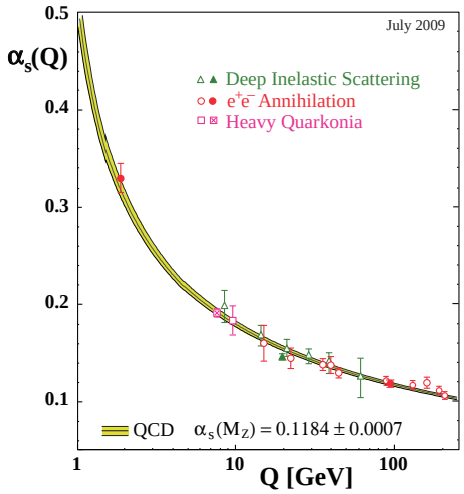

Figure 1.2: Flow of coupling strength with energy as obtained from [39].

[2] See, for example, the book by Peskin and Schroeder [10]

1.1.2 Confinement

Although it is hard to prove confinement in QCD, the phenomenological evidences for the phenomenon are very strong. One does not observe free quarks and gluons in nature but they are confined inside hadrons. To understand how it might happen, consider a high energy scattering experiment where a quark is struck off from the rest of the hadron. As the quark separates, the color electric field around it would approach the one due to a single quark. If the energy stored in this field becomes too large it may lead to the production of a quark-antiquark pair. The antiquark can then bind to the struck quark and the quark from the pair with the rest of the hadron resulting in color singlet states in the final state. Such an experiment, therefore, will not let one measure the energy associated with the color electric field of a lone quark. One can, however, resort to a study of this energy through indirect means namely, the pattern of hadron spectrum called Regge trajectories and numerical simulations of the problem.

If one plots the square of the masses of hadrons with their angular momentum, one finds that hadrons with given flavor lie on nearly parallel straight lines referred to as Regge trajectories. This is a feature that is particularly characteristic of the hadron spectrum. If one picturises a meson as a string of constant mass per unit length (string tension) between the quark and antiquark, one arrives at a similar spectrum. This gives an indication towards a string picture of a meson. One possible way that such a string picture may arise from quarks and gluons is through the formation of a color electric flux tube in which the color electric field between a static quark and antiquark is confined to a thin cylindrical tube running between the two. Such a phenomenon would be similar to Meissner effect in which magnetic field inside a type II superconductor gets collimated into thin flux tubes. The electric-magnetic dual picture of this would give rise to a situation in which the electric field between the quark and anti-quark is collimated into a flux tube in a dual superconductor consisting of a monopole condensate.

Although, it has not been possible to derive such a result for QCD, it has been demonstrated in alternate theories similar to QCD. A prime example is provided by $\mathcal{N}$=2 SU(2) super Yang-Mills theories considered by Seiberg and Witten. Because of an exact electric-magnetic duality in the theory, the properties of the vacuum in the strongly coupled ‘electric’ theory can be deduced from the properties of a weakly coupled ‘magnetic’ theory. Confinement can be described perturbatively in the dual theory as monopole condensation [36].

The most reliable evidence of the static quark potential is obtained using computer simulations with very massive quarks where pair production can be ignored. These computations are carried out using lattice gauge theory, a non perturbative technique which we will briefly describe later. This involves computation of a Wilson loop from which the static quark potential can be derived. The Wilson loop is found to satisfy an area law, indicating that the static potential between a quark and an

antiquark grows linearly with the pair separation. This makes it highly probable that the phenomenon of confinement is present in strong interactions.

1.1.3 Perturbative tests of QCD

Most experimental tests of QCD are based on perturbative calculations, which, as we saw now, are valid at high energies because the QCD coupling is small at high energies. This allows us to compare perturbative computations in QCD with scattering experiments involving exchange of momenta larger than a few times Λ_{QCD}. These comparisons have yielded a value $\Lambda_{\text{QCD}} \approx 200\text{MeV}$. This small value of the characteristic QCD scale explains the early onset of scaling and is responsible for the remarkable success of perturbative QCD in explaining a host of experimental data on many strong interaction processes [10]. In the following, we will briefly describe a few examples of such scattering experiments which have provided us with a large number of successful tests of QCD.

- e^+-e^- annihilation: In this process, an electron-positron pair collides at a large center of mass energy and annihilates into hadrons. The leading order Feynman diagram that contributes to this process is shown in Figure 1.3(a). This involves annihilation of the pair into an offshell photon which subsequently materialises into a quark-antiquark pair.

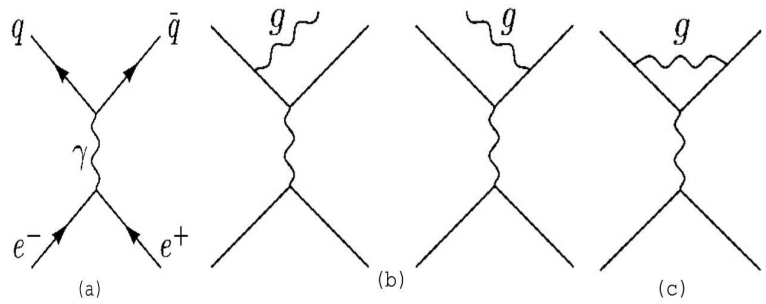

Figure 1.3: Feynman diagrams for e^+e^- scattering (adapted from [10]).

This diagram involves only QED interactions. However, the process receives corrections from diagrams involving QCD interactions too. The leading order correction in strong coupling is provided by the diagram in Figure 1.3(c) where the two quarks also exchange a gluon between them. The diagrams in Figure 1.3(b) show processes with a gluon emission which cancel the IR divergence present in the other. In all these, the quark, anti-quark and the radiated gluon subsequently hadronise through soft processes leading to hadrons as the final states in the scattering process. In the experiment, these appear as jets of hadrons shooting in different directions.

The scattering cross-section of the process can be computed using perturbation theory. After summing over all flavors (for quarks) and colors (for quarks and gluon) in the final state, it is

given by [10]

$$\sigma\Big(e^+e^- \to \text{hadrons}\Big) = 3\Big(\sum_{\text{i}} \text{e}_\text{i}^2\Big)\frac{4\pi\alpha^2}{3\text{s}}\Big(1 + \frac{\text{g}^2}{4\pi^2} + ...\Big), \tag{1.6}$$

where s is the standard Mandelstam variable and the dots represent corrections in higher orders of the QCD coupling. Here, we have neglected all masses, which makes sense for such high energy scattering processes. α is the electromagnetic fine structure constant and e_i is the electric charge of the quark with flavor i. The factor of 3 in the expressions depicts the number of colors. We may now worry how this cross-section is related to the cross-section for the experimentally observed process with hadrons in the final state. The key point is that the quarks and gluons in the final state of these QCD diagrams always hadronise with certainty. Hence the cross section for the whole process is given by equation (1.6) (to leading order in electromagnetic and strong couplings). This equation provides an additional way to experimentally verify the number of colors (the factor of 3).

One of the very important implications of this kind of scattering is due to the QCD process of the last two diagrams in the figure involving the radiated gluon. Let x_1, x_2 and x_3 be the fractions of energy of the annihilating electron-positron system in the center-of-mass frame shared by the quark, antiquark and the emitted gluon respectively. In terms of the the four momenta, they are given by $x_j = 2k_j.q/q^2$ for $j = 1, 2, 3$ and satisfy $\sum_{j=1}^{3} x_j = 2$. The differential cross section for this process is given by [10]

$$\frac{d^2}{dx_1 dx_2}\sigma = 3\Big(\sum_i e_i^2\Big)\frac{4\pi\alpha^2}{3s}\frac{g^2}{6\pi^2}\frac{x_1^2 + x_2^2}{(1-x_1)(1-x_2)}. \tag{1.7}$$

This expression has a singularity for $x_1 \to 1$ or $x_2 \to 1$. These limits pertain to the case when the quark (antiquark) is scattered with the maximum possible energy and the antiquark (quark) and the gluon are scattered in the opposite direction, collinear with each other. Thus, the process shows a very large differential cross section with the gluon emitted collinear to the quark or the antiquark. Subsequently, the quark, anti-quark and the gluon hadronise. However, with the gluon collinear to the quark or the anti-quark, one has two back-to-back hadron jets, indistinguishable from what happens in the processes without a gluon radiation. Such jets have been observed in PETRA and LEP experiments [26]. One can have a tri-jet of hadrons only when the gluon has a significant transverse momentum. In practice, this is implemented by imposing an angular cut-off on separations of the jets. It has been possible to distinguish such tri-jet events in LEP [26]. One can also have a four jet event, providing evidence of gluon self interactions. It is extremely difficult to carry out the experimental analysis for this but the

evidence of a three gluon interaction emerges [26].

- Deep inelastic scattering: This experiment involves scattering of a lepton (electron, muon or a neutrino) from a nucleon (a proton or a neutron) at very high momentum transfers. The lepton undergoes an electromagnetic interaction with one of the quarks inside the hadron (see Figure 1.4). When the momentum transferred to the quark is high enough, it is ripped off from the

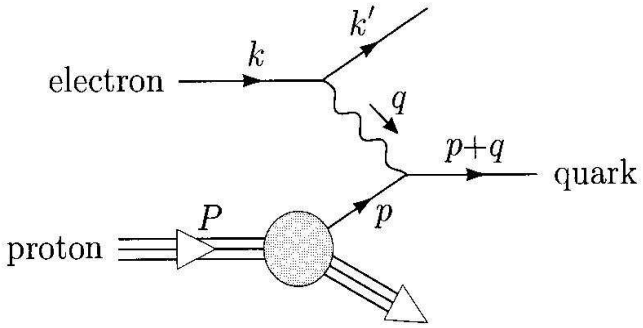

Figure 1.4: Deep inelastic scattering (adapted from [10]).

rest of the hadron. Let the four momentum of the lepton be k and that of the quark be p. Let the (space-like) momentum transferred to the quark be $q = k - k'$. Deep inelastic scattering pertains to the scenario when $Q^2 = -q^2$ is large such that the QCD coupling is small at this scale. Because of this, strong interactions can not prevent the quark from getting ripped off from the rest of the hadron. The quark, however hadronises through subsequent soft processes, as in all QCD processes.

To find out the cross-section in deep inelastic scattering, it is useful to go to the centre-of-mass frame of the lepton-hadron system. As the momenta of the lepton and the hadron are very large, one may neglect their masses. Further, at high enough momentum, the hadron may be thought of as being composed of quarks and gluons with momenta longitudinal to the hadron momentum itself. This is because, the constituents can gain a large transverse momentum only through the exchange of hard gluons. Such a process will be highly suppressed due to the smallness of the strong coupling at high energies. Hence, the momentum p of the quark undergoing the interaction may can be written as $p = xP$, where $x \in [0, 1]$. However, the probability distribution for the quark to have a momentum fraction x cannot be derived in perturbative QCD. This depends on the soft processes involved in confinement of constituents of a hadron, which is beyond the purview of a perturbative analysis.

The standard way to treat this is to parametrize our ignorance of the hadronic wave functions in terms of probabilities that a quark or a gluon carries a fraction of the momentum of the

hadron. These are known in the QCD literature as parton distribution functions. One relies on experimental observations to determine these distribution functions. The leading contribution to the cross-section in deep inelastic scattering in terms of these functions is given by [10]

$$\sigma(l + \text{hadrons} \to l' + \text{hadrons}) = \int_0^1 dx \sum_i f_i(x)\sigma\Big(l(k)q(xP) \to l(k') + q(q + xP)\Big), \quad (1.8)$$

where $f_i(x)$ denotes the distribution functions. In the leading approximation, one gets the differential cross-section

$$\frac{d^2}{dxdQ^2}\sigma\Big(l + \text{hadrons} \to l' + \text{hadrons}\Big) = \sum_i f_i(x)e_i^2\frac{2\pi\alpha^2}{Q^4}\{1 + (1 - Q^2/xs)^2\}, \quad (1.9)$$

where $q^2 = -Q^2$ and s is the standard Mandelstam variable of the lepton-hadron scattering. Notice that if we remove the kinematic dependence of the QED cross section, $\frac{1+(1-Q^2/xs)^2}{Q^4}$, rest of the the term depends only on x and not on Q^2. This is known as Bjorken scaling and implies that the structure of a hadron appears the same independent of the momentum transfer by the probe. However, higher order QCD corrections lead to violation of the scaling law. The quark undergoing electromagnetic interaction with the lepton can lead to emission of gluons and quarks through soft processes. Processes with collinear emission of gluons or quarks lead to large corrections, of the order of, $\alpha_s(Q^2)\ln(Q^2/m^2)$ to the Parton distribution function, where m is the mass of a quark. Thus, the distribution function is actually given by $f_i(xQ^2)$ which flows logarithmically in Q^2, as governed by Altarelli-Parisi equations [10].

One of the earliest of the deep inelastic scattering experiments, the SLAC-MIT deep inelastic scattering experiments, was done in 1960 (see [10]). These used a 20 GeV electron beam that was scattered from a hydrogen target. The scattering rate was measured for large deflection angles which correspond to deep inelastic scattering of electron off a proton. The largest part of the cross-section came from deep inelastic scattering where the end state is comprised of a large number of hadrons (apart from the deflected electron). The results from the parton model well described the observations from these experiments. The experiments also showed that Bjorken scaling holds true at 10 percent level for values of Q upto about 1 GeV [10, 27]. Because of a slow logarithmic flow of the parton distribution function with energy, violation of the scaling is seen only after accumulating more data over a large range of energy transfers.

- Hard scattering processes: Apart from the type of processes discussed above, yet another class providing perturbative tests of QCD is the hard scattering of high energy hadrons off each other. However, this is the messiest class since in all such processes the particles in both the initial and final states are hadrons. In this case, even initial states will involve some soft

interactions of quarks and gluons with only a small transverse momentum being exchanged. Such interactions can not be dealt with perturbatively. However, the underlying QCD process in the hard scattering part can be computed perturbatively. Consider the example of two high energy protons colliding with each other and leaving e^+e^- in the final state in addition to other hadrons as shown in Figure 1.5. The leading order contribution to the scattering cross-section

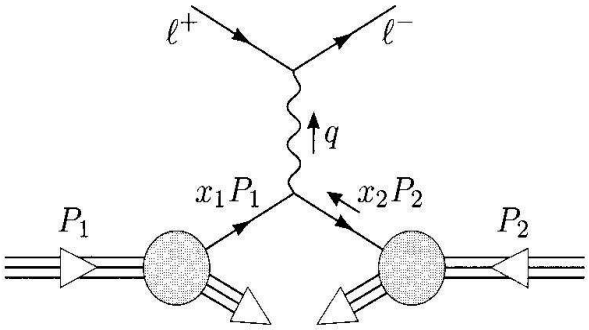

Figure 1.5: Hard scattering (adapted from [10]).

(in the centre of mass frame) computed using perturbative QCD, is written as

$$\sigma\Big(pp \to e^+e^- + \text{hadrons}\Big) = \int_0^1 dx_1 \int_0^1 dx_2 \sum_i f_i(x_1) f_{\bar{i}}(x_2) \sigma\Big(\bar{q}_i(x_1P_1) q_i(x_2P_2) \to e^+e^-\Big),$$
$$\sigma\Big(\bar{q}_i q_i \to e^+e^-\Big) = \frac{e_i^2}{3} \frac{4\pi\alpha^2}{3\hat{s}}, \tag{1.10}$$

where x_1 and x_2 denote the fractional momenta of the quark and the anti-quark and $\hat{s}$ is the standard Mandelstam variable for the underlying QCD process. Thus, using inputs on parton distribution functions derived, for example, from deep inelastic scattering experiments one can calculate the cross section in hard scattering processes and compare with experiments.

Historically, the first of scattering experiments to study strong interactions was in proton-proton collision [10]. At energies higher than 10 GeV or so, large number of pions were observed. The characteristic feature of these experiments was that the pions were mostly found to be collinear with the collision axis. Only a few events are observed where there are pions with large transverse momentum. It has been possible to analyse such events in perturbation theory and compare with experimental results. As an example, two-jet invariant mass distribution in $p\bar{p}$ collisions at 1.8TeV was measured by the CDF collaboration [10]. The results were found to be comparable with leading order QCD calculations.

1.1.4 Non-perturbative QCD

Although a non-perturbative study of non-abelian gauge theories is a difficult subject, considerable progress has been made in this direction over the last 40 years. Some of the techniques which have proven to be very important in this progress are as follows:

Lattice gauge theory

This is one of the most widely used techniques in non-perturbative QCD which allows numerical computation of various experimentally measurable quantities in hadronic Physics. Lattice gauge theory (LGT), invented by Wilson [23], is based on computation of Feynman path integral on a lattice of Euclidean space-time restricted to a finite volume (see [28] for an introduction). The space-time points are assumed to lie on the sites of a hyper-cubic lattice of size L with a unit cell of size a (see Figure 1.6). The finite lattice size provides an ultra violet cutoff while the finite volume provides an infra red cutoff thereby making the theory finite and well defined. As one takes the limit $a \to 0$ and $L \to \infty$, one approaches the infinite continuum space-time in Euclidean signature. Physical predictions for the continuum Minkowski space-time are then extracted by an analytic continuation.

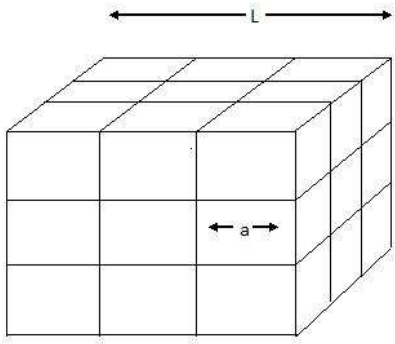

Figure 1.6: Space-time lattice.

The QCD action in such a discrete space-time involves quark fields sitting at the sites and gauge fields on the bonds of the lattice. One is, therefore, faced with computing *only* a finite number of integrals in evaluating the Feynman path integral. The smaller the lattice spacing a and the larger the size L, larger the number of integrals needed to evaluate the path integral. With faster and faster computers one could approach the infinite continuum (Euclidean) space-time. One expects that the results in actual space-time can be attained as a continuum limit of the results in finite discrete space-time. Nevertheless, with the advent of very powerful computers, it has now been possible to carry out lattice computations with dynamical fermions also in many cases. The computations are, by no means, trivial and one has to address various issues as discussed in the following:

- *Doubling problem*: If one naively extends the QCD action to discrete space-time one finds that the fermion propagator has extra poles leading to the well known *doubling problem* of fermions on a lattice. Removing these doublers requires one to add extra terms to the lattice action. This, however, destroys the chiral symmetry of the action even in the limit of zero quark mass. Other forms of action have been proposed which remove the doublers and restore chiral symmetry in the continuum limit.

- *Discretization error*: In writing the lattice action, space-time derivatives have to be written as finite differences. This leads to a discretization error. One is required to add a suitable combination of irrelevant operators to cancel the errors order by order in a. This increases the reliability of the results and may often be necessary due to limitations of computer power [38].

- *Computation of background gauge field configuration*: The Feynman path integrals are associated with a factor of exp(-S) in Euclidean space-time. Thus, the contribution to the path integral is dominant from configurations near which S is minimised. Such configurations can be generated using a Markov chain. The path integral, then, is carried out using Monte Carlo techniques.

- *Computation of quark propagator*: Computation of quark propagator involves inversion of the Dirac operator from a quark of a given spin and color at a site to a quark of another spin and color at a different site. One is required to compute this between all the space-time points, which turns out to be the most computationally expensive part in the problem. This makes one often work in the quenched approximation where the quarks in the QCD action are assumed to be non-dynamical. In other words, they are assumed to be infinitely heavy.

Lattice calculations indicate that there is confinement of quarks inside hadrons and that there is chiral symmetry breaking. Because of lattice gauge theory, it has also been possible to study hadronization of jets through soft interactions of quarks and gluons. Another very important contribution of LGT has been in calculating hadron masses and their decay constants. In many cases, the technique yields values which are quite close to the experimentally measured values within the error bounds. A summary of the achievements of the technique can be found in [26, 30]. A lot of progress has been made in lattice gauge theory recently. One of the major issues before LGT has been regarding the extrapolation of quark mass down to the physical values of up and down quarks. The next to leading order (NLO) correction in chiral perturbation theory (ChPT) for pion decay constant predicts a non-analytic behaviour $-m_\pi^2 \ln m_\pi^2$. The LGT simulation performed by the MILC collaboration found a pion mass as low as 250 MeV and showed the existence of the chiral log [24].

LGT has also come a long way in the prediction of fundamental QCD parameters like the strong coupling constant, light quark masses and heavy quark masses. The HPQCD collaboration carried out three loop computations with dynamical quarks and obtained results for the coupling constant with substantially reduced errors due to higher order terms [25]. These calculations have also been used to obtain light quark masses to a good deal of accuracy (see [30] for a review). LGT calculations have also been carried out in Kaon Physics, in particular to obtain mixing angles, with encouraging results.

Another application of LGT has been in the sector of finite temperature. At high temperatures and densities quarks and gluons inside hadrons are believed to deconfine into a free state known as quark-gluon plasma (QGP). There has been a lot of work in LGT literature that probed the nature of this transition. Recent 2+1-flavor LGT calculations done using staggered fermions have shown that there is no true phase transition but thermodynamic variables undergo a rapid crossover in a small interval of temperature [32]. Because of this, quantities like the chiral condensate have a sharp peak at some transition temperature. LGT calculations in [33] indicated it to be around $T_c = 176$ MeV. Using LGT calculations it has also been possible to evaluate equation of state at high temperatures. At temperatures large compared to T_c, QGP is found to approach the ideal gas state. Some of the recent calculations can be found in [34, 35].

Large N

This technique was invented by 't Hooft [45]. Many features of QCD can be understood by studying a 'slightly' different gauge theory where one considers an SU(N) gauge group instead of SU(3) and then takes the limit $N \to \infty$. In this limit one is required to keep g^2N fixed for a sensible expansion. This combination of N and g^2, usually denoted as λ , is known as 't Hooft coupling. The key feature in this technique is that the perturbation theory can be arranged in a double expansion in λ and $1/N$. In the large-N limit, one is then left with a perturbation series in $1/N$, each term of which is a further expansion in the coupling λ. There is a prescription which associates diagrams at each order of $1/N$ with surfaces of a given topology. The double expansion, can then be written as a genus expansion for surfaces of different topologies taking a form

$$\sum_{g=0}^{\infty} N^{2-2g} f_g(\lambda), \tag{1.11}$$

where $f_g(\lambda)$ arises in summing up all the diagrams with genus g. The leading order (in $1/N$) diagrams are associated with the topology of a sphere and are referred to as planar diagrams. In a pure gauge theory, the first subleading diagrams in $1/N$ are associated with the topology of a torus. In the presence of fundamental flavors however, the first subleading diagrams have the topology of a disc. The main crux is that, for large N one may neglect higher order terms in $1/N$ in the genus expansion, thus

drastically reducing the number of diagrams to calculate. Even though SU(N) gauge theory with large N is different from QCD, it is believed that many of the qualitative features of QCD are preserved in this limit. A detailed review of this method applied to QCD can be found in [46].

Although the large N limit leads to an immense simplification, calculations in asymptotically free gauge theories turn out to be quite hard to carry out even in this limit. This is because one is still left with an infinite number of planar diagrams (the expansion in λ) to sum over. However, with the emergence of AdS/CFT correspondence [3] it has now become possible to overcome this difficulty, at least in some corners of the parameter space.

AdS-CFT correspondence

The AdS/CFT correspondence, first discussed by Maldacena and Klebanov, Polyakov and Gubser [48, 49], conjectures a duality between an SU(N) gauge theory and string theory in one higher dimension. When the value of 't Hooft coupling of the gauge theory is large, the string theory reduces to a theory of gravity. The duality then is between a quantum theory of gravity and a strongly coupled gauge theory which lives on the boundary of the bulk space-time in which the theory of gravity lives. Further, in the limit of large N, the quantum corrections in the bulk theory are suppressed, giving rise to a classical theory of gravity. Thus, in the limit of large N and strong coupling, AdS/CFT becomes a very useful tool to study strongly coupled gauge theories by computations in a classical theory of gravity, which are often quite simple to carry out, certainly simpler than summing up the series of planar diagrams in the gauge theory!

The original work of Maldacena discussed the correspondence between a strongly coupled $\mathcal{N} = 4$ super Yang-Mills theory (which is obtained in the low energy limit in a setup of large number of overlapping $D3$ branes) and a classical bulk AdS space. A precise rule exists for calculating correlation functions of operators in the boundary gauge theory from computations in the bulk gravity theory. Following this work, various authors have investigated the duality in a variety of settings. We will provide a brief review of the working rules of the correspondence in the next chapter as we will be using them extensively in this thesis.

1.2 Chiral symmetry breaking

In QCD, the scale of chiral symmetry breaking (χSB) is close to the confinement scale. As a consequence, χSB in QCD is a strong coupling problem, not amenable to perturbative techniques. So it has been difficult to study this phenomenon analytically in QCD. However, in the large N_c analogue of QCD some general results can be obtained analytically since corrections, which are down by

[3] AdS stands for anti-deSitter space and CFT for conformal field theory

powers of $1/N_c$, can be controlled in this approximation [46]. An argument for χSB in large-N_c QCD was presented by Coleman and Witten in [59]. The argument is based on the following assumptions: 1) the large-N_c QCD is confining, 2) χSB is characterised by an order parameter given by a fermion bilinear that transforms as a bifundamental under the chiral group, 3) vacuum corresponds to a state obtained by minimizing an effective potential as a function of the order parameter, and 4) the various minima obtained do not have any accidental degeneracy with respect to the chiral group. In order to calculate the effective potential a s a function of the chiral bilinear, one needs to sum up the connected diagrams. In the limit of $N_c \to \infty$, diagrams with more than one quark loop drop out. One is eventually left with a form for the potential that involves a single trace over flavors. Using this and the assumption that there is no accidental degeneracy, the authors argued that there is a spontaneous breaking of $\mathrm{U}(N_f) \times \mathrm{U}(N_f)$ chiral symmetry to vector $\mathrm{U}(N_f)$ in an $\mathrm{SU}(N_c)$ gauge theory. An exact derivation of both χSB and confinement in a supersymmetric setup was given by Seiberg and Witten in [36, 37]. χSB has been studied using large N techniques also in models which do not show the phenomenon of confinement. One such model which has been extensively studied in literature, and is also a topic in this thesis, is the Nambu−Jona-Lasinio(NJL) model [41, 42]. The importance of this model lies in the fact that it can be argued to arrive in the low energy limit of large N_c QCD. We briefly review the model in the following.

1.2.1 NJL model

In their original paper, Nambu and Jona-Lasinio considered their work as a model for nucleons interacting through a four-fermi term. A nucleon-antinucleon bound state was identified as a pion. If the nucleons are replaced by quarks, one gets NJL model for quarks. It has been argued [43, 44] that such a model likely emerges from QCD as an effective low energy theory. The Lagrangian density of this model is given by

$$\mathcal{L} = \overline{q}_{L\alpha j} i\gamma^\mu \partial_\mu q_{L\alpha j} + \overline{q}_{R\alpha j} i\gamma^\mu \partial_\mu q_{R\alpha j} + g^2 (\overline{q}_{L\alpha j} q_{R\alpha k})(\overline{q}_{R\beta k} q_{L\beta j}), \tag{1.12}$$

where q_L and q_R denote Dirac spinors for left-handed and right-handed quarks respectively, α, β are color indices and j, k are flavor indices. Note that the Lagrangian is symmetric under chiral transformation

$$q_{L\alpha j} \to \mathrm{U}_{L\,jk} q_{L\alpha k},\ q_{R\alpha j} \to \mathrm{U}_{R\,jk} q_{R\alpha k}, \tag{1.13}$$

where U_L, U_R are unitary matrices in flavor space. The four-fermi term in the Lagrangian gives rise to an attractive interaction between the quarks of the two chiralities. This leads to the formation of a

chiral condensate in the vacuum through a dynamical breaking of chiral symmetry.

It is believed that at energies below the QCD scale $\Lambda_{\rm QCD}$, the model captures the dynamics of QCD. There is no systematic way of integrating out the gauge fields in QCD to derive a low energy effective theory of fermions. However, a scenario for how one may try to do so was described in [43, 44]. The basic point is that the integration of the gauge fields would lead to an effective multi-fermi interaction that should be of short range of order $1/\Lambda_{\rm QCD}$. The leading term corresponding to one gluon exchange diagrams gives rise to a four-fermi term as in the NJL model. One important fact about the NJL model is that it is not renormalisable and has to be thought of with a finite energy cutoff. This cutoff should be of the order of QCD scale for applications to QCD.

The Lagrangian in (1.12) is equivalent to

$$\mathcal{L} = \overline{q}_L i\gamma^\mu \partial_\mu q_L + \overline{q}_R i\gamma^\mu \partial_\mu q_R + \overline{q}_L M q_R + \overline{q}_R M^\dagger q_L - \frac{1}{g^2}{\rm tr}(M^\dagger M). \tag{1.14}$$

where M is color invariant. The operator 'tr' represents the trace on the spinor index. Solving the equation of motion for M and $M^\dagger$ and plugging into equation (1.14), one reproduces (1.12). This is true even at the quantum level since the Lagrangian is quadratic in M and $M^\dagger$. The bosonic field M plays the role of a chiral bilinear of the quarks given by

$$M_{ij} = g^2 \overline{q}_{Rj} q_{Li}, \tag{1.15}$$

where we have now made the flavor indices explicit. The rhs involves a sum over N_c colors.

To discuss symmetry breaking in this model, let us first express the action in (1.14) in terms of Dirac spinor q such that the chiral spinors are given as $q_L = P_L q$ and $P_R q$. The action then takes the form

$$\mathcal{L} = \overline{q} i\gamma^\mu \partial_\mu q + \overline{q}(M P_R + M^\dagger P_L) q - \frac{1}{g^2}{\rm tr}(M^\dagger M). \tag{1.16}$$

We now need to integrate out the fermion q to get an effective action purely in terms of the bosonic fields, M, $M^\dagger$:

$$\begin{aligned} S_{eff} &= N_c[\ln \det D - \frac{1}{N_c g^2}\int d^4x {\rm tr}(M^\dagger M)], \\ D_{x,y} &= (i\gamma^\mu \partial_\mu + iMP_L + iM^\dagger P_R)\delta^4(x-y). \end{aligned} \tag{1.17}$$

For large N_c the effective dynamics becomes classical since fluctuations are suppressed by factors of $1/N_c$. Chiral symmetry breaking leads to a non trivial v.e.v for the chiral bilinear which can be found from the classical equation of motion. In terms of the bosonic fields M and $M^\dagger$, it means a non

trivial vev for M itself. For a Poincare invariant vacuum, the v.e.v for M should be a constant matrix. Now, chiral symmetry of the Lagrangian (1.12) can be seen from its invariance under the following transformation:

$$\begin{aligned} q'_L = U_L q_L,\ q'_R = U_R q_R, \\ M' = U_L M U_R^\dagger. \end{aligned} \tag{1.18}$$

The matrix M can be written as HU where H is a Hermitian matrix and U a unitary matrix. Thus, using the chiral transformation $U_L = UU_R$, we can go to a frame where M is transformed into a real diagonal matrix diag(λ_1, λ_2,...,λ_{N_f}). Using the relation ln det$D$ = Tr ln$D$, we get the effective action as

$$S_{eff} = N_c \sum_{i=1}^{N_f} \Big(\mathrm{Tr} \ln(i\gamma^\mu \partial_\mu + i\lambda_i) - \frac{1}{g^2 N_c} \lambda_i^2 \int d^4x \Big). \tag{1.19}$$

In the above, we use the notation 'Tr' for trace on space-time and Dirac indices. Clearly, the action is symmetric with respect to interchange of λ_is. Hence, in the absence of accidental degeneracies, the vacuum must be characterised by the same value for all the λ_is. Let us denote this value as R. The equation of motion (gap equation) in R is given by

$$i\mathrm{Tr}\Big\langle \frac{1}{i\gamma^\mu \partial_\mu + iR} \Big\rangle = \frac{2R}{g^2 N_c}. \tag{1.20}$$

The lhs can be computed in momentum space as follows:

$$\begin{aligned} i\mathrm{Tr}\Big\langle \frac{1}{i\gamma^\mu \partial_\mu + iR} \Big\rangle &= i\mathcal{V}_4 \int \frac{d^4k}{(2\pi)^4} \mathrm{Tr}_{\text{spinor}} \frac{\gamma^\mu k_\mu - iR}{k^2 + R^2} \\ &= 4R\mathcal{V}_4 \int \frac{d^4k}{(2\pi)^4} \frac{1}{k^2 + R^2}. \end{aligned} \tag{1.21}$$

The integral can be evaluated by analytically continuing to Euclidean time. Before we do that, recall that NJL model is not renormalisable and requires an explicit UV cutoff. Thus the integral on k in (1.21) should be computed with a cutoff Λ. With this, the gap equation yields

$$R\left(1 - \frac{N_c g^2}{8\pi^2}(\Lambda^2 - R^2 \ln(1 + \frac{\Lambda^2}{R^2}))\right) = 0. \tag{1.22}$$

This has two possible solutions: $R = 0$ and $1 - \frac{R^2}{\Lambda^2}\ln\Big(1 + \frac{\Lambda^2}{R^2}\Big) = \frac{8\pi^2}{\Lambda^2 g^2 N_c}$. The first one corresponds to a vacuum that preserves chiral symmetry and the second one breaks it. However, the second solution exists only when the four-fermi coupling exceeds a critical value g_c given by $g_c^2 N_c = \frac{8\pi^2}{\Lambda^2}$. Further, one

finds that for all values of coupling above g_c, only the second solution is the true vacuum solution. To see this, consider the second derivative of the effective action wrt R. The Euclidean action gives the Hamiltonian up to a sign change. Therefore, in the limit $R \to 0$, the second derivative of energy wrt R is given by

$$\frac{d^2E}{dR^2} = -2\frac{d^2S_{eff}}{dR^2} \tag{1.23}$$

$$= \mathcal{V}_4\Big(\frac{1}{g^2} - \frac{1}{g_c^2}\Big). \tag{1.24}$$

For values of g above the critical value, this expression is negative showing that $R = 0$ is a maximum of energy. Thus, for such values of g, the vacuum with broken chiral symmetry is the true vacuum. For values of g below the critical value, the second derivative is positive and $R = 0$ is the true vacuum.

The breaking of chiral symmetry is associated with massless Goldstone bosons. (The analogs of these in QCD, for $N_f = 2$, are the pions.) In order to demonstrate this, let us consider the NJL action given by (1.16). One can decompose the matrix M as $M = H(x)\exp(ig\pi(x))$ where $H(x)$ is a Hermitian and the exponential is a unitary matrix of rank N_f. The matrix field $\pi(x)$ will turn out to be the field representing the Goldstone boson. Clearly, $\pi(x)$ does not appear in the last term of (1.16). We will now argue that it can also be transformed away from the other non-kinetic term. To see this, consider the following change of variable $q(x) = exp(ig\gamma_5\pi(x)/2)q'(x)$, $H(x) = e^{ig\pi/2}H'e^{-ig\pi/2}$. Under this change of variables, the middle term in (1.16) can be expressed as

$$\begin{aligned}\overline{q}(MP_R + M^\dagger P_L)q &= \overline{q}'e^{ig\gamma_5\pi/2}(He^{ig\pi}P_R + e^{-ig\pi}HP_L)e^{ig\gamma_5\pi/2}q' \\ &= \overline{q}'H'q'.\end{aligned} \tag{1.25}$$

The field $\pi(x)$ is completely removed from this term. However, these now reappear in the first term of (1.16) on re expressing this term in the action in terms of q'. The $\pi(x)$ dependence of the action would now be purely through derivative terms. Thus there can't be any potential term for pions in the effective action and hence they are massless.

Much of the work done in this thesis pertains to a scenario close to NJL model. We study various aspects of chiral symmetry breaking in a string theory model known as Sakai-Sugimoto model that gives rise to a non-local version of NJL model in the low energy, weak coupling limit. The model can also be studied in the strong coupling limit for which one requires the use of the AdS/CFT correspondence. In the following chapter we will present a brief discussion on the correspondence and its working rules.

Chapter 2

AdS/CFT correspondence and holographic QCD

The large-N limit of a field theory is a mean field approximation in which one can study quantum fluctuations as $1/N$ corrections. However, despite this drastic simplification because of large N limit, it has not been possible to exactly identify the mean field in any gauge theory. This is because even in the limit of $N \to \infty$ one is left with an infinite perturbation series in 't Hooft coupling which can be evaluated only to a few orders. In recent years, however, the status has dramatically changed with the emergence of a new tool to study large-N gauge theories at strong coupling: the AdS/CFT correspondence [48]. This has been one of the very important conceptual and technical advances in the subject. Providing a duality with a theory containing gravity, it leads to a dramatic simplification of the problem and allows one to identify the mean fields involved. In many cases, the AdS/CFT correspondence has also aided quantitative study of strongly coupled gauge theories.

The origin of the correspondence dates back to 1997 when Maldacena conjectured a duality between a gauge theory in $(3+1)$-dimensions and a string theory in an $AdS_5 \times S^5$ space-time [48, 49]. This was not the first time that a connection between string theory and a gauge theory was made. In QCD, the phenomenon of confinement has been conjectured to give rise to an electric analog of the standard Meissner effect for magnetic flux in a superconductor [20]. In this dual superconductor, color electric flux lines between quarks and antiquarks arise due to condensation of color magnetic monopoles in the QCD vacuum. This gives rise to effective string like degrees of freedom between quarks and antiquarks. Although, in QCD itself it remains a conjecture, this picture has been verified in a closely related supersymmetric analog of QCD [36]. However, attempts to explain these features using fundamental strings did not meet with success. This is because fundamental strings give rise to a spectrum of particles (like massless spin-2 states) which can not be seen in experiments. This, along with the emergence of QCD as a successful theory of strong interactions shifted the focus of

string theory to Planck scale physics. Slowly it began to emerge as the prime candidate for a quantum theory of gravity. This string theory, also referred to as the theory of fundamental strings, is in a very different context and is based on the assumption that the fundamental particles arise from string-like degrees of freedom. The AdS/CFT correspondence arose from a rather surprising connection between string theories and strongly coupled field theories uncovered in connection with studies of dualities in string theory.

To make the thesis self-contained, in the following, we will briefly review some salient features of the AdS/CFT correspondence and its application to QCD-like theories. Since there are many excellent reviews (e.g. [55]) of the subject available, we will not go into details and will concentrate only on those aspects which are of direct relevance to our work in the thesis.

2.1 The Conjecture

One of the plausibility arguments for a connection between a gauge theory and a string theory is based on large N limit of an SU(N) gauge theory. As mentioned before, the Feynman diagrams in the perturbation series can be arranged into a genus expansion as

$$\sum_{g=0}^{\infty} N^{2-2g} f_g(\lambda). \tag{2.1}$$

In the presence of only adjoint fields, the connected diagrams in the genus expansion are associated with closed surfaces. The leading contribution comes from surfaces of spherical topology and subleading contributions from spheres with one or more 'handles'. This is similar to what one finds in the perturbation series of closed oriented strings if one identifies $1/N$ with the closed string coupling constant. In spite of such indications for a connection, attempts at a derivation by reformulating gauge theory in terms of the gauge-invariant Wilson line operators met with only a limited success and to this date this program remains incomplete (see [52] and references therein).

The work of Maldacena in [48] provided a different handle on this problem. He conjectured that there exists a one to one correspondence between a string theory in $(d+1)$-dimensional space-time and a gauge theory living in the d-dimensional boundary of this bulk space-time. Since it was first proposed various examples of this duality have been constructed and tests have been devised. Perhaps the simplest of these is the original proposal of Maldacena of a duality between $\mathcal{N}=4$ super Yang-Mills theory in 4 space-time dimensions and a string theory in $AdS_5 \times S^5$. The gauge theory arises in the world volume of overlapping $D3$ branes [1] at weak coupling in the decoupling limit, which is defined as the limit in which the string length $l_s \to 0$ keeping the field theory quantities fixed. Strong

[1] An extensive discussion on D-branes can be found in [51].

coupling limit of the same system gives rise to an $AdS_5 \times S^5$ geometry in the near horizon limit. This indicates a connection between the two seemingly different kinds of theories. In the following, we elaborate on this connection.

2.1.1 Overlapping $D3$ branes

D-branes are objects in string theory on which open strings end. A Dp brane, in particular, is a p-dimensional extended object whose excitations are given by open strings with ends fixed on the world volume spanned by the Dp brane. One may also consider a set of overlapping Dp branes. An extensive study of branes and such systems of branes can be found in [51]. We briefly present properties of such a system in this subsection.

Consider a set of N_c overlapping Dp branes. Each open string describing the fluctuations of these branes is associated with two Chan-Paton indices at the ends, each running from 1 to N_c. Effectively, the open string spectrum gives rise to an adjoint representation of U(N_c). The branes can also source closed strings. They have N_c units of charge for a (p+1)-form RR potential. The interaction between D-branes can be studied using interactions between open strings. The D-brane interaction can be treated perturbatively for weak string coupling. For N_c overlapping D-branes, perturbation theory remains valid for $g_s N_c \ll 1$.

In this approximation one may now like to study the system in the low energy limit. In this limit, the brane system gives rise to a U(N_c) gauge theory in $(p+1)$-dimensions with 16 supercharges with the coupling given by $g_s N_c$. The case $p = 3$ is particularly interesting as this gives rise to superconformal field theory in (3 + 1)-dimensions: $\mathcal{N} = 4$ SU(N_c) super Yang-Mills theory [2]. The spectrum consists of gauge fields, six scalars [3] and four spinors, all transforming as adjoint under the SU(N_c) gauge group. This is a CFT with the conformal symmetry group SO(2, 4). There is an $\mathcal{R}$-symmetry group SU(4) that rotates the spinors and scalars among themselves. In all, the theory has a symmetry under the superconformal group SU(2,2|4). One of the key things that makes the theory simple to study is that due to superconformal symmetry the coupling $g_s N_c$ does not get renormalised.

A single D-brane in flat space does not backreact on the geometry strongly since for small string coupling the coupling to gravity is also weak [4]. However, when we consider a very large number of D-branes, the system leads to a significant backreaction if $g_s N_c > 1$. In this case, the system can not be studied perturbatively. However, there exists classical solutions to supergravity theories that arise from string theories in the low energy limit which have properties expected of a system of overlapping

[2] The extra U(1) symmetry in U(N_c) describes only the dynamics of center of mass degree of freedom of the brane system

[3] The six scalars correspond to six directions transverse to the branes along which they can be separated in the 10-dimensional space-time in which string theory lives

[4] mass $\propto 1/g_s$ and Newton's constant $\propto g_s^2$

$D3$ branes. To look at what these solutions are, consider a black hole solution in type II string theory with an electric charge N_c for the same (3+1)-form RR potential as carried by the set of $D3$ branes. In the string frame, the metric and the dilaton of the supergravity solution with the same quantum numbers as that of the brane system are given by

$$\begin{aligned} ds^2 &= -f_-^{-1/2}(\rho) f_+(\rho) dt^2 + f_-^{1/2}(\rho) \sum_{i=1}^{3} dx^{i2} + \frac{1}{f_+(\rho) f_-(\rho)} d\rho^2 + \rho^2 d\omega_5^2, \\ e^{\phi} &= g_s, \quad f_\pm(\rho) = 1 - r_\pm^4/\rho^4. \end{aligned} \tag{2.2}$$

In the above, t, x_i are the physical directions arising from the world volume of the D-branes. The parameters $r_\pm$ are related to the RR charge N_c and the mass per unit volume M as

$$r_+ r_- = \sqrt{4\pi g_s N_c} l_s^2, \quad 5r_+^4 - r_-^4 = 8(2\pi)^8 g_s^2 l_s^8 M. \tag{2.3}$$

There is a horizon at r_+ and a singularity at r_-. The horizon should cover the singularity, i.e. $r_+ \geq r_-$ to ensure that there is no time-like naked singularity. The extremal case, $r_+ = r_-$ is particularly interesting as it preserves one half of the supersymmetries in ten dimensions (16 supercharges). This is similar to what we have in the $D3$ brane system. Defining a new radial coordinate r, by $r^4 = \rho^4 - r_+^4$, the extremal solution looks like

$$\begin{aligned} ds^2 &= H^{-1/2}(r)\left(-dt^2 + \sum_{i=1}^{3} dx^{i2}\right) + H^{1/2}(r)\left(dr^2 + r^2 d\omega_5^2\right), \\ e^{\Phi} &= g_s, \quad H(r) = 1 + r_+^4/r^4, \quad r_+^2 = \sqrt{4\pi g_s N_c} l_s^2. \end{aligned} \tag{2.4}$$

In the new radial coordinate the horizon is at $r = 0$. At this stage we should note that this description requires the supergravity approximation of string theory. This is allowed only when the curvature of the space-time is much smaller than the string scale. This requires $r_+ \gg l_s$ and hence $g_s N_c \gg 1$. We have already learnt that $\mathcal{N} = 4$ super Yang-Mills theory arises from a system of N_c overlapping $D3$ branes in the weak coupling limit ($g_s N_c \ll 1$) at low energies. Here we see a classical solution of the supergravity theory with quantum numbers identical to a system of overlapping N_c $D3$ branes, which is a valid solution only in the semiclassical limit which requires $g_s N_c \gg 1$. [5]

In effect, we may have a completely different looking gravity description in the strong coupling limit of a large-N_c gauge theory. In fact, as we will discuss in the next section, it is the near horizon region of the above geometry that emerges as the dual of the $\mathcal{N} = 4$ super Yang-Mills theory. In the

[5] Also note, to suppress string loop diagrams, the dilaton must be small which requires $g_s \ll 1$. Thus, the strong coupling limit and suppression of string loops together also require $N_c \gg 1$.

near horizon limit ($r \ll r_+$), the metric in (2.4) reduces to

$$ds^2 = \left(\frac{r}{r_+}\right)^2\left(-dt^2 + \sum_{i=1}^{3} dx^{i2}\right) + \left(\frac{r_+}{r}\right)^2 dr^2 + r_+^2 d\omega_5^2. \tag{2.5}$$

This is an $AdS_5 \times S_5$ geometry where both the spaces are of radius r_+. The AdS space has a boundary at $r \to \infty$. (A light ray can travel to $r \to \infty$ in finite time.) The boundary at infinite r can be added to the space and the metric can be written in Poincare coordinate $z = r_+^2/r$ which includes it:

$$ds^2 = \frac{r_+^2}{z^2}\left(-dt^2 + d\vec{x}^2 + dz^2\right) + r_+^2 d\omega_5^2. \tag{2.6}$$

In these coordinates, the boundary of the AdS_5 is at $z = 0$. Further, it is easy to see that the metric is conformally flat near the boundary $z = 0$.

One of the important things to note about the geometry in (2.6) is its isometry group. Clearly, the S^5 in the product space leads to an SO(6) symmetry. The isometries of AdS_5 are most easily seen in the coordinates in which the space is defined as the following hyperbolic surface:

$$X_0^2 + X_5^2 - \sum_{i=1}^{4} X_i^2 = r_+^2. \tag{2.7}$$

The AdS_5 metric is inherited from the flat metric of the underlying space:

$$ds^2 = -dX_0^2 - dX_5^2 + \sum_{i=1}^{4} dX_i^2. \tag{2.8}$$

It can be verified that this gives rise to the AdS_5 metric by comparing with its form in Poincare coordinates in (2.6) using the following substitution:

$$\begin{aligned} X_0 &= \frac{z}{2}\left(1 + \frac{r_+^2 + \vec{x}^2 - t^2}{z^2}\right), \quad X_4 = \frac{z}{2}\left(1 - \frac{r_+^2 - \vec{x}^2 + t^2}{z^2}\right) \\ X_5 &= \frac{r_+}{z}t, \quad X^i = \frac{r_+}{z}x^i \quad \text{for } i = 1, 2, 3. \end{aligned} \tag{2.9}$$

The form in equations (2.7), (2.8) shows that the AdS_5 space has an isometry group SO(2,4). This is also the conformal symmetry group of $\mathcal{N} = 4$ super Yang-Mills theory in (3 + 1)-dimensions. The SO(6) symmetry can also be compared to the $\mathcal{R}$-symmetry in the super Yang-Mills theory. On inclusion of fermions, the isometry of near horizon geometry gets enhanced to SU(2,2|4). This is precisely the super conformal symmetry of the $\mathcal{N} = 4$ super Yang-Mills theory, indicating strongly a connection between these two descriptions of a system of N_c overlapping $D3$ branes.

2.1.2 The duality

In order to understand the duality in our example of overlapping $D3$ branes more precisely, let us compare the two pictures of the system again. In the first picture of overlapping $D3$ branes at weak coupling, one has open strings with ends confined on the branes and closed strings sourced by them propagating in the bulk of (9 + 1)-dimensional space-time. The low energy effective action obtained after integrating out the massive string states is of the form

$$S_{tot} = S_{brane} + S_{bulk} + S_{int}. \tag{2.10}$$

The part S_{brane} is given by the $\mathcal{N}$=4 super Yang-Mills theory and higher derivative corrections coming from integrating out the massive string modes. S_{bulk} is the supergravity action in the bulk plus its higher derivative corrections. S_{int} gives the interaction between the Yang-Mills fields and the supergravity fields, which will also have higher derivative corrections. However, in the decoupling limit (explained below), the rhs of (2.10) essentially reduces to the super Yang-Mills action plus a free supergravity action. Let us see in detail how this happens.

The decoupling limit of the above system is defined as the limit in which $l_s \to 0$ keeping field theory energy scales and Yang-Mills coupling $g_s N_c$ fixed. In this limit Newton's constant $\kappa \sim g_s l_s^4 \to 0$. Therefore, gravity decouples from the Yang-Mills degrees of freedom and gives rise to a free supergravity action. In this limit, the higher derivative corrections to the Yang-Mills part of the action also drop out and S_{brane} reduces to pure $\mathcal{N} = 4$ super Yang-Mills theory. The total effective action is thus given by the sum of two decoupled parts: the $\mathcal{N} = 4$ Yang-Mills action and the free supergravity action.

Let us now study the system using the black 3-brane supergravity solution given by (2.4). Because of the gravitational potential, the energy E_r of a particle at r is redshifted as measured by an observer at infinity since $E_\infty = H^{-1/4}(r)E_r$. If the observer now decides to study the low energy excitations, he will have to study two kinds of modes: the long wavelength (low energy) modes propagating in the bulk and all modes (including short wavelength) propagating in the near horizon region of the geometry which appear redshifted (at $r \to \infty$). In the decoupling limit, the size of the horizon shrinks ($r_+ \to 0$) for a fixed wavelength of the bulk modes. Thus, the interaction between the low energy modes in the bulk and the modes in the near horizon region is also turned off at low energies. One is finally left with two decoupled theories: the bulk super gravity theory in flat space-time and the supergravity theory in the near horizon region given by an $AdS_5 \times S^5$ space-time. Thus, we find that the bulk supergravity theory in flat space-time is a common decoupled part in each of the two descriptions of the system. This strongly motivates us to identify the leftover parts, the $\mathcal{N} = 4$ super-Yang Mills theory with supergravity (type II superstring theory) in $AdS_5 \times S^5$.

AdS/CFT correspondence gives a precise recipe for calculating correlation functions of observables in the gauge theory using the bulk string theory. These bulk calculations get simplified for a large N_c boundary field theory in the strong coupling limit as explained before. To explain the recipe, let us consider a massive scalar field $\phi(z, x)$ in the bulk of AdS_{d+1} space-time whose value in the boundary is given by a field $\phi_0(x)$. AdS/CFT correspondence prescribes a relation between a field in the bulk and a field theory operator in the boundary CFT. Thus, there is some operator $\mathcal{O}$ in the boundary theory which corresponds to the bulk scalar field.

Let us denote the string (or supergravity) partition function for the scalar field $\phi(z, x)$ in the bulk (which becomes $\phi_0(x)$ at the boundary) by $\mathcal{Z}[\phi_0(x)]$. The AdS/CFT correspondence states that

$$\mathcal{Z}[\phi_0(x)] = \left\langle \exp\left(\int_{M^d} \phi_0(x)\mathcal{O}(x) \right) \right\rangle_{CFT}. \tag{2.11}$$

In principle, the *lhs* can be computed independently of the rhs from the string theory propagating in the bulk. In practice, this becomes simple essentially only in the semiclassical supergravity limit in which we can set $\mathcal{Z}[\phi_0(x)] = \exp(-I[\phi_0(x)])$, where $I[\phi_0(x)]$ is the classical onshell action for the field in the bulk with the boundary value given by $\phi_0(x)$. The *rhs* gives the partition function of the boundary theory evaluated after deforming it by a source term for the boundary CFT operator $\mathcal{O}(x)$. It is also clearly the generating function of correlation functions of the boundary operator $\mathcal{O}(x)$. These can be computed by taking appropriate derivatives w.r.t. $\phi_0(x)$.

For our example of scalar field in the bulk, the classical supergravity action can be computed in the following way. Consider the AdS_{d+1} metric in Poincare coordinates given earlier, which we repeat here for convenience

$$ds^2 = \frac{1}{z^2}(\eta_{\mu\nu}dx^\mu dx^\nu + dz^2). \tag{2.12}$$

As explained z is the extra spatial direction and $\eta_{\mu\nu}$ is the d-dimensional boundary (which is approached as $z \to 0$) Minkowski metric in the mostly positive signature. In the above, we have chosen the AdS radius to be unity without any loss of generality. The action for the scalar field with mass m in the bulk AdS space-time is given by

$$I = \int_{AdS} d^{d+1}x \sqrt{g} \left(g^{mn}\partial_m\phi\partial_n\phi + m^2\phi^2 \right), \tag{2.13}$$

where x^m denotes the coordinates (z,x^μ) and g^{mn} is the $AdS_{(d+1)}$ metric in Poincare coordinates. For simplicity, let us consider the x-independent solutions. The z dependence is given by the equation of

motion

$$z^2\partial_z^2\phi + z\partial_z\phi - (m^2 + \frac{d^2}{4})\phi = 0. \tag{2.14}$$

The solutions to the equation of motion has the UV (small z) behaviour given by

$$\phi(z) = \phi_- z^{h_-} + \phi_+ z^{h_+} \tag{2.15}$$

where

$$h_\pm = \frac{d}{2} \pm \frac{1}{2}\sqrt{d^2 + 4m^2}. \tag{2.16}$$

The second term in (2.15) is referred to as the normalisable solution and the first term as the non-normalisable solution. This nomenclature can be understood as follows. Consider the on shell action for the scalar field ϕ. It is given by the boundary term

$$\begin{aligned} S_{o.s.} &= \lim_{z\to 0}\int dz d^d x\, \sqrt{g} g^{zz}\phi\partial_z\phi \\ &= \lim_{z\to 0}\int dz d^d x z^{(1-d)}\phi\partial_z\phi. \end{aligned} \tag{2.17}$$

For the solution containing the ϕ_+ term only the on-shell action is finite. It is in this sense a normalisable solution. The ϕ_- part is non-normalisable whenever $d^2 + 4m^2 > 1$. [6] A non-zero non-normalisable mode is required in the solution whenever the boundary CFT is deformed by the presence of a source term for the operator $\mathcal{O}$ dual to the scalar field. One can now compute the supergravity action for the scalar field (with x-dependence too) and the correlation functions for the operator $\mathcal{O}$. In particular, the two point correlator obtained after regularising the action [7], is given by

$$\langle \mathcal{O}(\vec{x}_1)\mathcal{O}(\vec{x}_2)\rangle = \frac{(2h_+ - d)\Gamma(h_+)}{\pi^{d/2}\Gamma(h_+ - d/2)}\frac{1}{|\vec{x}_1 - \vec{x}_2|^{2h_+}}. \tag{2.18}$$

We see that h_+ gives the conformal dimension of the CFT operator $\mathcal{O}$. This is in conformity with the interpretation of the non-normalisable part of the bulk field as the source for $\mathcal{O}$ since $h_+ + h_- = d$. One can also compute the vev of the operator $\mathcal{O}$:

$$\langle \mathcal{O}(\vec{x})\rangle = (2h_+ - d)\phi_+(\vec{x}), \tag{2.19}$$

where we have now given an $\vec{x}$ dependence to the parameter multiplying the normalisable solution.

[6] When $d^2 + 4m^2 < 1$, both the modes are normalisable and they give two equivalent descriptions of the same CFTs.
[7] Computation requires a careful renormalisation (see [56])

We thus see that there is a connection of the source of the operator in the boundary CFT with the non-normalisable mode of the bulk classical field and that of the *vev* of the boundary operator with the normalisable mode. Although in this example we have considered only scalar fields in the bulk, the duality actually extends to other kinds of fields too. As an example, the stress-energy tensor operator in the boundary CFT is dual to the metric field in the bulk.

One of the very important concepts of the AdS/CFT duality relates to the interpretation of the extra radial direction in the bulk as the energy scale of the boundary field theory and the IR/UV connection between the two dual descriptions. This relation can be motivated from the scaling symmetry of the AdS bulk metric in equation (2.5) (excluding the last term which denotes an S_5) under $(\vec{x} \to \lambda\vec{x}, t \to \lambda t, r \to r/\lambda)$. Since the boundary coordinates and the radial coordinate scale in the opposite way to keep the metric invariant, approaching the boundary of the AdS from the bulk side (which is the IR limit in this description) is equivalent to taking the UV limit in the boundary field theory.

It is well known that UV divergences appear in correlation functions in a quantum field theory. According to AdS/CFT correspondence, UV divergences in the boundary field theory should appear as IR divergences in the gravity theory in bulk. This gives rise to a novel prescription for dealing with boundary field theory divergences through renormalisation of the IR divergences in the bulk. This is called 'Holographic Renormalisation'. In fact, the results for the *vev* of the CFT operator and the two point correlator we quoted above are obtained only after performing a holographic renormalisation. To carry out this procedure one has to isolate the divergent terms of the bulk action at the boundary. One is then required to add boundary covariant counter terms which cancel out these divergences. This has developed into a whole new subject by itself and is beyond the scope of this short review of AdS/CFT correspondence. We refer the interested reader to the detailed analysis given in [57].

2.2 AdS/CFT in QCD

Originally, AdS-CFT correspondence was proposed only for special theories where the string theory lives in a bulk AdS space-time and the boundary field theory is a superconformal field theory. However, the general idea of AdS/CFT correspondence has been extended beyond this and dual pairs have been conjectured for theories with lesser number of supersymmetries and even for non-supersymmetric theories [53]. Gravity duals have also been suggested for QCD like theories. In practice, there are two approaches in applying AdS/CFT correspondence to QCD. In one approach, one starts with QCD and attempts to construct a five-dimensional bulk theory by fitting some of the parameters using QCD itself. This is usually referred to as AdS/QCD. In the other approach, one starts with a basic string theory setup and tries to derive a QCD-like theory using the duality. This

approach is known as holographic QCD.

2.2.1 AdS/QCD

In this approach, we look for a 5D bulk gravity theory with appropriate field content that reproduces the properties of QCD. There have been several attempts at deriving various quantities in QCD using such a setup. One of the first models to study χSB using AdS/QCD was discussed in [54]. In this work, the 5D theory has four free parameters. The number of colors fixes one of them and the other three parameters are fitted using the measured ρ-meson mass, the pion mass and the pion decay constant. Other hadronic properties can then be deduced from the model. For χSB, the important boundary operators are the chiral quark current and the chiral condensate. These are dual to bulk chiral gauge fields and a pseudo-scalar respectively. The space-time chosen is an AdS_5 space with a short distance cutoff (the AdS_5 metric in (2.6) with z cutoff before infinity). The cutoff in the metric provides a scale which is crucial for reproducing properties of a confining gauge theory like QCD. In this space-time one can solve for the classical configurations of the fields. The solutions have parameters which are fixed using the operator-field correspondence and the data on the ρ meson mass, pion mass and pion decay constant. With this, one can calculate various other meson masses and decay constants.

2.2.2 Holographic QCD

As stated earlier, multiple overlapping D-branes realise non-abelian gauge theories in the low energy limit and therefore provide the basic setup to study holographic QCD theories. Flavor degrees of freedom can be also be added to this setup using additional D-branes intersecting the 'color' branes. Below, we will describe earliest models along these lines.

Witten's model

A holographic model for the Yang-Mills part of large N_c QCD was proposed by Witten [50]. At strong coupling, it is provided by the near horizon limit of the supergravity solution (in Type IIA theory) having the quantum numbers of N_c overlapping $D4$ branes, filling the (3 + 1)-dimensional space-time directions x^μ ($\mu = 1, 2, 3$ and 0) and wrapping a circle in the x^4 direction of radius R_k.

At weak coupling and at energies much smaller than the string scale, a set of overlapping $D4$ branes gives rise to gauge fields A_μ, fermions and massless scalars Φ_i, i being the index for directions transverse to the $D4$ branes. All these fields arise from the massless open strings stretching between the $D4$ branes and are in the adjoint representation of U(N_c), giving rise to a (4+1)-dimensional super

Yang-Mills theory with 't Hooft coupling

$$\lambda_5 = (2\pi)^2 g_s l_s N_c. \tag{2.20}$$

If one of the directions x_4 is compactified on S^1 with radius R_k and we impose an antiperiodic boundary condition on the fermions, then all the fermions will become massive with masses of the order of the Kaluza-Klein scale, $1/R_k$. Furthermore, scalars will also acquire masses of the same order from fermion loops. This leaves out only the massless gauge fields at low energy. Supersymmetry is completely broken and at energies much lower than the Kaluza-Klein scale, the theory on the $D4$ branes reduces to a pure U(N_c) Yang-Mills theory in (3 + 1) dimensions.

In the dual bulk picture, the decoupling limit for a set of overlapping $D4$ branes allows us to replace it by the dual geometry. This geometry can be obtained from the type IIA supergravity solution for non-extremal $D4$-branes by making wick rotation of one of Euclidean spatial directions into a time direction. In the near horizon limit, it is given by

$$\begin{aligned} ds^2 &= \left(\frac{U}{R}\right)^{3/2}\left(\eta_{\mu\nu}dx^\mu dx^\nu + f(U)\,(dx^4)^2\right) + \left(\frac{R}{U}\right)^{3/2}\left(\frac{dU^2}{f(U)} + U^2 d\Omega_4^2\right), \\ e^\phi &= g_s\left(\frac{U}{R}\right)^{3/4}, \qquad F_4 = \frac{2\pi N_c}{V_4}\epsilon_4, \qquad f(U) = 1 - \frac{U_k^3}{U^3}, \end{aligned} \tag{2.21}$$

where $\eta_{\mu\nu} = \text{diag}(-1, +1, +1, +1)$ and U_k is a constant parameter of the solution. R is related to the 5-d Yang-Mills coupling by $R^3 = \frac{\lambda_5 \alpha'}{4\pi}$. Also, $d\Omega_4$, ϵ_4 and $V_4 = 8\pi^2/3$ are respectively the line element, the volume form and the volume of a unit S^4.

The above metric has a conical singularity at $U = U_k$ in the $U - x^4$ subspace which can be avoided only if x^4 has a specific periodicity. This condition relates the radius of the circle in the x^4 direction to the parameters of the background as

$$R_k = \frac{2}{3}\left(\frac{R^3}{U_k}\right)^{\frac{1}{2}}. \tag{2.22}$$

For $\lambda_5 >> R_k$ the curvature is small everywhere and so the approximation to a classical gravity background is reliable. Thus, the model presents a setup suitable for studying strongly coupled gauge theories without supersymmetry. Extensive studies of confinement have been carried out in the model by Witten [50] and Gross and Ooguri [64].

An important fact to note is that the the model actually gives rise to the gauge part of a U(N_c) QCD only in the weak coupling regime, i.e., when $\lambda_5 << R_k$. Consider the confinement scale generated

through dimensional transmutation in the effective Yang-Mills theory in (3 + 1) dimensions,

$$\Lambda \sim \frac{1}{\pi R_k} \exp(-48\pi^3 R_k/11\lambda_5). \tag{2.23}$$

In the weak coupling region, it is much smaller than the Kaluza-Klein scale, which is the high energy cut-off for the effective theory. In the strong coupling regime, $\lambda_5 >> R_k$, this relation gives the two scales to be of the same order. Therefore, in this regime there is no separation between the masses of glueballs and Kaluza-Klein states. Since the supergravity regime is obtained precisely in the strong coupling limit, the bulk theory cannot exactly reproduce U(N_c) Yang-Mills. However, one might expect, qualitative features like confinement and χSB, which are easy to study in the strong coupling regime, survive tuning of the dimensionless parameter λ_5/R_k to low values. Another difficulty with the model in the strong coupling limit is that the background solution for the dilaton (hence the string coupling) diverges with U (see (2.21)).

Models with Flavors

So far, our discussion of AdS/CFT correspondence has not included flavors. In the large-N_c limit, $1/N_c$ expansion gets reorganised like a genus expansion in closed string theory. Since the addition of fundamental flavor leads to surfaces with boundaries in the 't Hooft expansion, we expect that we will need to consider open strings in the dual bulk theory. This can be achieved by the addition of branes in the bulk. These branes are referred to as flavor branes. The first work that incorporated flavor branes was due to Karch and Katz [62]. They considered $D3-D7$ system where the overlapping $D3$ branes discussed earlier, realise the gauge theory and $D7$ branes provide flavor degrees of freedom. Flavors were also added to Witten's model in [63] where the authors considered $D6$ flavor branes intersecting the $D4$ system.

In general, one may consider N_f flavor branes intersecting N_c color branes. In the region of their intersection there are massless open strings between the flavor and color branes transforming like fundamentals under both U(N_c) and U(N_f). These provide the fundamental flavor degrees of freedom. One might worry that a holographic treatment of an intersecting brane system will turn out to be immensely difficult even in the supergravity limit. However, if the number of the flavor branes, $N_f \ll N_c$, the backreaction of the flavor branes on the background geometry due to the N_c color branes can be ignored. They can then be considered as probes in the background geometry of the overlapping color branes. With this qualification, the authors of [63] used the DBI action of the a $D6$ probe brane in $D4$ background and showed that the model displays an abelian chiral symmetry breaking and gives rise to a massless Goldstone boson analogous to pion (which corresponds to a massless quark). A more elaborate model due to Sakai and Sugimoto [67] has been extensively studied since this model

exhibits non-abelian χSB. The model involves a set of $D8$ and anti-$D8$ branes intersecting the $D4$ branes in Witten's model. In the strong coupling limit, it gives rise to a holographic description for a QCD-like theory. The model provides a geometrical description for χSB in which, separated $D8$ and anti-$D8$ branes meet each other in Witten's background. It gives rise to states which can be identified with analog of massless pions. In the following, we will elaborate further on this model at appropriate places since it is the core work of this thesis.

Chapter 3

Sakai Sugimoto model and χSB at weak coupling

In this chapter, we intend to study the phenomenon of chiral symmetry breaking (χSB) in the low energy and weak coupling limit of Sakai-Sugimoto model (SS model) [67]. In this limit, the model gives rise to a weakly coupled QCD-like theory and is therefore particularly interesting to study. As we will see in detail, the model provides a one parameter deformation to U(N_c) QCD with N_f flavors, tuning which, it is possible to separate χSB scale from confinement scale making the phenomenon accessible to perturbative methods. This is one of the most important features of the model that allows us to find χSB solutions. In the next section we will give a brief review of the SS model at weak coupling and in the remaining sections of this chapter we will present our work on χSB in the model carried out in [70], giving references to the original literature wherever appropriate.

3.1 SS model at weak coupling

SS model is an intersecting brane model with N_f $D8$ and anti-$D8$ ($\overline{D8}$) branes intersecting the N_c $D4$ branes in Witten's model discussed in the previous chapter (see Figure 3.1). The configuration may also be summarised as below (circles denoting the world volume of branes):

	0	1	2	3	(4)	5	6	7	8	9
D4	∘	∘	∘	∘	∘					
D8-$\overline{D8}$	∘	∘	∘	∘		∘	∘	∘	∘	∘

(3.1)

Here, the direction x^4 is compactified on S_1 and the common (3+1)-dimensional world volume of the flavor and color branes is parametrised by x^μ, $\mu = 0, 1, 2, 3$.

As mentioned in the last chapter, the massless open string spectrum on $D4$ branes in Witten's

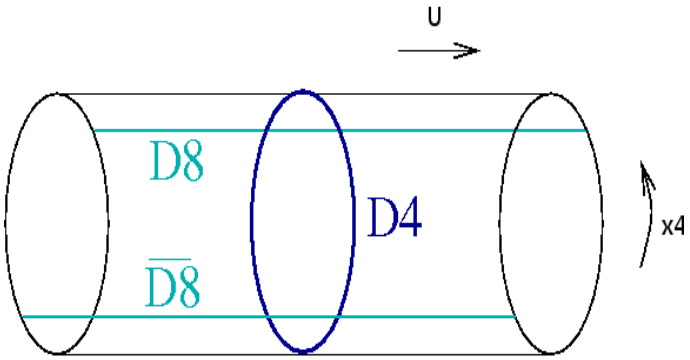

Figure 3.1: The brane configuration in weakly coupled SS model (adapted from [67]).

model leads to the realisation of a U(N_c) gauge theory in (3+1)-dimensions. In SS model, the additional flavor branes ($D8$ and $\overline{D8}$) lead to massless open string states arising from $4-8$ and $4-\overline{8}$ strings living in the common region of intersection with the $D4$ branes. These transform as fundamentals under both the U(N_c) and U(N_f) groups. This is because one of the ends of such strings lies on N_c $D4$ branes and has a Chan-Paton index running from 1 to N_c and the other on $D8$ branes running from 1 to N_f. The Ramond sector states arise, as usual, because the contribution to zero point energy, a_R vanishes. All states in the Neveu-Schwarz sector are massive. This is because the contribution to the zero point energy $a_{NS} = -1/2 + \nu/8 = 1/4$ (in string units), since ν, which denotes the number of Neumann-Dirichlet directions of the intersecting brane system [66], equals 6 for the present system. Thus, the massless sector emerges only from the Ramond sector. Further, the worldsheet fermions can have zero modes only along the directions common to the $D4$-$D8$ or $D4$-$\overline{D8}$ world volume along which the string can be freely moved. These zero modes in the Ramond sector give rise to (3+1)-dimensional space-time fermions. To get the physical states we must impose the GSO projection which leaves fermions of opposite parity arising from $4-8$ strings and $4-\overline{8}$ strings [67]. Without any loss of generality, the former can be identified with left-handed quarks and the latter with right-handed quarks.

The model also gives rise to massless $8-8$ and $\overline{8}-\overline{8}$ open strings. At low energies, they lead to an $(8+1)$-dim super Yang-Mills theory with coupling $g_9^2 = (2\pi)^6 g_s l_s^5$. In the decoupling limit where we take $l_s \to 0$ with λ_5 in equation (2.20) held fixed, g_9 vanishes. Thus, the states arising from the $4-4$, $4-8$ and $4-\overline{8}$ strings are decoupled from the $8-8$ and $\overline{8}-\overline{8}$ states. This allows us to study the model with the low energy spectrum consisting of left-handed fermions q_L, right-handed fermions q_R and color gauge fields only. The left-handed fermions live in the (3+1)-dimensional common world volume of the $D4$ with $D8$ branes and the right-handed fermions in that of $D4$ branes with $\overline{D8}$ branes. These fermions interact with each other through the exchange of $D4$ brane gauge fields A_M, ($M = \mu$,4) living in (4+1) dimensions. At energies much below the Kaluza-Klein scale $1/R_k$, one is left with a

(3+1)-dim U(N_c) QCD-like theory.

3.2 Low energy action

Having motivated the low energy spectrum of the brane system in the weak coupling limit, we can now write down the action that describes the low energy dynamics of the system. Before we do that, it is important to discuss the hierarchy of scales involved in the low energy limit we will be discussing here. The model has the following scales: L, which is the $D8-\overline{D8}$ separation; R_k, which is the radius of the compact S_1; g_5^2, the $D4$ brane gauge coupling which has dimensions of length; and of course the string length l_s. Here, we will be interested in the the hierarchy of scales given by $g_5^2 N_c \ll l_s \ll L \ll R_k$. The condition $l_s \ll L$ allows us to neglect non trivial dilaton and RR fields created by the $D8$ branes [72] while $g_5^2 N_c \ll l_s$ allows us to neglect string loop corrections. Further, as we will see later, the condition $L \ll R_k$ allows us to study χSB perturbatively.

We can now write the low energy action of the weakly coupled SS model as

$$\begin{aligned} S &= -\frac{1}{4g_5^2}\int d^4x \int_0^{2\pi R_k} dx^4\, (F^a_{MN}(x,x^4))^2 + \int d^4x\, q_L^{i\dagger}(x)\bar{\sigma}^\mu\Big(i\partial_\mu + t^a A^a_\mu(x,-L/2)\Big)q_L^i(x) \\ &+ \int d^4x\, q_R^{i\dagger}(x)\sigma^\mu\Big(i\partial_\mu + t^a A^a_\mu(x,L/2)\Big)q_R^i(x), \end{aligned} \tag{3.2}$$

where q_L and q_R denote two-component left-handed and right-handed fermions respectively. The indices μ, ν refer only to the (3+1)-dimensional physical space-time while M, N also include the compact direction x^4. Rest of the indices are the same as in (1.1). The matrices σ^μ have been defined right below equation (1.2). Notice that the gauge fields are in the world volume of $D4$-branes and hence the first term involves an integral over all the five directions. However, the fermions are located at the intersections of the $D4$-$D8$ and the $D4$-$\overline{D8}$ branes. Therefore, the left-handed fermions interact only with $A_\mu(x,-L/2)$ and the right-handed fermions interact only with $A_\mu(x,+L/2)$, where we assume that the $D8$ branes are located at $x^4 = -L/2$ and the $\overline{D8}$ branes at $x^4 = L/2$. We have included the effects of Kaluza-Klein modes which will turn out to be crucial for separating χSB scale from the confining dynamics of QCD. For the given hierarchy of scales, this is the first non-trivial effect away from the extreme low energy limit.

3.3 Non-local NJL model from the $D4-D8-\overline{D8}$ system.

The direction x^4 being compact, the gauge fields $A_M(x,x^4)$ must be periodic in x^4. Hence, the dependence of the $D4$ brane gauge fields on the x^μ and x^4 directions can be separated out using a

Kaluza-Klein expansion given by

$$A_M^q(x,x^4) = A_M^{q(0)}(x) + \sum_{n=1}^{\infty}\Big(A_M^{q(n)}(x)e^{inx^4/R_k} + A_M^{q(n)*}(x)e^{-inx^4/R_k}\Big). \tag{3.3}$$

Using this expression, action (3.2) can be written in terms of the fields in $(3+1)$ dimensions given by the Kaluza-Klein modes in equation (3.3).

In our studies of χSB, we are interested in knowing how q_L and q_R effectively interact with each other. Although there is no explicit coupling between the two in the action, the gauge fields lead to an effective interaction between q_L and q_R. Further, at weak coupling this interaction is primarily mediated by one gauge particle exchange diagrams. Notice that the component $A_4^q(x,x^4)$ does not interact directly with the fermions. Any effective interaction of the fermions with A_4 through A_μ is suppressed in the coupling. Hence, the component $A_4^q(x,x^4)$ can be neglected in the leading order approximation in which we are working.

With the mode expansion (3.3), the action splits into two parts, one purely consisting of the zero mode of the gauge field, its interaction with fermions and the kinetic term of the fermions and the other purely of the non-zero modes of the gauge fields and their interaction with the fermions. We call the first term S_0 and the second S_1 so that,

$$S = S_0 + S_1 \tag{3.4}$$

with

$$S_0 = -\frac{1}{4g_4^2}\int d^4x\,(F_{\mu\nu}^{a(0)}(x))^2 + \int d^4x\,\bar{q}^i(x)\gamma^\mu\Big(i\partial_\mu + t^a A_\mu^{a(0)}(x)\Big)q^i(x), \tag{3.5}$$

where, we have defined the 4-dimensional YM coupling as $g_4^2 = g_5^2/2\pi R_k$. The part S_0 is a QCD-like action in (3+1) dimensions with the YM coupling given by g_4. The second part is given by

$$\begin{aligned} S_1 &= \frac{1}{g_4^2}\sum_{n=1}^{\infty}\int d^4x\Big(-\frac{1}{2}|\partial_\mu A_\nu^{a(n)}(x) - \partial_\nu A_\mu^{a(n)}(x)|^2 + \frac{n^2}{R_k^2}|A_\mu^{a(n)}(x)|^2\Big) \\ &\quad + \sum_{n=1}^{\infty}\int d^4x\Big(J_n^{a\mu*}(x)A_\mu^{a(n)}(x) + J_n^{a\mu}(x)A_\mu^{a(n)*}(x)\Big) \end{aligned} \tag{3.6}$$

with the current $J_n^{a\mu}(x)$ defined as

$$J_n^{a\mu}(x) = \Big(q_L^\dagger(x)\bar{\sigma}^\mu t^a q_L(x)e^{inL/2R_k} + q_R^\dagger(x)\sigma^\mu t^a q_R(x)e^{-inL/2R_k}\Big). \tag{3.7}$$

In writing equation (3.6), we have neglected cubic and quartic interaction terms of the gauge fields.

This is because we are interested in the first non-trivial contribution to the effective interaction between the left-handed and right-handed fermions and this arises from one gauge particle exchange diagrams. In the weak coupling limit, the cubic and quartic interactions give rise to contributions which are higher order in the coupling and therefore smaller. Both S_0 and S_1 need to be considered to get the effective interaction between the left-handed and right-handed fermions.

3.3.1 Fermion effective action from S_1

Let us begin with the computation of the effective interaction between fermions that arises out of S_1 in equation (3.6). The non-zero modes of the gauge fields in S_1 are massive, and in the weak coupling can be easily integrated out to arrive at a fermion effective interaction. For this, it is useful to write the action S_1 in terms of momentum space fields. Putting into (3.6) the Fourier transforms defined through the equations

$$\begin{aligned} A_\mu^{a(n)}(x) &= \int \frac{d^4k}{(2\pi)^4} A_\mu^{a(n)}(k) e^{ik.x} \\ J_{n\mu}^a(x) &= \int \frac{d^4k}{(2\pi)^4} J_{n\mu}^a(k) e^{ik.x}, \end{aligned} \tag{3.8}$$

we get

$$\begin{aligned} S_1 &= \sum_{n=1}^{\infty} \frac{1}{g_4^2} \int \frac{d^4k}{(2\pi)^4} \left\{ -A_\mu^{a(n)}(k) \left(\left(k^2 - \frac{n^2}{R_k^2} \right) \eta^{\mu\nu} - k^\mu k^\nu \right) A_\nu^{a(n)*}(k) \right\} \\ &+ \sum_{n=1}^{\infty} \int \frac{d^4k}{(2\pi)^4} \left(J_n^{a\mu *}(k) A_\mu^{a(n)}(k) + J_n^{a\mu}(k) A_\mu^{a(n)*}(k) \right). \end{aligned} \tag{3.9}$$

Leading interaction between left-handed and right-handed fermions can be obtained from this action simply by substituting classical solution for the gauge field in it. Doing this in the transverse gauge, $k^\mu A_\mu^{a(n)} = 0$, we get the effective interaction. (Of course, the result is gauge invariant.) Using equations (3.7) and (3.8), it can be written as follows:

$$S_{1eff} = 2g_4^2 \sum_{n=1}^{\infty} \int \frac{d^4k}{(2\pi)^4} \frac{\cos(nL/R_k)}{k^2 - n^2/R_k^2} \int d^4x \int d^4y \left(q_{\alpha L}^{\dagger i}(x) \bar{\sigma}^\mu t_{\alpha\beta}^a q_{\beta L}^i(x) \right) \left(q_{\gamma R}^{\dagger j}(y) \sigma^\mu t_{\gamma\delta}^a q_{\delta R}^j(y) \right) e^{ik.(x-y)} + ... \tag{3.10}$$

where the dots indicate interactions among the fermions of the same parity. Since these terms will not contribute to χSB, henceforth they will be dropped in the rest of this chapter. The *rhs* of equation

(3.10) can be further simplified using the Fierz identity[1]

$$\left(q^{\dagger i}_{\alpha L}(x)\,\bar{\sigma}^{\mu}\,q^{i}_{\beta L}(x)\right)\,\left(q^{\dagger j}_{\gamma R}(y)\,\sigma^{\mu}\,q^{j}_{\delta R}(y)\right) = -2\left(q^{\dagger i}_{\alpha L}(x)\,q^{j}_{\delta R}(y)\right)\,\left(q^{\dagger j}_{\gamma R}(y)\,q^{i}_{\beta L}(x)\right), \tag{3.11}$$

and relation among the generators given by

$$t^{a}_{\alpha\beta}\,t^{a}_{\gamma\delta} = \frac{1}{2}\,\delta_{\alpha\delta}\,\delta_{\beta\gamma}. \tag{3.12}$$

This gives

$$S_{1eff} = 2g_4^2\int d^4x\,d^4y\Big(\sum_{n=1}^{\infty}\cos\Big(\frac{nL}{R_k}\Big)\Delta_n(x-y)\Big)[q^{\dagger i}_L(x)q^{j}_R(y)][q^{\dagger j}_R(y)q^{i}_L(x)], \tag{3.13}$$

where the massive propagator is given by

$$\Delta_n(x-y) = -\int\frac{d^4k}{(2\pi)^4}\frac{e^{ik.(x-y)}}{(k^2-n^2/R_k^2)}, \tag{3.14}$$

signifying an exchange of a whole tower of particles of masses $\frac{n}{R_k}$.

The sum in (3.14) can be carried out in the Euclidean momentum space using the identity 1.445.2 given in [90]:

$$\sum_{n=1}^{\infty}\frac{\cos ns}{n^2+a^2} = \frac{\pi}{2a}\frac{\cosh a(\pi-s)}{\sinh\pi a} - \frac{1}{2a^2}. \tag{3.15}$$

The final result we get is

$$S_{1eff} = g_4^2\int d^4x\,d^4y\,G_1(x-y)[q^{\dagger i}_L(x)q^{j}_R(y)][q^{\dagger j}_R(y)q^{i}_L(x)], \tag{3.16}$$

where the propagator G_1 is given by

$$\begin{aligned} G_1(x) &= \int\frac{d^4k}{(2\pi)^4}\,e^{ik.x}\,\tilde{G}_1(k), \\ \tilde{G}_1(k) &= \frac{\pi R_k\cosh\bar{k}(\pi R_k - L)}{\bar{k}\sinh\bar{k}\pi R_k} - \frac{1}{\bar{k}^2}. \end{aligned} \tag{3.17}$$

Here, $\bar{k}^{\mu}$ is the Euclidean continuation of the four momentum k^{μ} and $\bar{k} = \sqrt{-k^2}$. In arriving at equations (3.16), (3.17), we have assumed the weak coupling limit and neglected stringy corrections and have as yet not applied any constraint on the relation between L and R_k (though, of course,

[1]This can be derived from equations (3.77) and (3.80) in [10].

$L \leq \pi R_k$). This is because, we have included the effect of all the Kaluza-Klein modes.

So far, we have considered the effective interaction between the left-handed and right-handed fermions mediated by massive Kaluza-Klein modes of the $D4$ gauge fields. An effective interaction also arises due to the zero modes. Before we go on to study this effect, it is interesting to look at the Euclidean propagator $\tilde{G}_1(k)$ in (3.17) in various limits of parameters. An interesting case arises when we take the non-compact limit, $R_k \to \infty$, with L fixed. In this limit, the propagator can be approximated to

$$\begin{aligned} \tilde{G}_1(k) &\approx \frac{\pi R_k}{\bar{k}} e^{-\bar{k}L} - \frac{1}{\bar{k}^2} \\ &\approx \frac{\pi R_k}{\bar{k}} e^{-\bar{k}L}, \end{aligned} \tag{3.18}$$

where in the last line we have neglected the power law in favour of the exponentially decaying term because the latter has a factor of R_k associated with it. This function reflects a UV cutoff $1/L$ in the limit of infinite R_k. On the other hand, for finite values of R_k, and at momenta much smaller than $1/\pi R_k$ i.e., $\bar{k} \ll 1/\pi R_k$, the Green's function reduces to

$$\begin{aligned} \tilde{G}_1(k) &\approx \frac{\pi R_k}{\bar{k}} e^{-\bar{k}L} \left\{1 + e^{-2(\pi R_k - L)\bar{k}}\right\} \left\{1 - e^{-2\pi R_k \bar{k}}\right\}^{-1} - \frac{1}{\bar{k}^2} \\ &\approx \frac{1}{\bar{k}^2} + \frac{1}{3}\pi^2 R_k^2 - \frac{1}{\bar{k}^2}. \end{aligned} \tag{3.19}$$

Thus, in this limit, the singularity at $\bar{k} = 0$ cancels out between the two terms of $\tilde{G}_1(k)$ and we are left with a constant. This can be understood from the fact that at momenta much lower than the Kaluza-Klein mass, propagator is essentially given by a constant $1/m^2 \sim R_k^2$.

In the other extreme limit given by $\bar{k} \gg 1/L$, which of course also means that $\bar{k} \gg 1/\pi R_k$, $\tilde{G}_1(k)$ has the behaviour

$$\tilde{G}_1(k) \approx \frac{\pi R_k}{\bar{k}} e^{-\bar{k}L} - \frac{1}{\bar{k}^2}. \tag{3.20}$$

The leading behaviour of this Green's function is given by $-\frac{1}{\bar{k}^2}$ since for very large $\bar{k}$, $e^{\bar{k}L} \gg \bar{k}$ (for fixed L and R_k). As we will see in the next subsection, the contribution coming from S_{0eff} to the full effective action cancels this term leaving behind the result for the full Green's function, $\frac{\pi R_k}{\bar{k}} e^{-\bar{k}L}$. This result can be understood as due to an effective UV cutoff on the momentum at $1/L$.

3.3.2 Fermion effective action from S_0

In this subsection we will compute the leading S_0 contribution to the full effective fermion action. We have seen that S_0 is given by a QCD-like action in (3+1) dimensions. Unlike the non-zero modes of the $D4$ gauge field in S_1, $A_\mu^{a(0)}$ is massless and it can not be integrated out in a true sense. Consider, however, a scenario in which the energy scale of chiral symmetry breaking is made much higher than the confinement scale [2]. In this case, to study χSB, we need the effective fermion coupling at energies much above the confinement scale. At such high energies, asymptotic freedom allows a perturbative computation of the effective fermion coupling due to exchange of gauge fields $A_\mu^{a(0)}$. We do this in the following.

Since we wish to study only the effective interaction between the fermions, it suffices to consider the terms in S_0 involving the gauge fields. This can be written as

$$S_{0\ gauge} = -\frac{1}{4g_4^2}\int d^4x\ (F_{\mu\nu}^{a(0)}(x))^2 + \int d^4x J^{a\mu}(x)A_\mu^{a(0)}(x) \tag{3.21}$$

where the current is given by

$$J^{a\mu}(x) = \left(q_L^\dagger(x)\bar{\sigma}^\mu t^a q_L(x) + q_R^\dagger(x)\sigma^\mu t^a q_R(x)\right). \tag{3.22}$$

In the following parts of this subsection, we will drop the superscript (0) in the gauge field by $A_\mu^{a(0)}$ for convenience. Then, using the Fourier transforms

$$\begin{aligned} A_\mu^a(x) &= \int \frac{d^4k}{(2\pi)^4} A_\mu^a(k)e^{ik.x}, \\ J_\mu^a(x) &= \int \frac{d^4k}{(2\pi)^4} J_\mu^a(k)e^{ik.x}, \end{aligned} \tag{3.23}$$

we can write equation (3.21) as

$$S_{0\ gauge} = -\frac{1}{2g_4^2}\int \frac{d^4k}{(2\pi)^4}\ A_\mu^a(-k)\ \left(k^2\eta^{\mu\nu} - k^\mu k^\nu\right)\ A_\nu^a(k) + \int \frac{d^4k}{(2\pi)^4}\ J^{a\mu}(-k)\ A_\mu^a(k). \tag{3.24}$$

Proceeding as in the previous section and using the classical solution for gauge field in (3.24) we get the fermion effective interaction. The result can be written as

$$S_{0\ \text{eff}}^{int} = \frac{g_4^2}{2}\int d^4x\ d^4y\ G_0(x-y)\ J^{a\mu}(x)J_\mu^a(y), \tag{3.25}$$

[2] SS model has an extra parameter L/R_k that can allow this tuning.

where the propagator $G_0(x)$, given by

$$G_0(x) = \int \frac{d^4k}{(2\pi)^4}\tilde{G}_0(k)e^{ik.x}, \tag{3.26}$$

with $\tilde{G}_0(k) = -\frac{1}{k^2}$. This can be seen as coming from one gluon exchange between fermions in the tree level approximation. For Euclidean momenta $\bar{k}^\mu$, this is given by

$$G_0(k) = \frac{1}{\bar{k}^2} \tag{3.27}$$

This justifies the statement made after equation (3.20). As before, using Fierz identity, the full effective fermion action that arises from S_0 is given by

$$\begin{aligned} S_{0\,\text{eff}} &= i\int d^4x \left(q_L^{\dagger i}(x)\,\bar{\sigma}^\mu\,\partial_\mu q_L^i(x) + q_R^{\dagger i}(x)\,\sigma^\mu\,\partial_\mu q_R^i(x)\right) \\ &\quad + g_4^2\int d^4x\,d^4y\,G_0(x-y)\,\left(q_L^{\dagger i}(x)\,q_R^j(y)\right)\left(q_R^{\dagger j}(y)\,q_L^i(x)\right). \end{aligned} \tag{3.28}$$

3.3.3 The 'total' action

Putting the two pieces together, we get the total fermion effective action

$$\begin{aligned} S_{\text{eff}} &= i\int d^4x\left(q_L^{\dagger i}(x)\bar{\sigma}^\mu\partial_\mu q_L^i(x) + q_R^{\dagger i}(x)\sigma^\mu\partial_\mu q_R^i(x)\right) \\ &\quad + g_4^2\int d^4x\,d^4y\,G(x-y)[q_L^{\dagger i}(x)q_R^j(y)][q_R^{\dagger j}(y)q_L^i(x)], \end{aligned} \tag{3.29}$$

where

$$\begin{aligned} G(x) &= \int \frac{d^4k}{(2\pi)^4}\,e^{ik.x}\,\tilde{G}(k), \\ \tilde{G}(k) &= \tilde{G}_0(k) + \tilde{G}_1(k). \end{aligned} \tag{3.30}$$

A rather remarkable thing about the effective fermion action in equation (3.29) is that the four-fermi interaction is non-local. This is in contrast with the usual local four-fermi interaction in the NJL model. This can be understood as follows. The local NJL model is believed to emerge from QCD as an effective theory of quarks at energies of the order of the confinement scale Λ_{QCD}. The range of the interactions in the NJL model for quarks arises from the mass gap due to confinement in QCD. Therefore, at distances of the order of this range, the interaction looks essentially local. Is the non-locality in equation (3.29) relevant to the study of χSB in the present model? As we will show in the following by numerical computations, this model shows χSB at a length scale much smaller than Λ^{-1}. This provides a posteriori justification for retaining the non-locality in (3.29) for the study

of χSB in the present case.

Before we proceed to find χSB solutions, let us summarise the properties of the Green's function $\tilde{G}(k)$. Two regimes can be identified in the momentum space:

- $\bar{k} \gg \Lambda$: In this regime, we have obtained an exact expression for the propagator in the leading order of the coupling which is given by $\tilde{G}(k) = \frac{\pi R_k \cosh \bar{k}(\pi R_k - L)}{k \sinh k\pi R_k}$. Here, two further sub-regimes can be identified as follows :

  i) $\underline{\Lambda \ll \bar{k} \ll 1/\pi R_k}$: $\tilde{G}(k) \sim 1/\bar{k}^2$. In this region, like before, the Kaluza-Klein excitations are too heavy to appear and hence the four-dimensional physics with single gluon exchange at weak coupling is still a good approximation.

  ii)$\underline{\bar{k} \gg 1/\pi R_k}$: $\tilde{G}(k) \sim \pi R_k e^{-\bar{k}L}/\bar{k}$. In this regime, the physics is essentially five-dimensional since the whole tower of Kaluza-Klein modes comes into play. The high momentum cutoff present in the propagator is a reflection of the fact that the five-dimensional propagator is constant $\sim 1/L^3$ for four-dimensional distances much smaller than L.

- $\bar{k} \lesssim \Lambda$: In this regime, the theory is essentially given by a (3+1)-dimensional QCD-like theory and is confining. Our perturbative computation can not capture this physics. To proceed further, therefore, we simply assume that the propagator $\tilde{G}(k)$ essentially becomes a constant of order Λ^{-2} for such momenta. We will give evidence in the following that the precise value of Λ does not matter for determining properties of χSB in the present model. However, the fact of its existence does. It provides an IR cutoff on the interactions between quarks, limiting these to a finite range.

Putting together the two regimes, we can write

$$\begin{aligned} \tilde{G}(k) &= \frac{\pi R_k \cosh \bar{k}(\pi R_k - L)}{k \sinh k\pi R_k}, && \text{for } |\bar{k}| > \Lambda \\ &= \text{constant}, && \text{for } |\bar{k}| \lesssim \Lambda. \end{aligned} \tag{3.31}$$

For practical reasons, it is more convenient to use a smooth functional form for $\tilde{G}(k)$. A function that captures the properties of $\tilde{G}(k)$ in the various regimes discussed above is

$$\tilde{G}(k) = \left(\frac{1 + \pi R_k \bar{k}}{k^2 + \Lambda^2}\right) e^{-\bar{k}L}. \tag{3.32}$$

This is the form we have used for obtaining numerical solutions in this chapter. The solutions obtained using relation (3.31) have the same qualitative behaviour. This is discussed in appendix A.

3.3.4 Non-local NJL action and the chiral bilinear

We have now found a fermion effective action (3.29) arising from the SS model. However, only the dynamics of chiral bilinears of fermions is relevant for studying χSB. For this reason, let us introduce a bosonic auxiliary field $T^{ij}(x,y)$. We can write the action in equation (3.29) in terms of this auxiliary field as

$$\begin{aligned} S_{\text{eff}} &= i\int d^4x\Big(q_L^{\dagger i}(x)\bar{\sigma}^\mu\partial_\mu q_L^i(x)) + q_R^{\dagger i}(x)\sigma^\mu\partial_\mu q_R^i(x)\Big) \\ &\quad + \int d^4x\int d^4y\Big[-\frac{T^{ij*}(x,y)T^{ij}(x,y)}{g_4^2G(x-y)} + T^{ij*}(x,y)q_R^{\dagger j}(y)q_L^i(x) \\ &\qquad + T^{ij}(x,y)q_L^{\dagger i}(x)q_R^j(y)\Big]. \end{aligned} \tag{3.33}$$

This can be easily verified by substituting the equation of motion for the field $T^{ij}(x,y)$[3],

$$T^{ij}(x,y) = g_4^2\, G(x-y)\, q_R^{\dagger j}(y)q_L^i(x). \tag{3.34}$$

To study the dynamics of this bilinear, we can integrate out the fermions and arrive at an effective action for $T^{ij}(x,y)$. To do this, let us first consider the terms in equation (3.33) which contain fermionic fields:

$$\begin{aligned} S^f_{\text{eff}} &= i\int d^4x\Big(q_L^{\dagger i}(x)\bar{\sigma}^\mu\partial_\mu q_L^i(x)) + q_R^{\dagger i}(x)\sigma^\mu\partial_\mu q_R^i(x)\Big) \\ &\quad + \int d^4x\int d^4y\Big[T^{ij*}(x,y)q_R^{\dagger j}(y)q_L^i(x) \\ &\qquad + T^{ij}(x,y)q_L^{\dagger i}(x)q_R^j(y)\Big]. \end{aligned} \tag{3.35}$$

The partition function for this action can be written as

$$\mathcal{Z} = \int \mathcal{D}q\mathcal{D}\overline{q}\exp\left\{i\int d^4x\int d^4y\overline{q}^i(x)\left(i\delta^{ij}\delta^4(x-y)\gamma^\mu\partial_\mu + T^{ij}(x,y)P_R + T^{ij*}(x,y)P_L\right)q^j(y)\right\}. \tag{3.36}$$

Integration of the fermions gives rise to the fermion effective action

$$S^f_{\text{eff}} = N_c\text{Tr}\ln\left(i\delta^{ij}\delta^4(x-y)\gamma^\mu\partial_\mu + T^{ij}(x,y)P_R + T^{ij*}(x,y)P_L\right), \tag{3.37}$$

where we have explicitly written a factor of N_c obtained after integrating out fermions of N_c color degrees of freedom. The notation 'Tr' stands for a trace with respect to flavor degrees of freedom,

[3]Since the field $T^{ij}(x,y)$ appears only to quadratic order, the two forms are equivalent even in the quantum level.

Dirac indices and space-time. The bosonic field can now be broken into the classical and quantum parts: $T^{ij}(x,y) = T^{ij}_{cl}(x,y) + \frac{1}{\sqrt{N_c}} T^{ij}_q(x,y)$. (Since the effective action has an explicit factor of N_c, the factor of $1/\sqrt{N_c}$ with $T^{ij}_q(x,y)$ is required to give it a canonically normalised kinetic term.) In the large N_c limit, the quantum corrections drop out and the dominant part is the classical contribution. For a Poincare invariant vacuum which is also invariant under vector U(N_f) transformation, we should have $T^{ij}_{cl}(x,y) = \delta^{ij} T(|x-y|)$. With this, we can now compute the *rhs* of equation (3.37) and add this to the non-fermionic part of (3.33). We get the total effective action for the function $T(|x|)$ (in Euclidean space-time) as

$$\frac{S^E_{eff}}{VN_cN_f} = \frac{1}{\lambda}\int d^4x \frac{|T(x)|^2}{G^E(x)} - \int \frac{d^4\bar{k}}{(2\pi)^4} \ln\left(1 + \frac{|\tilde{T}(\bar{k})|^2}{\bar{k}^2}\right), \quad \lambda \equiv g_4^2 N_c, \tag{3.38}$$

where $G^E(x)$ is the Green's function in Euclidean space-time derived earlier.

As mentioned earlier, we will carry out the numerical computations using the momentum space (Euclidean) Green's function given by (3.32). The coordinate space Green's function can be written as

$$\begin{aligned} G^E(x) &= \int \frac{d^4\bar{k}}{(2\pi)^4}\tilde{G}(k)e^{-i\bar{k}.x} = \frac{1}{4\pi^2|x|}\int_0^\infty d\bar{k}\bar{k}^2 J_1(\bar{k}|x|)\left(\frac{1+\pi R_k\bar{k}}{\bar{k}^2+\Lambda^2}\right)e^{-\bar{k}L} = \frac{\Lambda^2}{4\pi^2}g(|x|\Lambda), \\ g(r) &\equiv \frac{R_\Lambda}{(L_\Lambda^2+r^2)^{3/2}} + (\cos L_\Lambda + R_\Lambda \sin L_\Lambda)\mathcal{I}_1(r) - (R_\Lambda \cos L_\Lambda - \sin L_\Lambda)\mathcal{I}_2(r), \end{aligned} \tag{3.39}$$

where in writing $g(r)$ we have used a notation in which all length scales with subscript Λ imply dimensionless quantities obtained after a scaling with respect to the confinement length scale Λ^{-1}. Thus R_Λ=$R_k\Lambda$ and L_Λ=$L\Lambda$. Also,

$$\begin{aligned} \mathcal{I}_1(r) &= \int_{L_\Lambda}^\infty ds \frac{\cos s}{(s^2+r^2)^{3/2}} = \frac{K_1(r)}{r} - \int_0^{L_\Lambda} ds \frac{\cos s}{(s^2+r^2)^{3/2}}, \\ \mathcal{I}_2(r) &= \int_{L_\Lambda}^\infty ds \frac{\sin s}{(s^2+r^2)^{3/2}} = \frac{1}{r} - \frac{\pi}{2r}(I_1(r) - \mathbf{L}_1(r)) - \int_0^{L_\Lambda} ds \frac{\sin s}{(s^2+r^2)^{3/2}}, \end{aligned} \tag{3.40}$$

where the functions $K_1(r)$ and $I_1(r)$ are Bessel functions and $\mathbf{L}_1(r)$ is a Struve function [90]. Numerical computation is easier to carry out with $g(r)$ written in terms of these functions and this is what we have used.

We can analytically find the behaviour of $g(r)$ in various regions as in the following. In the region $r \ll R_\Lambda$, it is given by

$$\begin{aligned} g(r) &\approx R_\Lambda/L_\Lambda^3 \quad \text{for} \quad r \ll L_\Lambda, \\ g(r) &\approx R_\Lambda/r^3 \quad \text{for} \quad L_\Lambda \ll r \ll R_\Lambda. \end{aligned} \tag{3.41}$$

This behaviour can be understood as follows. Since the region $r \ll R_\Lambda$ is associated with energies which can probe the Kaluza-Klein scale, the Kaluza-Klein modes must have an impact. Hence, the associated physics must be 5-dimensional. So we expect the propagator to be of the form of a 5-dimensional propagator as above. In the region $r \gg R_\Lambda$, the Green's function should be such that the

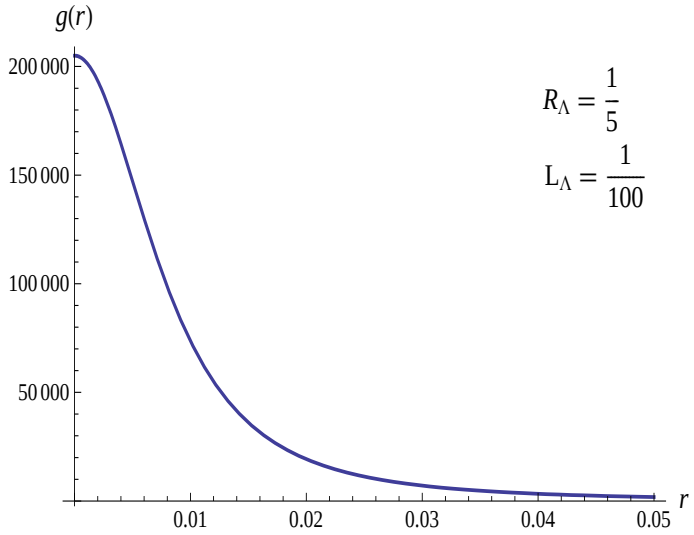

Figure 3.2: Variation of the kernel $g(r)$ with r. The figure shown corresponds to the set $R_\Lambda = 1/5$ and $L_\Lambda = 1/100$.

associated energies can't probe the Kaluza-Klein mass scale. So the 4-dimensional physics is a good approximation. In this region, $g(r)$ is given by

$$\begin{aligned} g(r) &\approx 1/r^2 \text{ for } R_\Lambda \ll r \ll 1, \\ g(r) &\approx \sqrt{\frac{\pi}{2}}\frac{e^{-r}}{r^{3/2}} - 3\frac{R_\Lambda}{r^5} \text{ for } r \gg 1. \end{aligned} \tag{3.42}$$

In the second line of equation (3.42), we have not kept the higher powers of $1/r$ although we have kept the exponentially decaying part. This is because, with a sufficiently small R_Λ, the exponentially decaying part may be significant. In fact, with

$$r \gg 1, \;\; r^{7/2} \gg 3\sqrt{\frac{2}{\pi}} R_\Lambda e^r, \tag{3.43}$$

the exponentially decaying term is dominant over the other. Thus, there is a region in r in which $g(r)$ is essentially exponentially decaying. For even larger values of r, however, the power law takes over. Because of the negative sign of the power law term, $g(r)$ can be negative for sufficiently large r. In fact, we see this in numerical computation. This is, presumably, an artifact of the choice of $\tilde{G}(k)$ that we made in (3.32). Physically we expect the Green's function to die-off exponentially beyond the confinement length scale. We will, therefore, assume this and impose a cutoff r_{max} on $g(r)$ beyond

which it will be set to zero. The cutoff r_{max} required becomes smaller as we increase R_Λ. Figure 3.2 shows the variation of $g(r)$ with r for a particular set of values $R_\Lambda = 1/5, L_\Lambda = 1/100$.

3.4 Chiral symmetry breaking

Let us now proceed to study chiral symmetry breaking in the non-local NJL action (3.38). A dynamical breaking of chiral symmetry gives rise to a non-zero vev of the chiral bilinear of fermions. As mentioned before, equation (3.34) then implies a non-trivial classical value for the bosonic field $T^{\alpha\beta}(x)$. In the limit of large N_c, one can ignore the quantum fluctuations of the bosonic fields. Therefore, its classical value can be obtained by solving its equation of motion, called the gap equation, which in momentum space is given by

$$\tilde{\phi}(k) = \frac{\tilde{T}(k)}{k^2 + |\tilde{T}(k)|^2}, \tag{3.44}$$

where $\tilde{\phi}(k)$ is the Fourier transform of $\phi(x)$ which is defined through

$$T(x) = 4\pi^2 \lambda G^E(x)\phi(x). \tag{3.45}$$

As can be seen using equation (3.34), $\phi(x)$ is the quark condensate,

$$\phi(x) = \frac{1}{N_c}\langle q_L^{\dagger\alpha}(x) q_R^{\alpha}(0)\rangle. \tag{3.46}$$

The field $\phi(x)$ is of mass dimension 3. Introducing a length scale l (as we will see later, this will turn out to be the χSB length scale), this fact may be expressed explicitly by writing $\phi(x)$ as follows:

$$\phi(x) = \frac{\phi_0}{4\pi^2 l^3}\varphi(|x|/l). \tag{3.47}$$

The field $\varphi(|x|/l)$ is dimensionless. We have introduced a normalisation factor $\phi_0/4\pi^2$ for later convenience. We can now find the Fourier transforms:

$$\begin{aligned}
&\tilde{\phi}(k) = l\phi_0 f(kl),\ f(p) \equiv \frac{1}{p}\int_0^\infty dy y^2 J_1(py)\varphi(y),\\
&\tilde{T}(k) = \lambda l\Lambda^2\phi_0 t(kl),\ t(p) \equiv \frac{1}{p}\int_0^\infty dy y^2 J_1(py) g(l_\Lambda y)\varphi(y),
\end{aligned} \tag{3.48}$$

where $f(kl)$ and $t(kl)$ are dimensionless. Also note that $l_\Lambda \equiv l\Lambda$. With this, the gap equation (3.44) can be expressed as

$$f(p) = \frac{\bar{\lambda} t(p)}{p^2 + \bar{\lambda}^2 \phi_0^2 t(p)^2} \equiv f_T(p), \quad \bar{\lambda} \equiv \lambda l_\Lambda. \tag{3.49}$$

All quantities appearing in this equation are dimensionless. We also notice that the cutoff Λ does not explicitly appear in the equation after we have used it to scale out various other dimensionful parameters.

3.4.1 Numerical solutions of the gap equation

Since equation (3.49) is non-linear, it is difficult to solve it analytically and we must resort to a numerical approach. However, we can make general observations in some limiting cases analytically. It can be seen from equation (3.48) that $t(p)$ gets a significant contribution only from the region $y \lesssim 1/l_\Lambda$ since $g(l_\Lambda y)$ decays exponentially beyond this region. Thus, for $p \ll l_\Lambda$, the Bessel function inside the integral is essentially linear in the argument. Therefore, for small enough values of p, $t(p)$ goes to a constant. In this limit then, the second term in the denominator of the *rhs* of (3.49) dominates, so that this equation becomes

$$f(p) \approx \frac{1}{\lambda \phi_0^2} \frac{1}{t(p)}, \tag{3.50}$$

which implies $f(p)t(p) \to$ constant for $p \to 0$. On the other hand, for very large values of p, the first term in the denominator of the *rhs* of (3.49) dominates. This is because $t(p)$ remains finite in the limit of $p \to \infty$. Therefore, in this limit the gap equation becomes

$$f(p) \approx \frac{\bar{\lambda} t(p)}{p^2}. \tag{3.51}$$

As we will see, numerical computations provide evidence for (3.50) and (3.51) in the two limits.

In order to solve the gap equation (3.49) numerically, we start with an ansatz for the solution given by

$$\varphi(r) = \frac{\exp(-r)}{(c^2 r^2 + 1)^\sigma}. \tag{3.52}$$

This form is motivated by the fact that the condensate must go to a constant at small distances and vanish beyond a certain length scale. We then adopt the following procedure. We choose values for the parameters R_Λ and L_Λ[4] consistent with the constraint $L_\Lambda \ll R_\Lambda \ll 1$. With this, we need to look

[4]This corresponds to a particular brane configuration.

for a solution with a set of values of the parameters l_Λ, ϕ_0, σ and c for different values of λ. It turns out, as we will explain later, that it is easier to fix l_Λ to a given value and then look for the set of values of $\bar{\lambda}$, ϕ_0, σ and c that would solve the equation. For this, we compute the difference of the *lhs* and the *rhs* of equation (3.49). We try to find values of the parameters $\bar{\lambda}$, ϕ_0, c and σ such that the ratio

$$\rho = \left(\int_0^\infty dp |f(p) - f_T(p)|^2 \right) / \int_0^\infty dp |f(p)|^2 \tag{3.53}$$

is minimised. We find that the value of c that gives the best fit always turns out to be l_Λ / L_Λ. This set of values (along with l_Λ) provides the χSB solution to equation (3.49) for the corresponding value of λ. This exercise is then repeated for various values of l_Λ.

We have carried out the numerical computations using 'Mathematica'. The equation solving essentially involves two parts. One is the computation of $f(p)$ and $t(p)$ using equation (3.48) and the ansatz (3.52), and the other is the minimisation of ρ. The first step involves numerical integration and is more computationally expensive than the second step. Computation of $t(p)$ depends on l_Λ whereas the parameters $\bar{\lambda}$ and ϕ_0 appear only in the second step. Therefore, it is numerically easier to choose a particular value of l_Λ and then adjust $\bar{\lambda}$ and ϕ_0 to minimise the value of ρ instead of choosing a value for $\bar{\lambda}$ and then trying to find the correct l_Λ and other parameters.

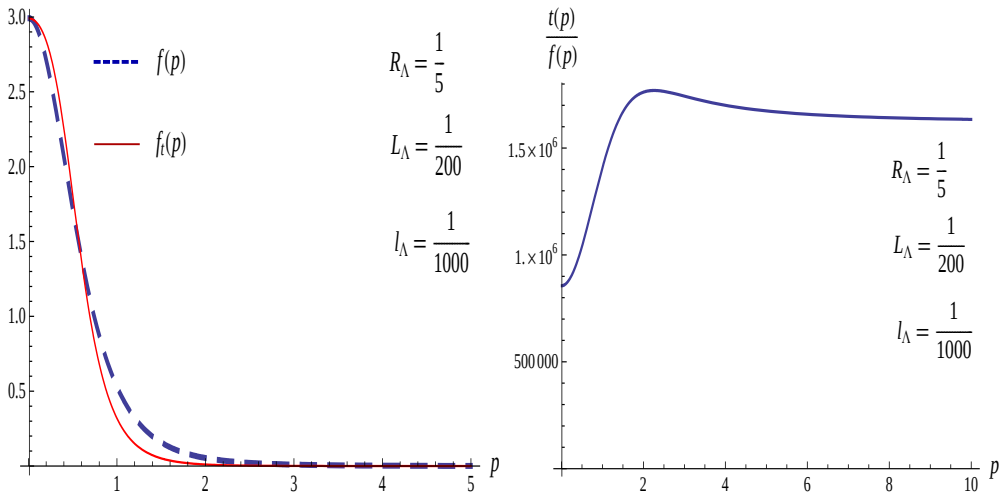

Figure 3.3: The first figure shows that there is no good matching between $f(p)$ and $f_T(p)$ for $l_\Lambda \ll L_\Lambda$ and the second shows that the ratio t(p)/f(p) becomes a constant which is impossible for a solution to the gap equation.

Before we discuss the numerical χSB solutions in detail, it is worthwhile pointing out a few important features of the solutions:

- Using equation (3.48) we can see that $t(p)$ gets a significant contribution only in the region $y \lesssim 1$ since $\varphi(y)$ decays exponentially beyond this region. Now let us look at the parameter regime with $l_\Lambda \lesssim L_\Lambda$. In this regime $g(l_\Lambda y)$ is essentially a constant because $g(r)$ is a constant for $r \lesssim L_\Lambda$

as can be seen from (3.41). Thus, $t(p) \propto f(p)$ and hence the gap equation (3.49) can not be satisfied. We conclude that there are no χSB solutions with $l_\Lambda \lesssim L_\Lambda$. Numerical computations confirm this as can be seen from Figure 3.3 which shows the best fit for a particular value of the parameters. The fit is clearly poor.

- Since χSB solutions exist only in the parameter regime $l_\Lambda \gtrsim L_\Lambda$, it follows that if we want χSB length scale to be much smaller than the confinement scale (as we have assumed in our derivation of the effective model) we must have $L_\Lambda \ll 1$. This can be attained by appropriately tuning L/R_k keeping the coupling λ fixed.

- Just like the local NJL model, it turns out that in the present case also there is a critical value of the coupling below which there is no χSB. This happens for $l_\Lambda \gtrsim 1$. We will see numerical evidence for this in the following subsection. This phenomenon can be understood as follows. In this parameter regime the non-local NJL model can essentially be approximated as a local NJL model[5] which is known to have a critical coupling for χSB. However, note that the near critical regime corresponds to a region where a perturbative treatment of the underlying gauge theory is not trustworthy.

3.4.2 Numerical results

Let us now discuss the best fit numerical χSB solutions of the gap equation in the parameter regime $l_\Lambda \gtrsim L_\Lambda$. As mentioned earlier, we choose a set of values for R_Λ and L_Λ consistent with the constraint $L_\Lambda \ll R_\Lambda \ll 1$ and then obtain the values for σ, λ and $\phi_{00} \equiv (\bar{\lambda}\phi_0)^2$ for each value of l_Λ that are consistent with the gap equation. Consider the set R_Λ=1/5, L_Λ=1/100. Table 3.1 lists all the parameters involved in the numerical solutions for this set for different values of the coupling λ. In order to show the numerical agreement, we provide figures for two representative values of l_Λ showing the fit between $f(p)$ and $f_T(p)$. Figure 3.4 shows the fits obtained for the values l_Λ= 1/10, 1. Numerical calculations also show that the UV behaviour of the solution is given by $t(p) \propto p^2 f(p)$ as derived analytically. This can be easily seen from Figure 3.5 where we plot the ratio $p^2 f(p)/t(p)$. The left panel of Figure 3.6 shows the variation of l_Λ with λ. We find that as we decrease λ from a large value, l_Λ slowly increases until it reaches a 'knee' where it rapidly starts increasing and hits a 'wall', an artifact of a critical coupling λ_c below which there is no χSB. This happens around $l_\Lambda = 1$. After that, the curve slowly turns back indicating two possible solutions for each λ. A more detailed investigation of this feature requires considerably longer computation time but is clearly desirable. It

[5]This can be understood by looking at the behaviour of the Green's function $G^E(x)$ in (3.39). Since $g(r)$ vanishes exponentially for $r \gtrsim 1$, $G^E(x)$ vanishes exponentially for $|x| \gtrsim l$ in the region $l_\Lambda \gtrsim 1$. Therefore, the Green's function essentially looks like a Dirac delta function at distances of the order or greater than the χSB length scale and hence approximates a local NJL model.

turns out that as we increase the value of l_Λ, the energy of the solution increases as shown in the right panel of Figure 3.6. This implies that among the two solutions for the same value of λ, the one with lower value of l_Λ is preferred.

Before we close this section, we would like to mention that we have obtained χSB solutions for multiple sets of values of R_Λ and L_Λ. All these solutions share the same qualitative features. For the sake of comparison, we provide the data and figures for two other sets $\{R_\Lambda$=1/20, L_Λ=1/300$\}$ and $\{R_\Lambda$=1/5, L_Λ=1/200$\}$ in the *list of tables and figures* at the end of this chapter.

R_Λ=1/5		L_Λ=1/100	
l_λ	σ	λ	ϕ_{00}
1/100	0.005	0.31266l	3.3538×10^{-10}
3/200	0.250	0.28873	5.6739×10^{-9}
3/100	0.500	0.2570	8.6961×10^{-7}
3/50	0.650	0.2363	0.00017609
1/10	0.730	0.2135	0.0097973
1/4	0.800	0.1988	12.5067
3/5	0.835	0.1972	12176.4
4/5	0.845	0.1983	121168
1	0.853	0.1969	724447
8/5	0.870	0.1944	3.2694×10^{7}
5/2	0.880	0.1976	1.1888×10^{9}
4	0.888	0.2031	5.2297×10^{10}
5	0.890	0.2085	3.1255×10^{11}

Table 3.1: Table of parameters for the solution to gap equation for the set R_Λ=1/5 and L_Λ=1/100.

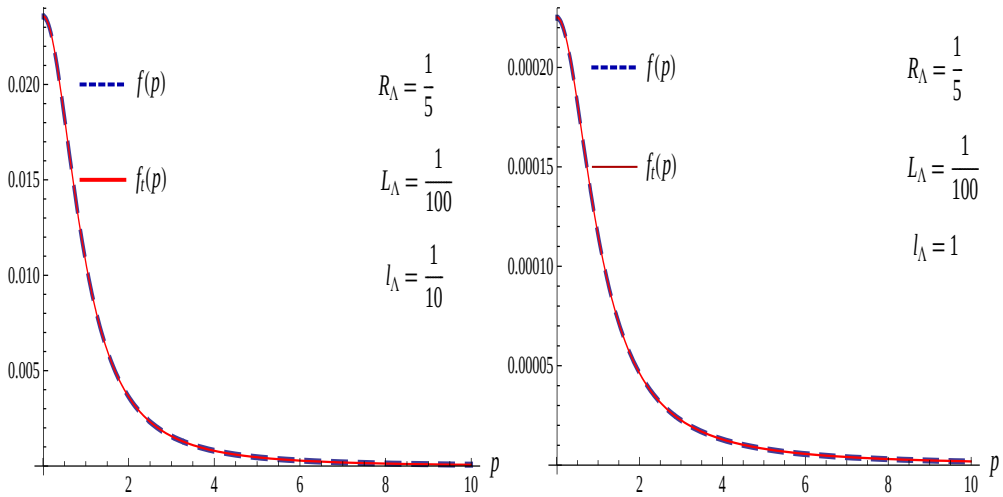

Figure 3.4: Fits between $f(p)$ and $f_T(p)$ for two different values of l_Λ with R_Λ=1/5 and L_Λ=1/100 corresponding to the data in Table 3.1.

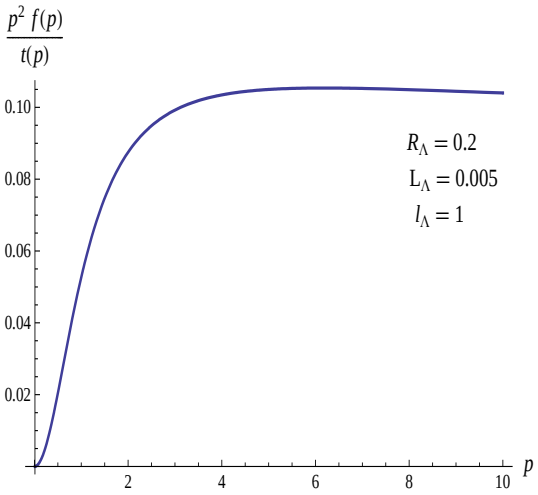

Figure 3.5: Plot to demonstrate the UV behaviour of the solution

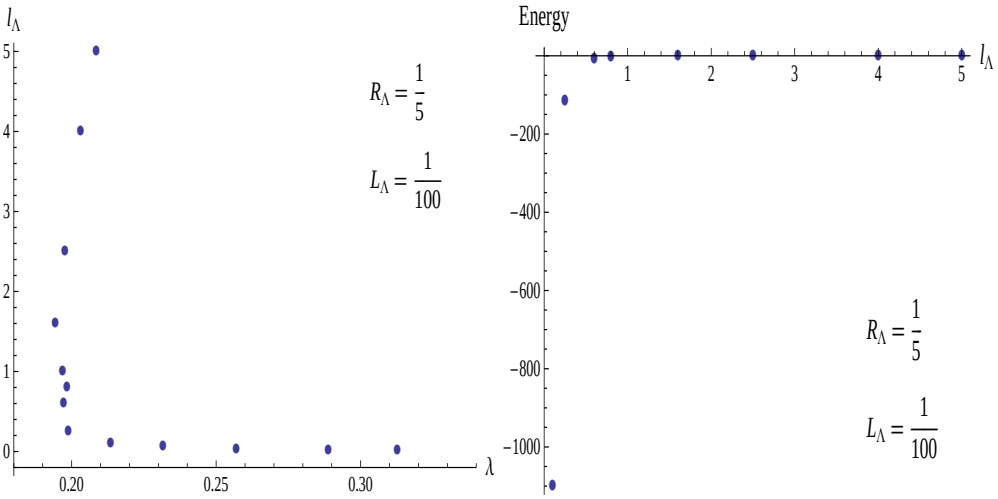

Figure 3.6: Left: Variation of l_Λ with λ for the set R_Λ=1/5, L_Λ=1/100; Right: Energy variation with l_Λ

3.5 The non-compact limit

Till now, we have considered a finite value for R_k that leads to a non-local NJL action with an effective (3+1)-dimensional 't Hooft coupling λ. We have presented strong numerical evidence that this theory has a critical value λ_c below which there is no dynamical breaking of chiral symmetry. We will now try to find out what happens when one takes a non-compact limit ($R_k \to \infty$). In order to keep intact the vital assumptions made in our computation of χSB solutions in this model, we must maintain the hierarchy of scales $L \ll R_k \ll \Lambda^{-1}$ as we take the non-compact limit. To incorporate confinement in this model, we would also like to use the relation among the quantities Λ, R_k and g_4^2 (hence g_5^2) as given by (2.23). If we define $\exp\left(-\frac{2\pi R_k}{\beta_0 g_5^2}\right)$ as b then with a scale transformation $R_k \to \eta R_k$, we get

$b \to b^\eta$. Further, equation (2.23) leads to a scaling of Λ such that $R_\Lambda \to R_\Lambda^\eta$. Since we are keeping L fixed as we take the non-compact limit, L_Λ scales as $L_\Lambda \to L_\Lambda R_\Lambda^{\eta-1}/\eta$. The model can now be studied in the non-compact limit by taking the $\eta \to \infty$ limit of the compact model.

From our numerical study of the compact case we have seen that there is a critical value of the coupling below which there is no χSB. This critical value is achieved for $l_\Lambda \approx 1$. We now wish to find what happens to λ_c as we take the non-compact limit. In order to carry out this exercise we begin with an initial set of values of R_Λ and L_Λ and find the value of λ_c and the corresponding χSB solution. We then try to find how this solution evolves as one approaches the non-compact limit by scaling R_Λ and L_Λ using the scale factor η as mentioned above. As we decrease $1/\eta$ from η=1, the value of λ_c starts decreasing linearly. Such a linear behaviour would give rise to a finite critical value for the 5-dimensional 't Hooft coupling. However, on further increasing η, we find that the linear behaviour is not satisfied any more. Rather the curve actually bends and apparently approaches a constant value, which would imply that the critical value of the 5-dimensional 't Hooft coupling blows up in the limit $\eta \to \infty$, leading to no sensible result. We present an example in which we choose the initial set of values, R_Λ=1/2 and L_Λ=1/100. The evolution of the χSB solution (corresponding to the critical coupling) with the scaling η has been tabulated in Table 3.2. Figure 3.7 shows the variation of the critical coupling with the scaling parameter η.

Initial R_Λ=1/2		Initial L_Λ=1/100	
η	σ	λ_c	ϕ_{00}
1.0	0.871	0.084302	1.5834×10^5
1.5	0.881	0.061379	1.6846×10^6
2.0	0.885	0.050870	1.1915×10^7
2.4	0.888	0.045603	5.2653×10^7
2.8	0.889	0.042359	2.1624×10^8
3.0	0.890	0.040758	4.3096×10^8
3.3	0.890	0.039170	1.1719×10^9
3.5	0.891	0.037928	2.2875×10^9
4.0	0.891	0.036500	9.8027×10^{10}
4.5	0.892	0.035382	5.9672×10^{10}
5.0	0.891	0.035535	2.9431×10^{11}
5.5	0.892	0.035071	1.4229×10^{12}
6.0	0.892	0.035423	6.7879×10^{12}

Table 3.2: Table of parameters for the solution to the gap equation with l_Λ=1 and initial R_Λ=1/2 and initial L_Λ=1/100

In the above approach to the non-compact limit, we have maintained the relation between scales implied by (2.23). However, since NJL model is a non-renormalisable model, it might be suitable to relax this condition. Nevertheless, we still want to maintain the hierarchy of scales $L \ll \pi R_k \ll \Lambda^{-1}$. A simple way to do this is to keep R_Λ fixed at a value much smaller than 1 and then take L_Λ to zero.

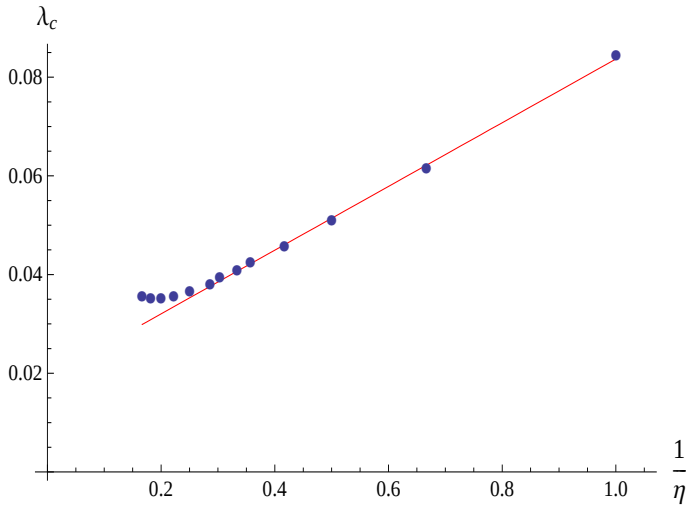

Figure 3.7: Variation of λ_c with $1/\eta$ for the set with starting values of R_Λ=1/2, L_Λ=1/100 corresponding to Table 3.2.

This corresponds to the scaling $R_k \to \eta R_k$, $\Lambda \to \Lambda/\eta$ so that, for a fixed L, $L_\Lambda \to L_\Lambda/\eta$. As above, here also we study the evolution of the critical coupling with the scale factor as we take the non-compact limit. In this case also we find that the 5-dimensional critical coupling blows up in the non-compact limit and hence this way of taking the non-compact limit also does not lead to a sensible result. We present an explicit example where the initial set of values are set to R_Λ=1/5 and L_Λ=3/200 . Figure 3.8 shows the variation of λ_c with the scaling parameter. The curve actually fits with the behaviour $\lambda_c = 0.271339/\eta^{0.817788}$ leading the 5-dimensional critical coupling to blow up in the non-compact limit. Thus, in both these ways of approaching the non-compact limit we have ended up unsuccessful. This may be an indication that there are no consistent χSB solutions in the non-compact limit of this model. This clears up a confusion in the treatment of χSB in [72] and indicates why the corresponding gap equation might not actually have any χSB solution.

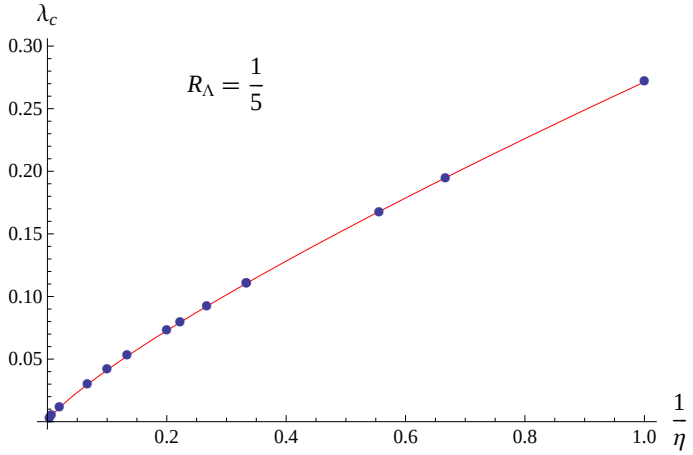

Figure 3.8: Variation of λ_c with $1/\eta$ for the set with starting values of R_Λ=1/5, L_Λ=3/200

3.6 Summary

The study of χSB in QCD is made complicated by the fact that the scale at which chiral symmetry is broken is of the order of the confinement scale. If QCD could be deformed to enable "tuning" of the χSB scale to be much smaller than the confinement scale, then one would have separated the complications of the dynamics of confinement from a study of χSB, which could then be handled by perturbative methods. The intersecting brane configuration of Sakai and Sugimoto, which gives rise to a QCD-like theory at low energies, admits just such a possibility; it has an additional parameter, the flavour brane-anti-brane separation, which can be tuned.

In this chapter, we have discussed the weakly coupled SS model in the low energy limit. For any finite radius R_k of the circle which the colour $D4$-branes wrap, there is confinement and a mass gap in the low energy theory. The interaction between the flavor branes can be described in terms of a non-local NJL model whose behaviour can be derived exactly at energies higher than the confinement scale. If the energy scale of χSB is also large, it allows one to study the phenomenon perturbatively. The NJL model reflects the confinement scale, Λ, in the length scale over which the non-local four-fermi interaction extends. The fact that this range is finite turns out to be crucial in getting consistent χSB solutions. In the large N_c limit, the question of χSB amounts to finding appropriate solutions to the non-linear gap equation. For solutions with χSB length scale l much larger than the confinement scale Λ^{-1}, it is reasonable to replace the non-local NJL model by the local NJL model. Hence these solutions must reveal the existence of a critical coupling, which is known to determine χSB in the local NJL model. In this work we have numerically solved the non-linear gap equation and verified the existence of a critical coupling below which chiral symmetry is unbroken. Roughly speaking, only solutions with χSB scale greater than the brane-anti-brane separation L exist. The χSB scale l increases as the 't Hooft coupling is decreased, until a critical value is reached for $l \sim \Lambda^{-1}$. Solutions with $l > \Lambda^{-1}$ do not lead to any further decrease in the coupling.

Our analysis is valid for any finite value of the radius R_k, which may be large. We have briefly addressed the question of what happens when $R_k \to \infty$. Two different ways of taking this limit, each one obtained from a well-motivated one-parameter scaling of the parameters of the SS model, were discussed. We found from our numerical data that neither of them leads to a sensible limit. The tentative conclusion is that simple ways of implementing this limit do not lead to a consistent picture of χSB in the non-compact version of the non-local NJL model. This seems to reinforce the critical role that the confinement scale plays in the compact model; the infrared cut-off provided by it enables the existence of consistent solutions to the gap equation. However, more work needs to be done to clarify this issue further.

Finally, most of the calculations reported in this chapter were done numerically because the gap equation is non-linear and we could not solve it analytically. It would, however, be useful to have

some analytic handle on the calculations, especially in the parameter region near the critical coupling. This could be important for a better understanding of the non-compact limit. A possible hint in this respect is the fact that excellent numerical solutions were obtained using the ansatz (3.52), with the constant c turning out to be almost exactly equal to l/L in all cases.

List of tables and figures

R_Λ=1/20, L_Λ=1/300				R_Λ=1/5, L_Λ=1/200			
l_λ	σ	λ	ϕ_{00}	l_λ	σ	λ	ϕ_{00}
1/300	0.01	0.40707	7.167×10^{-12}	1/1000	0.005	0.5	6.512×10^{-14}
2/300	0.27	0.3737	5.531×10^{-10}	1/200	0.01	0.16156	5.7492×10^{-12}
1/100	0.50	0.3336	1.792×10^{-10}	1/100	0.430	0.13945	9.98934×10^{-10}
4/100	0.7	0.28772	0.0005542	1/50	0.620	0.12410	1.76125×10^{-7}
1/10	0.775	0.268637	0.73002	3/50	0.765	0.10902	0.0008285
1/4	0.808	0.27007	893.65	1/10	0.810	0.10382	0.048126
3/5	0.833	0.27417	882330	1/4	0.850	0.10064	66.118
1	0.849	0.27274	5.3738×10^{7}	3/5	0.870	0.10382	67550.4
8/5	0.863	0.27094	2.4385×10^{9}	1	0.885	0.10302	4.1827×10^{6}
5/2	0.875	0.27013	9.29622×10^{10}	8/5	0.892	0.10583	1.797×10^{8}
4	0.886	0.26933	4.3044×10^{12}	5/2	0.890	0.11559	6.0005×10^{9}
5	0.889	0.27257	2.5899×10^{19}	5	0.890	0.12620	1.786×10^{12}

Table 3.3: Table of parameters for the solution to gap equation for the sets {R_Λ=1/20, L_Λ=1/300} and {R_Λ=1/5, L_Λ=1/200}

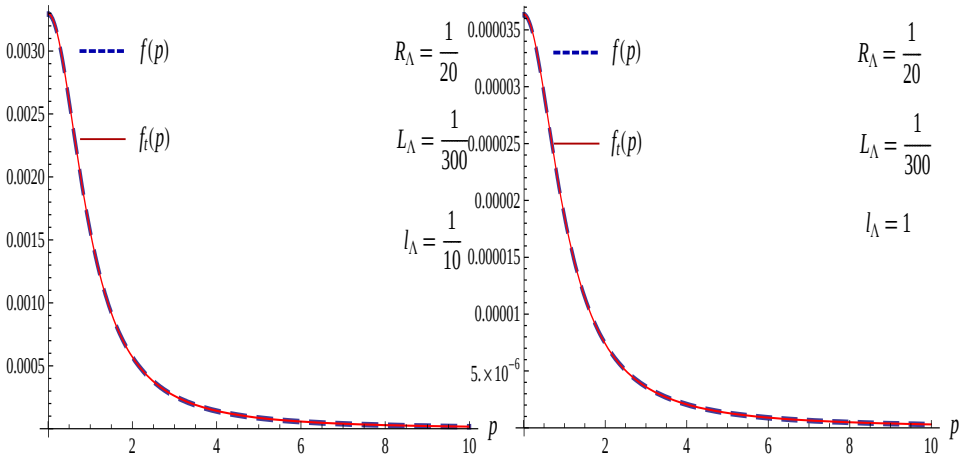

Figure 3.9: Fits between $f(p)$ and $f_T(p)$ for two different values of l_Λ with R_Λ=1/20 and L_Λ=1/300

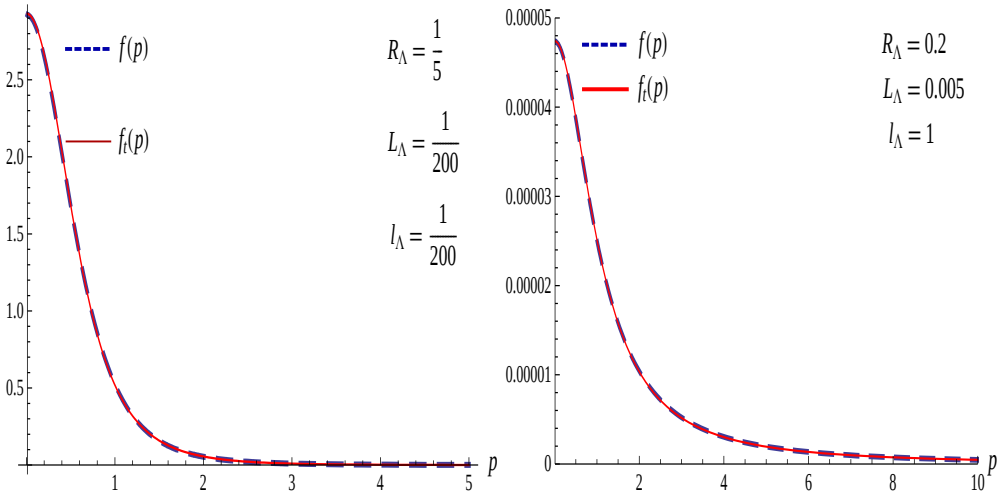

Figure 3.10: Fits between $f(p)$ and $f_T(p)$ for two different values of l_Λ with R_Λ=1/5 and L_Λ=1/200

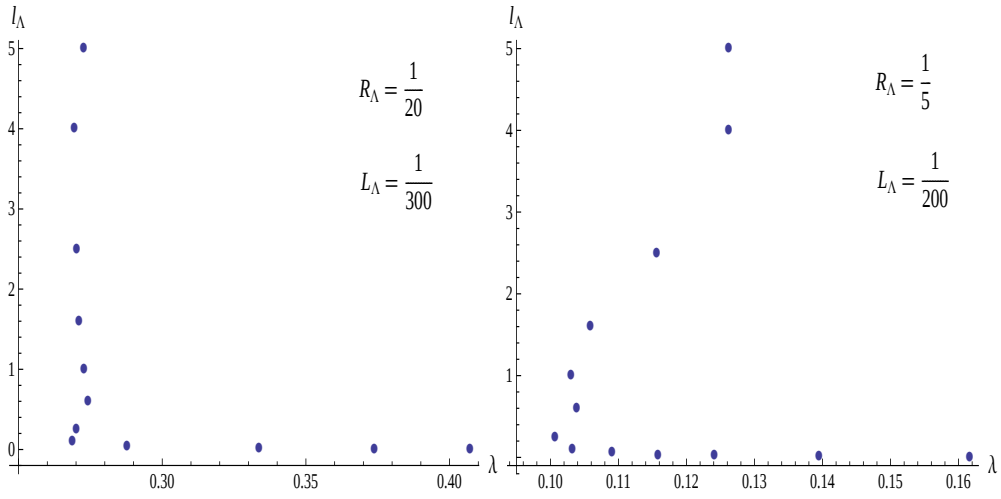

Figure 3.11: Variation of l_Λ with λ for the sets {R_Λ=1/20, L_Λ=1/300} and {R_Λ=1/5, L_Λ=1/200}

Chapter 4

A review of Sakai-Sugimoto model at strong coupling

In the previous chapter, we have discussed aspects of χSB in the weakly coupled limit of the SS model which gives rise to a modified QCD-like theory with an additional parameter. In this chapter, we will review the original work of Sakai and Sugimoto [67] in which they introduced the model and discussed its strong coupling limit obtained through an application of the AdS/CFT correspondence. In the strong coupling limit, the SS model reproduces many qualitative features of the non-perturbative aspects of QCD like confinement and a non-abelian chiral symmetry breaking. In particular, an elegant geometrical picture of chiral symmetry breaking emerges from the holographic dual bulk geometry. Here, we will only provide a compact review of the work of Sakai and Sugimoto and refer the interested reader to the original work [67] for a more detailed exposition. As we will see, while the SS model captures some aspects of χSB in an elegant way, other aspects require modification of the model.

4.1 The strong coupling description

In the discussion on Witten's model (p. 28), we have mentioned that at low energies and in the strong coupling limit a set of large number N_c of overlapping $D4$ branes can be replaced by the near horizon limit of the supergravity bulk solution having the quantum numbers of the brane system. Sakai and Sugimoto studied the strongly coupled model by considering the flavor branes $D8$ and $\overline{D8}$ as probes in the $D4$ background. Such a treatment is allowed provided the number of flavor branes is much smaller than the number of color branes ($N_f \ll N_c$) so that the backreaction of the flavor branes on

the geometry is small. In this limit, the dynamics of this system is captured by the action

$$S = S_{sugra} + S_{DBI} + S_{CS}. \tag{4.1}$$

The term S_{sugra} is the supergravity action of the $D4$ background and gives the holographic description for the pure gauge theory. The dynamics of the flavor branes is given by the DBI action for the $D8 - \overline{D8}$ system in the presence of this background geometry, S_{DBI}, and the Chern-Simons action, S_{CS}, arising from the interaction of the flavor brane gauge fields with the background RR field. Since this is the main focus of the SS model, in the following we will concentrate only on these terms in the full action (4.1).

In our study of the weakly coupled SS model, we saw that there is a U(N_f) symmetry associated with the each of the two sets of overlapping N_f $D8$ branes and $\overline{D8}$ branes. We studied the dynamics of the system and saw how a dynamical breaking of chiral U(N_f) symmetry occurs in it. In the strong coupling picture, the $D4$ background geometry leads the branes and the anti-branes to meet each other in the bulk leaving behind only a U(N_f) symmetry. This presents a geometrical picture of χSB in the model in the strong coupling limit. We will see a demonstration for this in the following.

4.1.1 The $D8$-$\overline{D8}$ profile

Although the model consists of N_f $D8-\overline{D8}$ pairs and leads to a non-abelian chiral symmetry breaking, it is instructive to consider the simpler case of $N_f = 1$ [1] which has most of the essential elements of the model. Sakai and Sugimoto consider the $D8 - \overline{D8}$ branes as probe $D8$ branes. They study the DBI action of a $D8$ in the $D4$ background which involves a scalar field corresponding to the position of the brane in the x^4 coordinate and the 8-brane gauge fields. The DBI action is given by

$$\begin{aligned} S &= -\mu_8 \int d^9\sigma\, e^{-\phi} \sqrt{-\det \mathcal{A}}, \\ \mathcal{A}_{ab} &= g_{MN}\partial_a x^M \partial_b x^N + 2\pi\alpha' F_{ab}, \end{aligned} \tag{4.2}$$

where $\mu_8 = 1/(2\pi)^8 l_s^9$. The integral is carried out in the $D8$-brane world volume. The first term in the second line of (4.2) gives the induced metric on the brane and the second one the field strength of the flavor gauge fields. The indices a, b run over the world-volume directions of the branes while the indices M, N run over the background ten-dimensional space-time directions. Here g_{MN} is the metric dual to the $D4$ brane system and ϕ is the dilaton. For the reader's convenience, we repeat the

[1] The associated U(1) chiral symmetry of the classical theory is broken by the well known quantum anomaly. In the large N_c limit, however, the anomaly vanishes. Therefore, it is meaningful to study U(1) χSB in this limit.

expressions for the dual fields given in (2.21):

$$\begin{aligned} ds^2 &= \left(\frac{U}{R}\right)^{3/2}\left(\eta_{\mu\nu}dx^\mu dx^\nu + f(U)\,(dx^4)^2\right) + \left(\frac{R}{U}\right)^{3/2}\left(\frac{dU^2}{f(U)} + U^2 d\Omega_4^2\right), \\ e^\phi &= g_s\left(\frac{U}{R}\right)^{3/4}, \qquad F_4 = \frac{2\pi N_c}{V_4}\epsilon_4, \qquad f(U) = 1 - \frac{U_k^3}{U^3}, \end{aligned} \tag{4.3}$$

where U_k is defined through relation (2.22) i.e. $U_k = 4R^3/9R_k^2$. The impact of $D4$ background on the configuration of the flavor branes can be seen by putting the flavor brane gauge fields to zero and then solving the equation of motion. Using the static gauge and assuming that x^4 depends on the coordinate U only, which is the case for a classical vacuum solution, the DBI action becomes

$$S = -\mathcal{T}_8 V_4 \int d^4x \int dU \left(\frac{U}{R}\right)^{-3/4} U^4 \sqrt{D}, \tag{4.4}$$

where $\mathcal{T}_8 = \mu_8/g_s$ is the $D8$ brane tension and

$$D = f(U)^{-1}\left(\frac{U}{R}\right)^{-3/2} + f(U)\left(\frac{U}{R}\right)^{3/2}\frac{x^{4\prime}(U)^2}{4}. \tag{4.5}$$

Here and in the following, a prime denotes derivative with respect to U.

In this setup, chiral symmetry breaking has a geometrical description where asymptotically separated branes meet each other in the bulk. This can be seen by explicitly solving the equation of motion for $x^4(U)$ obtained from the action (4.4). This equation is

$$\left(\frac{\left(\frac{U}{R}\right)^{13/4}}{\sqrt{D}}\frac{f(U)}{4}\left(\frac{U}{R}\right)^{3/2} x^{4\prime}(U)\right)' = 0, \tag{4.6}$$

which has the solution

$$x^4(U) = U_0^4 f(U_0)^{1/2}\int_{U_0}^{U} dy \frac{f(y)^{-1}\left(\frac{y}{R}\right)^{-3/2}}{\sqrt{y^8 f(y) - U_0^8 f(U_0)}}. \tag{4.7}$$

Thus, $x^4(U_0) = 0$ and the asymptotic value of $x^4(U)$ as $U \to \infty$ is a monotonically decreasing function of U_0. The maximal asymptotic values occurs for $U_0 = U_k$ and is $\pi R_k/2$. The $D8$ and $\overline{D8}$ are at antipodal points on the x^4 circle and are separated by a distance $l(U) = \pi R_k$. To see this, note from (4.6) that $x^{4\prime}(U) = 0$ is a solution. The background geometry is such that the radius of the circle x_4 remains fixed at R_k for all values of U. Therefore, the antipodal configuration is such that the separation $l(U)$ remains constant in U. In the generic case, the system comprises asymptotically separated brane and antibrane bending towards each other as they approach smaller values of U and

then smoothly meeting at $U = U_0$ as shown in Figure 4.1. Expanding around the point $U = U_0$, we

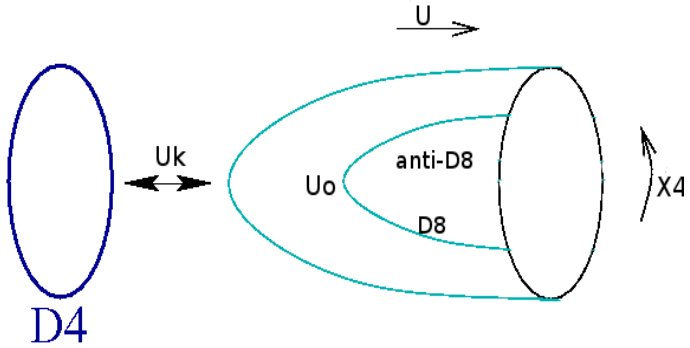

Figure 4.1: The brane configuration in strongly coupled SS model.

get from equation (4.7)

$$x^4(U) = \frac{R^{3/2}}{U_0\sqrt{f(U_0)}}\frac{(U-U_0)^{1/2}}{\sqrt{3+5f(U_0)}}[1+O(U-U_0)]. \tag{4.8}$$

It can be seen that $x^{4\prime}(U) \sim (U-U_0)^{-1/2}$ diverges at U_0, as required by a smooth joining of the brane with the anti-brane.

Excitations about the ground state are simpler to analyze for the antipodal configuration $U_0 = U_K$. In this case, it is useful to define the new coordinates (r, θ) through

$$U^3 = U_K^3 + U_K r^2, \quad \theta = \frac{3}{4}\frac{U_K^{1/2}}{R^{3/2}}x_4. \tag{4.9}$$

We can further define the coordinates (y, z) as

$$y = r\cos\theta, \quad z = r\sin\theta. \tag{4.10}$$

In these coordinates, the configuration of the $D8 - \overline{D8}$ can be expressed as the function $y(x^\mu, z)$. The antipodal configuration corresponds to $y(x^\mu, z) = 0$. The horizon, where the two branes meet, appears at $z = 0$ and the asymptotic infinity on the $D8$ and $\overline{D8}$ are at $z \to \infty$ and $z \to -\infty$. All computations carried out in the rest of this chapter will assume this configuration.

4.1.2 Mesons

In the discussion carried out till now, the flavor gauge fields have been neglected since we were interested only in the profile of the branes. However, chiral symmetry breaking must also be

associated with massless Goldstone bosons[2]. To see this, one needs to look at the excitations in the model. The mesonic excitations arise by switching on the flavor gauge fields on the $D8$ and $\overline{D8}$ branes, which, as we shall see, contain the Goldstone boson as well as the vector and axial-vector mesonic analogs of QCD. In principle, the index on the gauge field A_M can run over space-time and S_4 directions and the holographic direction z. The components along the directions of the space-time and z respectively will be denoted by A_μ and A_z. The components along the S_4 directions must be associated with an SO(5) symmetry. Since the intention here is to study the qualitative features of QCD, which does not have such a symmetry, these components are put to zero by hand. Further, the symmetry of the system also allows us to restrict the fluctuations to zero modes in S^4, so that A_μ and A_z do not have any dependence on the S^4 coordinates. With this, the action for the gauge field fluctuations is given by

$$S = -\mathcal{T}(2\pi\alpha')^2 \int d^4x dz \left(\frac{R^3}{4U_z} \eta^{\mu\nu}\eta^{\lambda\sigma} F_{\mu\lambda}F_{\nu\sigma} + \frac{9}{8}\frac{U_z^3}{U_K}\eta^{\mu\nu}F_{\mu z}F_{\nu z} \right) \tag{4.11}$$

where $U_z^3 = U_K^3 + U_K z^2$ and we have defined $\mathcal{T} \equiv \frac{2}{3}R^{3/2}U_K^{1/2}V_4\mathcal{T}_8$. Only terms upto quadratic order in fluctuations are kept. There is also a Chern-Simons action S_{CS} arising from the four-form background RR field strength and the flavor gauge fields. However, such a term is cubic in the flavor gauge field strength and is therefore neglected here in the fluctuations analysis.

The finiteness of the action (4.11) requires the field strength to vanish at $z \to \pm\infty$. By a choice of gauge we can assume that the gauge field vanishes at $z \to \pm\infty$. Note that this still allows a further gauge freedom

$$A_z \to A_z + \partial_z\Lambda(x,z), \;\; A_\mu \to A_\mu + \partial_\mu\Lambda(x,z) \;\text{ with } \lim_{z\to\pm\infty}\Lambda(x,z) = 0. \tag{4.12}$$

To proceed further, we use a mode expansion of the fields in terms of a complete set of functions in the holographic coordinate $Z \equiv z/U_K$:

$$A_\mu(x,Z) = \sum_n A_\mu^{(n)}(x)P_n(Z), \; A_Z(x,Z) = \sum_j \phi^{(j)}(x)Q_j(Z). \tag{4.13}$$

Since the gauge fields vanish at $z \to \pm\infty$, the functions $P_n(Z)$ and $Q_j(Z)$ must satisfy the same boundary condition. With this, the five dimensional action can now be written as

$$\begin{aligned} S = -\mathcal{T}(2\pi\alpha')^2R^3 \int d^4x dZ \Big\{ \frac{1}{4}K^{-1/3}F_{\mu\nu}^{(n)}F^{(m)\mu\nu}P_nP_m + \frac{K}{2R_k^2}\Big(A_\mu^{(m)}A^{(n)\mu}\partial_Z P_n\partial_Z P_m \\ + \partial_\mu\phi^{(i)}\partial^\mu\phi^{(j)}Q_iQ_j - 2\partial_\mu\phi^{(i)}A^{(n)\mu}Q_i\partial_Z P_n \Big)\Big\}, \end{aligned} \tag{4.14}$$

[2] As mentioned earlier, for $N_f = 1$, there is a single Goldstone boson in the large N_c limit.

where $K(Z)=1+Z^2$ and the repeated indices i, j, m, n are summed over. The set of functions $P_n(Z), n \geq 1$ can be chosen such that they satisfy

$$-K^{1/3}\partial_Z(K\partial_Z P_n) = \lambda_n P_n, \quad \mathcal{T}(2\pi\alpha')^2 R^3 \int dZ K^{-1/3} P_n(Z) P_m(Z) = \delta_{nm}. \tag{4.15}$$

With this, in the absence of the field $\phi^{(i)}$, the four dimensional action for $A_\mu^{(n)}$s would reduce to the action for a tower of massive vectors given by

$$S[A_\mu] = \int d^4x \sum_{n=1}^{\infty} \left(\frac{1}{4} F_{\mu\nu}^{(n)} F^{(n)\mu\nu} + \frac{m_n^2}{2} A_\mu^{(n)} A^{\mu(n)} \right), \tag{4.16}$$

where $m_n^2=\lambda_n/R_k^2$. The following orthonormality condition should be imposed on the set of functions Q_i:

$$\mathcal{T}(2\pi\alpha')^2 \frac{R^3}{R_k^2} \int dZ K Q_i Q_j = \delta_{ij}. \tag{4.17}$$

Note that the set of functions $Q_n = m_n^{-1}\partial_Z P_n (n \geq 1)$ satisfy the above condition. Now, the function $Q_0 = C/K$ also satisfies the orthonormality condition. Thus, the set $Q_i (i \geq 0)$ now provides a complete set of functions consistent with the orthonormality condition (4.17). Using this, the total action (4.14) then reduces to

$$\begin{aligned} S &= -\int d^4x \left\{ \frac{1}{2}\partial_\mu\phi^{(0)}\partial^\mu\phi^{(0)} + \sum_{n\geq 1} \left(\frac{1}{4} F_{\mu\nu}^{(n)} F^{(n)\mu\nu} + \frac{m_n^2}{2} (A_\mu^{(n)} - m_n^{-1}\partial_\mu\phi^{(n)})(A^{\mu(n)} - m_n^{-1}\partial^\mu\phi^{(n)}) \right) \right\} \\ &\equiv -\int d^4x \left\{ \frac{1}{2}\partial_\mu\phi^{(0)}\partial^\mu\phi^{(0)} + \sum_{n\geq 1} \left(\frac{1}{4} F_{\mu\nu}^{(n)} F^{(n)\mu\nu} + \frac{m_n^2}{2} B_\mu^{(n)} B^{\mu(n)} \right) \right\}. \end{aligned} \tag{4.18}$$

Let us now invoke the additional gauge freedom (4.12) we mentioned before. Since we have $\lim_{Z\to\infty} \Lambda(x,Z)=0$ [3], $\Lambda(x,Z)$ can be written in terms $P_n(Z)$s as $\Lambda(x,Z) = \sum_{n\geq 1} \Lambda^{(n)}(x) P_n(Z)$. It can be easily seen using this that the fields $\phi^{(0)}(x)$ and $B_\mu^{(n)}(x)$ are gauge invariant under this additional gauge degree of freedom and are therefore physical in nature. Sakai and Sugimoto numerically solved the eigenvalue equations for the basis functions and determined the parity of the fields. The field $\phi^{(0)}(x)$ is of odd parity and is identified with the analog of η' meson. The fields $B_\mu^{(n)}(x)$ give the analogs of the vector and axial-vector mesons. Although, for simplicity, we have discussed the case with single flavor, it is not difficult to analyse the case with multiple flavors. Using a non-abelian generalisation Sakai and Sugimoto show that the model gives rise to analogs of massless pions and massive vector and axial-vector mesons. The authors also reproduced the chiral anomaly in QCD

[3] We use Z instead of z.

using their model. This arises from the Chern-Simons action involving interaction between the RR 4-form field strength and flavor gauge field strength. The gauge transformation of the Chern-Simons term precisely matches the chiral anomaly of QCD and precisely reproduces the WZW term of chiral lagrangian. They have also studied baryons in the model. A baryon is realised as a $D4$ brane wrapped on S_4 which in turn can be realised as an instanton configuration of the flavor gauge fields. The Chern-Simons term leads to a potential for the vector U(1) part of the flavor gauge field fluctuation coupled to a point source of charge nN_c where n is the instanton number. This identifies the instanton configuration to a baryon with the instanton number giving the baryon number (since each baryon has N_c quarks). Just as in QCD, the baryon mass turns out to be $O(N_c)$.

4.2 Summary and discussion

Before we end this chapter, let us summarise some of the salient points of the model. The model is an important qualitative step towards a holographic description of a QCD-like theory. It reproduces many of the qualitative features of QCD-like theory including the strong coupling phenomena of confinement and chiral symmetry breaking. However, the model also has problems because of which it is actually expected to describe a theory that is different from QCD. The first problem is that at strong coupling, the masses of Kaluza-Klein modes are of the order of Λ_{QCD} as we have argued in the discussion on Witten's model. Thus, the model has infinitely many more glueball and meson states than in QCD. Moreover, there are no low lying states with spin higher than 2, these having been pushed to very high masses (of the order of string scale). This makes it different from properties expected of QCD.

The second problem is the absence of any parameter corresponding to the quark mass deformation. The quarks in the Sakai-Sugimoto model are massless and there is no simple way of switching on a quark mass. This masslessness of quarks can be deduced from the masslessness of the Goldstone bosons of the χSB. The model has no parameter describing massive quarks. For phenomenological reasons, having nonzero quark masses is important. The first of these problems is generic to all holographic models of QCD. The hope is that despite this, many qualitative features survive the tuning of coupling from weak to strong. One of the main aims of this thesis is to present a proposal to solve the second problem. We will do this in the next two chapters. Our proposal is to modify the SS model by taking into account the tachyon fluctuations which we expect to be relevant in the region where the branes meet. As we will see, introduction of the tachyon will allow the model to accommodate a non-zero quark mass.

Chapter 5

Quark mass deformation of SS model

In the last chapter, we saw a beautiful geometrical picture of spontaneous breaking of chiral symmetry arising in the strongly coupled Sakai-Sugimoto model. In the dual geometry of the $D4$-branes, the global chiral symmetry of asymptotically separated $D8$ – $\overline{D8}$ branes is broken in the bulk where the branes meet. The model also gives rise to a meson spectrum where the associated massless pseudoscalar Goldstone bosons can be identified with some of the flavor gauge field fluctuations of the $D8$-$\overline{D8}$ branes. As mentioned before, however, one of the main drawbacks of the model is that it does not have any parameter corresponding to quark masses. Further, it lacks an order parameter for χSB too.

In this chapter and the following, we present a proposal for overcoming these drawbacks. Our proposal provides a setup in which one can take into account a non-zero quark mass. Our setup also has an explicit order parameter for χSB. The model is a modification of the strongly coupled SS model involving a study of the dynamics of the open string tachyon between $D8$ and $\overline{D8}$ branes in the $D4$ background. Note that the open string tachyon between the flavor branes transforms as a bifundamental under the flavor group. Thus, it couples to a chiral bilinear of fermions in the boundary field theory. Therefore, condensation of this field can potentially lead to the analog of a quark mass term in the boundary QCD-like theory. The transformation under the flavor group also suggests that it can give rise to an order parameter for χSB. In this chapter, we will provide details of our proposal and in the following chapter, we describe the meson spectrum and study the impact of a non-zero quark mass on it. The matter covered in these two chapters is based on our work in [121, 122].

5.1 Modified Sakai-Sugimoto model with tachyon

In the last chapter we discussed the strongly coupled SS model in which the $D8$ and $\overline{D8}$ branes attain a U-shaped configuration in the $D4$ background. In order to arrive at such a configuration one may have

to study the tachyon dynamics arising from open strings between the $D8$ and $\overline{D8}$ branes. For a large separation, these modes are massive. However, it is natural that they give rise to tachyonic modes whenever the $D8-\overline{D8}$ separation is smaller than the string scale. In the region of small separation where the $D8$ and $\overline{D8}$ branes meet each other, the tachyonic mode is expected to become important and can no longer be neglected. This requires us to consider the effect of the tachyon in the $D8$-$\overline{D8}$ DBI action. In particular, its coupling with the flavour gauge fields modifies the spectrum of the mesons. It turns out that the tachyonic mode has a parameter for the quark mass which gives rise to a non-zero mass to the pseudo-Goldstone boson analogous to pion and also one for the order parameter associated with chiral symmetry breaking, i.e., the chiral condensate. We will see this in detail in the following.

5.2 Brane-antibrane pair with tachyon

Studies of various aspects of tachyon dynamics on a non-BPS D-brane have been carried out in superstring theory. The proposed tachyon effective action for a non-BPS Dp-brane in flat space is given by [100] - [106]:

$$\begin{aligned} S &= -\int d^{p+1}x V(\tau)\sqrt{-\det \mathcal{A}}, \\ \mathcal{A}_{ab} &= \eta_{ab} + \partial_a T\partial_b T + \partial_a X^i \partial_b X^i + F_{ab}, \\ F_{ab} &= \partial_a A_b - \partial_b A_a, \end{aligned} \tag{5.1}$$

where $0 \le a, b \le p$ are the indices for the directions in the Dp brane world-volume and $(p+1) \le i \le 9$ is the index for the transverse directions. The field A_a is the Dp brane gauge field and X^is are the transverse scalars. τ denotes the tachyon field. $V(\tau)$ is the tachyon potential and depends only on the magnitude $T = |\tau|$ of the tachyon. It is believed to satisfy the following general properties [107]:

- $V(T)$ has a maximum at $T = 0$ and a minimum at $T = \infty$ where it vanishes.
- The normalization of $V(T)$ is fixed by the requirement that with tachyon put to zero it should correctly produce the Dp brane tension, so that $V(0) = \mathcal{T}_p = 1/(2\pi)^p\, l_s^{p+1}\, g_s$.
- The expansion of $V(T)$ around $T = 0$ up to terms quadratic in T gives rise to a tachyon with mass-squared equal to $-1/2\alpha'$.

There are several proposals for $V(T)$ which satisfy these requirements [107], although no rigorous derivation exists. Examples are (i) the potential used in [114, 115, 116] for calculation of decay of

unstable D-branes in two-dimensional string theory

$$V(T) = \mathcal{T}_p \text{ sech } \sqrt{\pi} T; \tag{5.2}$$

and (ii) the potential obtained using boundary string field theory computation [117, 118, 119, 120]

$$V(T) = \mathcal{T}_p \, e^{-\frac{\pi}{2} T^2}. \tag{5.3}$$

Both these potentials satisfy the properties listed above. Note that the asymptotic form of the potential in (5.2) for large T is $\sim e^{-\sqrt{\pi} T}$. The linear growth of the exponent with T should be contrasted with the quadratic growth for the potential in (5.3).

A generalisation of (5.1) was proposed to describe the tachyon effective action for the brane-antibrane system by Sen in [108]. It is given by

$$\begin{aligned} S &= -\int d^{p+1}x V(T, X^i_{(1)} - X^i_{(2)})(\sqrt{-\det \mathcal{A}_{(1)}} + \sqrt{-\det \mathcal{A}_{(2)}}), \\ \mathcal{A}_{(J)ab} &= \eta_{ab} + F^{(J)}_{ab} + \partial_a X^i_{(J)} \partial_b X^i_{(J)} + \frac{1}{2}(D_a\tau)^\star (D_b\tau), \\ F^{(J)}_{ab} &= \partial_a A^{(J)}_b - \partial_b A^{(J)}_a, \quad D_a\tau = (\partial_a - iA^{(1)}_a + iA^{(2)}_a)\tau, \end{aligned} \tag{5.4}$$

where τ is complex and T is its magnitude. For small values of T, the potential has a behaviour given by

$$V(T, X^i_{(1)} - X^i_{(2)}) = \mathcal{T}_p \Big[1 + \frac{1}{2} \Big\{ \Big(\frac{X^i_{(1)} - X^i_{(2)}}{2\pi} \Big)^2 - \frac{1}{2} \Big\} T^2 + O(T^4) \Big]. \tag{5.5}$$

Although the form of the action is not based on an exact derivation but it satisfies the following consistency conditions:

- The action is invariant under the gauge transformation given by

$$\tau \to e^{i(\lambda_1(x) - \lambda_2(x))}\tau, \; A^{(1)}_a \to A^{(1)}_a + \partial_a \lambda_1(x), \; A^{(2)}_a \to A^{(2)}_a + \partial_a \lambda_2(x).$$

- With tachyon τ put to zero we get the sum of the actions of two BPS D-branes.

- If we demand that the fields be invariant under $(-1)^{F_L}$ that interchanges the brane and anti-brane then we have

$$\tau = \text{real}, \; A^{(1)}_a = A^{(2)}_a, \; X^i_{(1)} = X^i_{(2)}.$$

  With this the action becomes proportional to that of a single non-BPS Dp-brane given by (5.1). In [109], Sen investigated the result of orbifolding (modding wrt $(-1)^{F_L}$) a Dp-$\overline{Dp}$ system. He

showed that the result is a single non-BPS Dp brane. Thus, the present case is consistent with this result.

A proposal for the brane-antibrane effective action was also made by Garousi in [110, 111]. The line of argument for this proposal is based on the work done in [101] which proposes an effective action for multiple non-BPS Dp branes in a given background space-time. It uses a non-abelian generalisation of the action for a single non-BPS Dp brane. It is the easiest to obtain such a non-abelian generalisation for multiple non-BPS $D9$ branes which have no transverse scalars. One can then find the effective action for Dp branes using a T-duality along the (9-p) directions. The effective action for Dp-$\overline{Dp}$ is then found from the effective action for two non-BPS Dp-branes by restricting the Chan-paton factors to the subgroup corresponding to the Dp-$\overline{Dp}$ system. The effective action so generated is consistent with disk level S-matrix elements in string theory [110, 111].

An alternate proposal for the effective action for a Dp-$\overline{Dp}$ pair has also been made in [112] building upon the work carried out in [113] describing the dynamics of the system. This is based on the abelian tachyon-DBI action for a single non-BPS $D(p+1)$ brane. The Dp-$\overline{Dp}$ system arises as a kink-antikink solution in this description. (Kink solution in non-BPS D-brane was previously studied by Sen in [108].) The complex tachyon, the U(1)×U(1) gauge field and the additional transverse scalars are emergent quantities in this setup.

In the following, we apply the proposal made in [110, 111] to the $D8$-$\overline{D8}$ system in $D4$ background. The simplest case occurs when the brane and antibrane are on top of each other since in this case all the transverse scalars are set to zero. This is the situation considered in [85]. To retain the nice geometrical picture of χSB of the SS model, one needs to separate the brane and anti-brane. This requires an effective tachyon action on a brane-antibrane pair interacting with the transverse scalars. Although the work carried out in [110, 111] proposes an effective action with the brane and antibrane separated along a noncompact direction, a generalization of this action to the case when the brane and antibrane are separated along a periodic direction (like ours) is not known. However, for small separation $l(U)$ compared to the radius R_k of the circle, the action in [110] should provide a reasonable approximation to the compact case. In the following we will assume this to be true. A posteriori justification for this assumption, as we shall see later, is provided by the classical solutions for the brane-antibrane profile. In these solutions, for small asymptotic separation, the brane and antibrane meet far away from the central region. In this case, to a good approximation, the factor $f(U)$ in the background metric can be set to identity, which is equivalent to setting the radius R_k to infinity.

With this, the effective low-energy tachyon action for a $D8$ and $\overline{D8}$-brane pair for $l(U) << R_k$ is given, in the $D4$ background by

$$\begin{aligned} S &= -\int d^9\sigma\, V(T,l)e^{-\phi}\left(\sqrt{-\det \mathcal{A}_{\rm L}} + \sqrt{-\det \mathcal{A}_{\rm R}}\right), \\ (\mathcal{A}_i)_{ab} &= \left(g_{MN} - \frac{T^2l^2}{2\pi\alpha' Q} g_{M4}g_{4N}\right)\partial_a x_i^M \partial_b x_i^N + 2\pi\alpha' F^i_{ab} + \frac{1}{2Q}\Big(2\pi\alpha'(D_a\tau(D_b\tau)^* + (D_a\tau)^* D_b\tau) \\ &\quad + il(g_{a4} + \partial_a x_i^4 g_{44})(\tau(D_b\tau)^* - \tau^* D_b\tau) + il(\tau(D_a\tau)^* - \tau^* D_a\tau)(g_{4b} - \partial_b x_i^4 g_{44})\Big), \end{aligned} \tag{5.6}$$

where

$$Q = 1 + \frac{T^2l^2}{2\pi\alpha'} g_{44}, \quad D_a\tau = \partial_a\tau - i(A_{L,a} - A_{R,a})\tau, \quad V(T,l) = g_s V(T)\sqrt{Q}. \tag{5.7}$$

$T = |\tau|$, $i = L, R$ and we have used the fact that the background does not depend on x^4. $V(T)$ is called the tachyon potential. The complete action also includes terms involving Chern-Simons couplings of the gauge fields and the tachyon to the RR background sourced by the $D4$-branes. In the following, we will be interested in knowing the classical vacuum configuration of the $D8 - \overline{D8}$ system in which the gauge fields A_L and A_R do not acquire any vev. The Chern-Simons terms vanish in the absence of gauge fields and therefore play no role in determining the vacuum configuration. In the next chapter also, we will study only the implications of the vacuum configuration we determine here, on the flavor gauge field fluctuations. Therefore, we omit the Chern-Simons terms. It may, however, be important to mention that a study of chiral anomaly requires one to take into account these terms.

We end this section with the following observation. It can be easily seen that in the decoupling limit all factors of α' scale out of the entire action, without requiring any scaling of the transverse scalar l or the tachyon τ. In fact, the entire action can be rewritten in terms of λ_5 and U, quantities that are kept fixed in the scaling limit. Henceforth, we will use the convention $2\pi\alpha' = 1$.

5.3 Classical equations for brane profile and tachyon

In this section, we look for an appropriate classical ground state solution of the brane-antibrane-tachyon system. We, therefore, set the gauge fields to zero and assume that T and x_i^4 depend only on U. Guided by symmetry and with no loss of generality, we choose $x_L^4 = l(U)/2$ and $x_R^4 = -l(U)/2$ so that the separation between the brane and antibrane is l. With this, the action (5.6) in the static gauge, simplifies to

$$S = -V_4 \int d^4x \int dU\, V(T)\left(\frac{U}{R}\right)^{-3/4} U^4\left(\sqrt{D_{L,T}} + \sqrt{D_{R,T}}\right), \tag{5.8}$$

where $D_{L,T} = D_{R,T} \equiv D_T$ and

$$D_T = f(U)^{-1}\left(\frac{U}{R}\right)^{-3/2} + f(U)\left(\frac{U}{R}\right)^{3/2}\frac{l'(U)^2}{4} + T'(U)^2 + T(U)^2 l(U)^2. \tag{5.9}$$

It is convenient to remove the dependence on R (except for an overall factor in the action) through a redefinition of variables,

$$U = u/R^3, \quad l(U) = R^3 h(u), \quad U_k = u_k/R^3. \tag{5.10}$$

In terms of the new variables, we get

$$S = -V_4 R^{-9}\int d^4x \int du\, u^{13/4}\, V(T)\left(\sqrt{d_{L,T}} + \sqrt{d_{R,T}}\right), \tag{5.11}$$

where

$$d_{L,T} = d_{R,T} \equiv d_T = f(u)^{-1}u^{-3/2} + f(u)\, u^{3/2}\frac{h'(u)^2}{4} + T'(u)^2 + T(u)^2 h(u)^2, \tag{5.12}$$

with $f(u) = (1 - u_k^3/u^3)$.

The effective potential for the tachyon can be obtained from this action by setting $T' = h' = 0$ and is given by

$$V_{\text{eff}}(T, l) \sim \text{sech}\,\sqrt{\pi}T\,\sqrt{1 + u^{3/2}T^2h^2}. \tag{5.13}$$

In Figure 5.1 we have plotted V_{eff} as a function of T for various values of u. We see that a perturbatively stable minimum at $T = 0$ for large values of u turns into an unstable maximum at a sufficiently small value of u. This is true for any fixed, non-zero value of h. Moreover, the value of u at which there is an unstable maximum at $T = 0$ increases as h decreases.

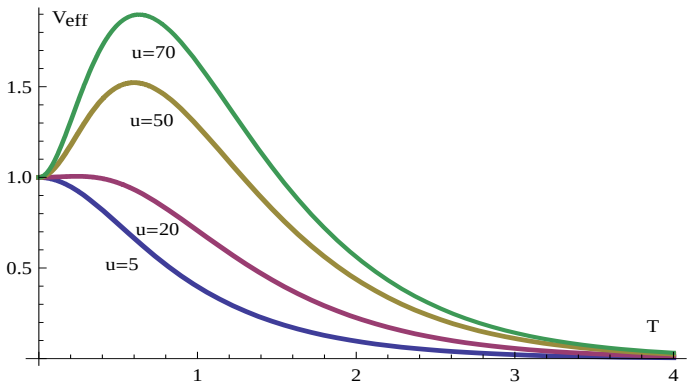

Figure 5.1: The effective potential V_{eff} as a function of T for different values of u for a fixed non-zero value of h.

The equations of motion obtained from the action (5.11) are given by

$$\left(\frac{u^{\frac{13}{4}}}{\sqrt{d_T}}T'(u)\right)' = \frac{u^{\frac{13}{4}}}{\sqrt{d_T}}\left[T(u)h(u)^2 + \frac{V'(T)}{V(T)}(d_T - T'(u)^2)\right], \tag{5.14}$$

$$\left(\frac{u^{\frac{13}{4}}}{\sqrt{d_T}}\frac{f(u)}{4}u^{\frac{3}{2}}h'(u)\right)' = \frac{u^{\frac{13}{4}}}{\sqrt{d_T}}\left[T(u)^2h(u) - \frac{V'(T)}{V(T)}\frac{f(u)}{4}u^{\frac{3}{2}}h'(u)T'(u)\right], \tag{5.15}$$

where the 'prime' on $V(T)$ denotes a derivative w.r.t. its argument T (and not a derivative w.r.t. u). This is a complicated set of coupled nonlinear differential equations which can be solved completely only numerically. However, for large u and u near the place in bulk where the brane and anti-brane join, these equations simplify and can be treated analytically. To get some insight into the kind of solutions that are possible, we will, therefore, first analyse these equations in these two special cases before proceeding on to describe the complete numerical solutions which we have obtained [121, 122]. Note that we are looking for solutions in which the brane and antibrane have a given asymptotic separation h_0, i.e. $h(u) \to h_0$ as $u \to \infty$, and they join at some interior point in the bulk, i.e. $h(u) \to 0$ at $u = u_0 \geq u_k$ (since u_k provides a lower bound on u). Such a solution will help us preserve the geometrical picture of χSB in SS model. Moreover, we desire the tachyon solution to vanish as $u \to \infty$. This implies that in the UV limit, the vev of the tachyon vanishes and the full chiral symmetry is preserved, as in the massless QCD action. The tachyon solution is also desired to blow up as u approaches u_0. As we will see, this will allow us to relate bulk calculations with boundary field theory quantities in the UV only. This is because the tachyon potential becomes zero when the tachyon blows up.

5.3.1 Solution for large u

Here we seek a solution in which $h(u)$ approaches a constant h_0 and T becomes small as $u \to \infty$. For small T one can approximate $V'/V \sim -\pi T$ which follows from the general properties of the potential discussed in section 5.2. If T and h' go to zero sufficiently fast as $u \to \infty$ then to the leading order, one might approximate $d_T \sim u^{-3/2}$. With this, (5.14) can be approximated to

$$\left(u^4\, T'(u)\right)' = h_0^2\, u^4\, T. \tag{5.16}$$

The general solution of this equation is

$$T(u) = \frac{1}{u^2}(T_+ e^{-h_0 u} + T_- e^{h_0 u}). \tag{5.17}$$

In writing this solution we have ignored a higher order term in $1/u$ for consistency with other terms in equation (5.14) of this order that we have neglected.

The fact that the tachyon becomes small for large u makes it irrelevant for the leading asymptotic behaviour of h. Thus, (5.15) simplifies to

$$\left(u^{\frac{11}{2}}h'(u)\right)' = 0, \tag{5.18}$$

which has the solution

$$h(u) = h_0 - h_1 u^{-9/2}. \tag{5.19}$$

Here h_1 is restricted to positive values so that the branes come together in the bulk. For SS model without the tachyon, $h_1 = \frac{4}{9}u_0^4 f_0^{1/2}$, where $f_0 = f(u_0)$, u_0 being the value of u where the branes meet in the bulk.

It is easy to convince oneself that the only solution to equations (5.14) and (5.15) in which T vanishes asymptotically and h goes to a constant is (5.17) with $T_- = 0$. In particular, for example, these equations have no solutions in which T vanishes asymptotically as a power law.

5.3.2 Solution for $u \sim u_0$

Here we look for a solution in which $h \to 0$ and $T \to \infty$ as $u \to u_0$. Let us assume a power law ansatz, namely

$$h(u) \sim (u - u_0)^\alpha, \qquad T(u) \sim (u - u_0)^{-\beta}. \tag{5.20}$$

For a smooth joining of the brane and antibrane at u_0, the derivative of h must diverge at this point, which is ensured if $\alpha < 1$. With this ansatz, the leading contribution to d_T comes from T'^2. Hence, we can approximate $d_T \sim T'(u)^2$. We will also need the asymptotic form of the potential $V(T)$ for large T, which depends on the specific potential being used. The tachyon potential in (5.2) leads to an asymptotic form given by $V'(T)/V(T) \sim -\sqrt{\pi}$, while for the potential in (5.3), we get $V'(T)/V(T) \sim -\pi T$. Using this in (5.14) and (5.15), it is easy to verify that the equations cannot be satisfied by the ansatz for the potential (5.3). They are, however, satisfied for the potential in (5.2). In fact, in this case the powers as well as the coefficients all get fixed:

$$h(u) = \sqrt{\frac{26}{\pi u_0 f_0}}u_0^{-3/4}(u - u_0)^{1/2} + \cdots, \tag{5.21}$$

$$T(u) = \frac{\sqrt{\pi}}{4} f_0 u_0^{3/2}(u - u_0)^{-2} + \cdots, \tag{5.22}$$

where $f_0 = f(u_0)$.

An important feature of the above solution is that it depends only on a single parameter, namely the value of u_0. We have checked that this feature persists in the next few higher orders in a power series expansion in $(u-u_0)$. This is in sharp contrast to the asymptotic solution (5.17), (5.19) which depends on all the four expected parameters, $T_+,\ T_-,\ h_0,\ h_1$. This reduction in the number of parameters is similar to what happens in the SS model where the solution for $u \sim u_0$ depends only on one parameter, although the asymptotic solution depends on two parameters. In the present case the reduction in the number of parameters is even more severe; the solution for $u \sim u_0$ matches with only a one-parameter subspace of the four-parameter space of asymptotic solutions. As we will discuss later, this one-parameter freedom of the classical solution turns out to be analogous to the freedom to add a bare quark mass in QCD.

For completeness, we note that there exists another solution in which T does not diverge but goes to a nonzero constant as $u \to u_0$. In this case we can approximate $d_T \sim f(u)u^{3/2}h'(u)^2/4$. Substituting in (5.14) we see that the *lhs* diverges as $(u-u_0)^{-\alpha}$. The first term on the *rhs* vanishes as a positive power, but the second term diverges as $(u-u_0)^{\alpha-1}$, since $\alpha < 1$. For consistency we must have $\alpha = 1/2$. The resulting solution

$$h(u) = \frac{4}{u_0}(f_0(5f_0+3))^{-1/2}(u-u_0)^{1/2} + \cdots, \tag{5.23}$$

$$T(u) = t_0 + \frac{2u_0^{-1/2}}{(5f_0+3)}\frac{V'(u_0)}{V(u_0)}(u-u_0) + \cdots, \tag{5.24}$$

also satisfies (5.15). Note that no special condition was required for the tachyon potential to get this solution; this solution exists for any potential.

5.4 Quark mass and the ultraviolet cut-off

In the tachyon solution (5.17), the exponentially falling part satisfies the approximations under which (5.16) was derived for any large value of u. The exponentially rising part will, however, eventually become large and cannot be self-consistently used. This is because for sufficiently large u, there is no consistent solution for T which grows exponentially or even as a power-law to the original equations (5.14) and (5.15), if we impose the restriction that $h(u)$ should go to a constant asymptotically. This puts a restriction on the value of u beyond which the generic solution (5.17) cannot be used. The most restrictive condition comes from the approximation $d_T \sim u^{-3/2}$. This requires the maximum value, $u_{\rm max}$, to satisfy the condition

$$T_+^2 e^{-2h_0 u_{\rm max}} + T_-^2 e^{2h_0 u_{\rm max}} << \frac{u_{\rm max}^{5/2}}{2h_0^2} \tag{5.25}$$

For generic values of $|T_\pm|$ and h_0, this inequality determines a range of values of $u_{\rm max}$ for which the solution (5.17) can be trusted. The value $T_- = 0$ is special since in this case there is no upper limit on $u_{\rm max}$, except the cut-off that comes from the fact that the 10-dimensional description of the background geometry breaks down beyond some very large value ($\sim N_c^{4/3}$) of u. However, as is clear from (5.25), for nonzero $|T_-|$ one needs to choose a much smaller value of $u_{\rm max}$. Numerical calculations reported in the next section bear out this expectation.

It is important to emphasize that the ultraviolet cut-off we are talking about here does not merely play the usual role of a cut-off needed in any example of AdS/CFT with a non-normalizable part present in a solution to the bulk equations. The point is that there is no growing solution to the tachyon equation in the ultraviolet which is consistent with a brane profile that goes to a finite asymptotic brane-antibrane separation. This constraint limits the value of u up to which the asymptotic solutions, (5.17) and (5.19), can be trusted.

One way to think about the inequality (5.25) is the following. Suppose for given values of $|T_\pm|$ we have chosen the largest value of $u_{\rm max}$ consistent with (5.25). Increasing $u_{\rm max}$ further would then be possible only if $|T_-|$ is decreased appropriately, while $|T_+|$ can be kept fixed, as $u_{\rm max}$ is increased. To be concrete, let us keep $|T_+|$ and $|T_-|e^{h_0 u_{\rm max}}$ fixed as $u_{\rm max}$ is increased. The process of "removing the cut-off" can then be understood as increasing $u_{\rm max}$ and simultaneous decreasing $|T_-|$ while keeping $|T_+|$ and the combination $|T_-|e^{h_0 u_{\rm max}}$ fixed. In this process, at some point $|T_+|e^{-h_0 u_{\rm max}}$ would become much smaller than $|T_-|e^{h_0 u_{\rm max}}$. As we shall see in the next section, however, limitations due to numerical accuracy prevent us from tuning $|T_-|$ to very small values, or equivalently tuning $u_{\rm max}$ to be very large. Thus we are numerically restricted to rather small values of $u_{\rm max}$. For values of u larger than $u_{\rm max}$, the inequality (5.25) breaks down and consequently the asymptotic solution (5.17) is not applicable. Clear evidence for this breakdown is seen in the numerical calculations reported in the next section.

It is natural to associate T_- with the quark mass since this parameter comes with the growing solution. Evidence for this will be given in later where we will show that for a small nonzero value of this parameter, the mass of the pseudo-Goldstone boson analogous to pion is nonzero and proportional to it. It is also natural to associate T_+ with the chiral condensate because it comes with the normalizable solution. It turns out that this association too is consistent, though this part of the story is somewhat more complicated, as we shall see in section 5.10.

It is interesting to mention here that keeping the combination $|T_-|e^{h_0 u_{\rm max}} = \rho$ fixed as the cut-off becomes large implies an exponential dependence of $|T_-|$ on the $u_{\rm max}$, i.e. $|T_-| = \rho e^{-h_0 u_{\rm max}}$. A similar dependence of the quark mass on the cut-off has been observed in [124, 125], though the methods used for computing quark mass in these works are quite different from ours. In [124] the cut-off arises from the location of a $D6$-brane, which is additionally present in that model, thereby giving a physical meaning to the cut-off.

5.5 Numerical solutions

The equations (5.14), (5.15) cannot be solved analytically. One needs to use numerical tools to get a solution. We have made use of Mathematica for this. Also, for numerical calculations we have chosen the potential (5.2), since there is no diverging solution for $T(u)$ for $u \sim u_0$ for the potential (5.3), as discussed above.

The numerical calculations are easier to do if we start from the $u = u_0$ end and evolve towards the large u end. This avoids the fine-tuning one would have to do if one were to start from large values of u, where the general solution has four parameters, and end on a one-parameter subspace for $u \sim u_0$. We must also satisfy the requirement of working in the parameter region of the background geometry corresponding to the strong coupling. In addition, we need to ensure that the asymptotic separation between flavour branes and antibranes is small compared to the radius of the x^4 circle. Mathematically, these requirements are $\lambda_5 = 8\pi^2 R^3 \gg 2\pi R_k$ and $l_0 \ll \pi R_k$. Using (2.22) and (5.10), one gets $R^3 = \frac{3}{2} R_k \sqrt{u_k}$. Then, these requirements become $\frac{1}{36\pi^2} \ll u_k \ll \frac{4\pi^2}{9h_0^2}$. Throughout our numerical calculations we will work with $u_k = 1$, which satisfies the first condition easily, while it requires from the second that $h_0 \ll \frac{2\pi}{3}$. As we shall see below, the asymptotic separation decreases with increasing value of u_0, as is the case for the SS model. Therefore, the condition is easily satisfied by choosing $u_0 \gg u_k = 1$. For such values of u_0, $f(u) \sim 1$ for all $u \geq u_0$.

The boundary conditions are imposed using (5.21), (5.22) at a point $u = u_1$ which we choose as close to u_0 as allowed by numerics. Generally we were able to reduce $(u_1 - u_0)$ down to about 0.1 percent of the value of u_0. Starting from the values of $T(u_1)$, $T'(u_1)$, $h(u_1)$ and $h'(u_1)$ obtained from (5.21), (5.22) at $u = u_1$, the system was allowed to evolve to larger values of u. Figure 5.2 shows an example for $u_0 = 12.7$. Solutions for both $h(u)$ and $T(u)$ are shown.

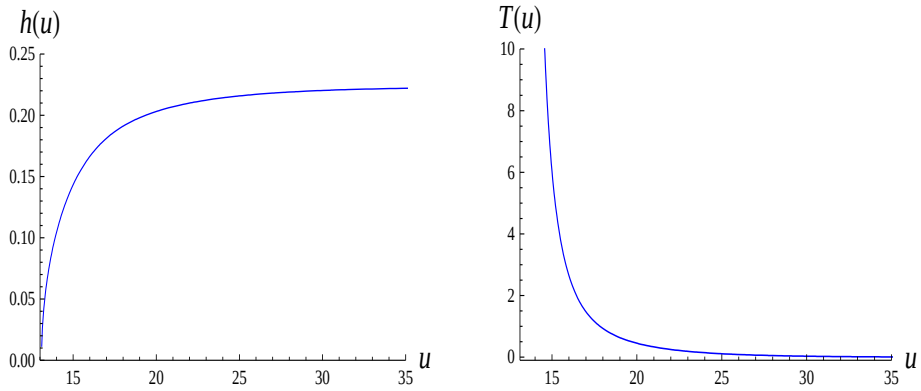

Figure 5.2: The brane profile and the tachyon solution for $u_0 = 12.7$.

5.6 Verification of the UV and IR analytic solutions

From the numerical solutions one can verify that $h(u)$ and $T(u)$ are given by the forms (5.21), (5.22), for $u \sim u_0$. Figure 5.3 shows the impressive fits between the numerical data and the analytical expectations for the powers of $(u - u_0)$ for $h(u)$ and $T(u)$. We have plotted $h(u)/h'(u)$ and $T(u)/T'(u)$, calculated from the numerical solutions, as functions of u. The numerical data are plotted in dashed lines while the theoretical solutions are plotted in solid lines. As one can see, these graphs are linear at the IR end and their slopes turn out to be close to the expected values 2 and -0.5 respectively. In fact, the numerical and the theoretical curves entirely overlap in the IR region of u, as shown in Figure 5.3. At the other end also, namely for large u, one can verify that the numerical solutions have the

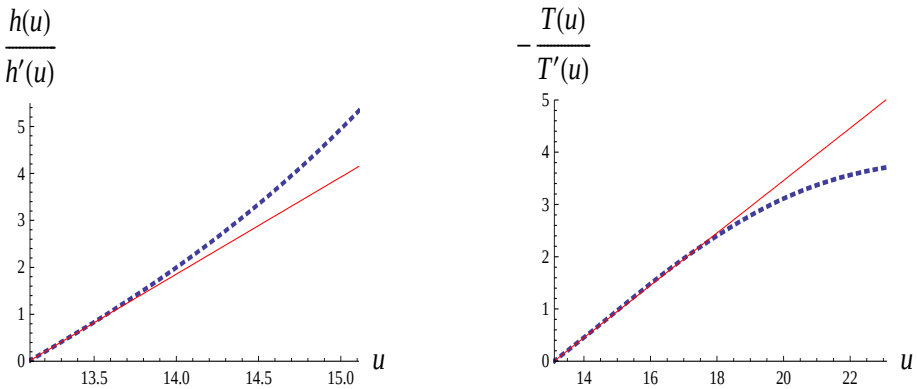

Figure 5.3: Numerical verification of exponents in the IR behaviour of brane profile and tachyon. The fits give the two exponents respectively to be 0.50 and -2.07 for $u = 13.1$.

analytic forms (5.19), (5.17). The goodness of the fits of these analytic forms to numerical data is shown in Figure 5.4 where again the two curves overlap in the asymptotic region of u. The fits yield values of the four parameters: $h_0 = 0.224$, $h_1 = -16068$, $T_+ = 29194.5$, $T_- = -1.25 \times 10^{-4}$ for $u_0 = 13.1$. It may be noted here that the numerical relation between the IR parameter u_0 and the UV parameters may depend on the cutoff u_{max}. However, we find that they are actually quite robust with respect to small changes in u_{max}. We discuss this issue in detail in appendix B.

5.7 Behaviour of the non-normalizable part

For $T_- \neq 0$, extending numerical calculations much beyond the values of u shown in Figure 5.2 meets with a difficulty. It turns out that for small u_0, T_- is positive. Since T_- is the coefficient of the rising exponential in $T(u)$, for a sufficiently large value of u this term dominates and so $T(u)$ begins to rise. Eventually, T becomes so large that the conditions under which the asymptotic solutions (5.19), (5.17) were obtained no longer apply. Figure 5.5 illustrates this; it shows the solutions for $u_0 = 12.7$ for two different large values of u. In Figure 5.5(a), after falling very fast, T rises and then falls again. Almost

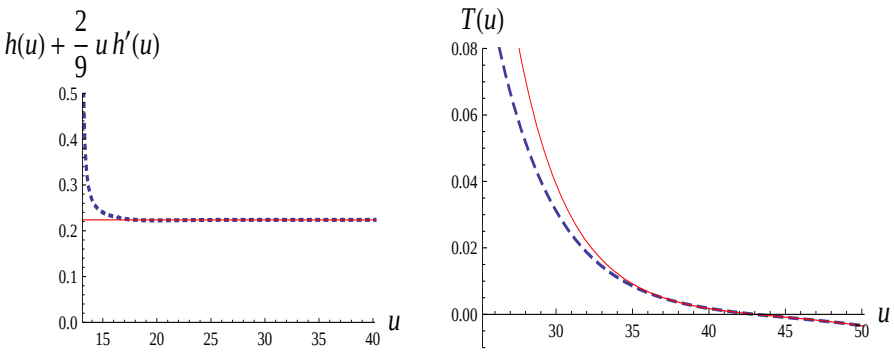

Figure 5.4: Numerical verification of the asymptotic form of the brane profile and the tachyon.

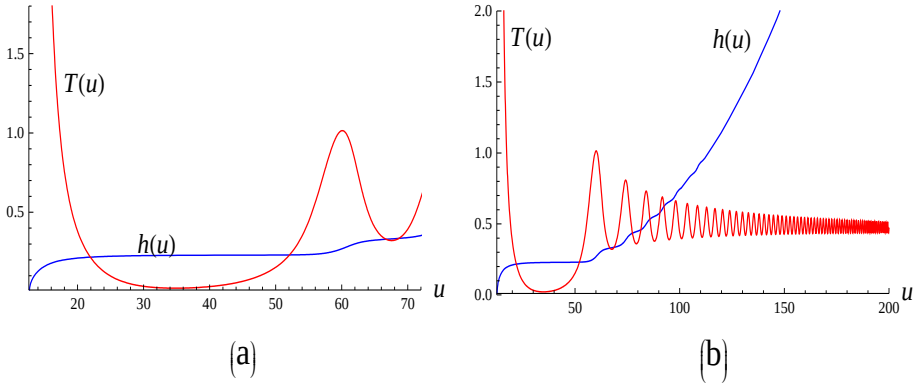

Figure 5.5: Solutions for two different large values of u.

simultaneous with this is a rapid rise of h from one nearly constant value to a higher constant value. Evidently, this behaviour continues indefinitely with u, as can be seen in Figure 5.5(b).

The value of T_- decreases with increasing u_0. This can be easily deduced from the fact that the maximum value of u up to which the asymptotic solutions (5.17), (5.19) apply, namely before the oscillations begin, increases with increasing u_0. Figure 5.6 illustrates this by showing the solutions for increasing values of u_0, close to where T_- is small. As one can see, increasing the value of u_0 by a very small amount, from $u_0 = 13$ to $u_0 = 13.0878$, dramatically increases the threshold for oscillatory behaviour of T from $u \sim 50$ to $u \sim 120$! As u_0 increases further, T_- decreases, becomes zero [1] and

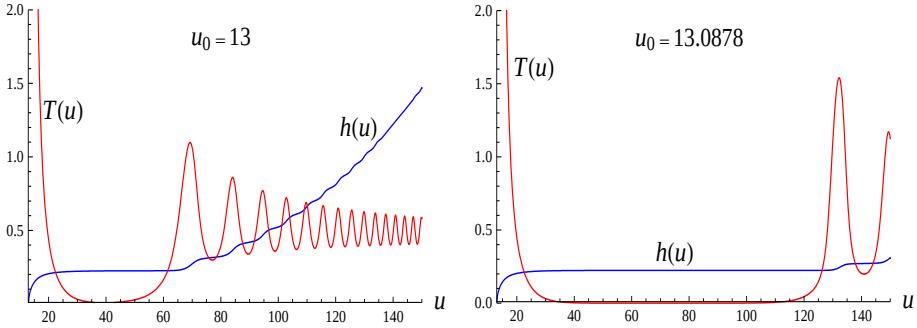

Figure 5.6: Numerical solutions for increasing values of u_0 for positive T_-.

eventually negative. Since we want to interpret T_- as the bare quark mass parameter, negative values for it are allowed. However, a large value for $|T_-|$ will eventually again make T large in magnitude for large enough u. So once again we expect that at some sufficiently large u, T will become so large that the conditions under which the asymptotic solutions (5.17), (5.19) were obtained no longer apply. So, as before, one should find oscillations in $T(u)$, which now start at smaller and smaller u as u_0 grows. This is indeed seen to be the case, as is evident in Figure 5.7. This happens because $|T_-|$ grows with

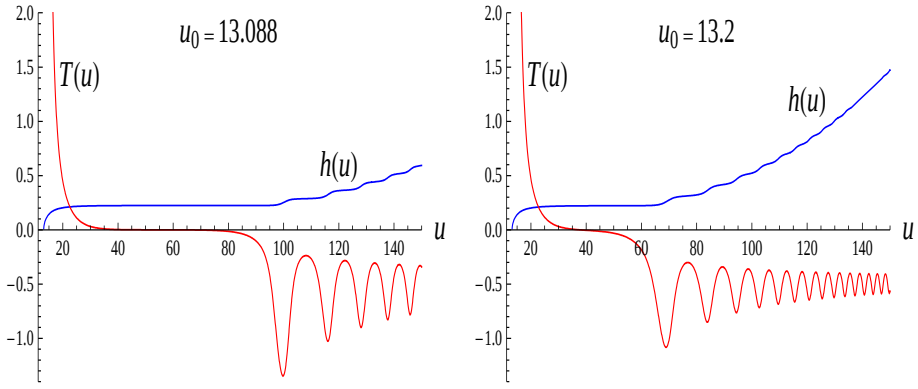

Figure 5.7: Numerical solutions for increasing values of u_0 for negative T_-.

u_0, beyond the value at which it becomes zero. Figure 5.8 shows the change of T_- with u_0. We see

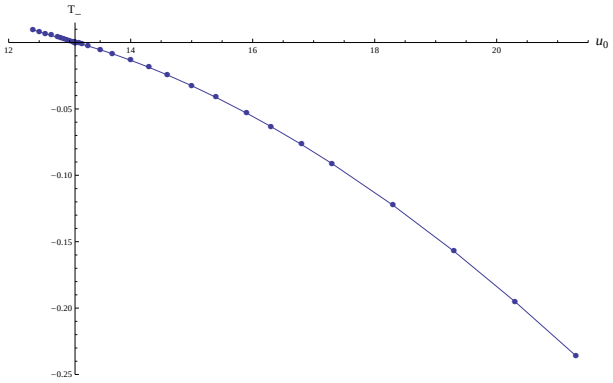

Figure 5.8: T_- as a function of u_0.

that T_- vanishes at $u_0 \sim 13.0878$ and $|T_-|$ grows on both sides away from this value. It is hard to understand what is special about this value of u_0. One might have thought that the role of zero mass would be played by the antipodal configuration, which has $u_0 = u_k$, and is beyond our approximation. It is possible that this is an artifact of using the approximate action, (5.6), valid for a noncompact x^4 coordinate, although the value $u_0 \sim 13.0878$ is fairly large and seems to be within the validity of our approximation. We also note that for negative T_-, negative $T(u)$ can be avoided by imposing a

[1]We have found that $T_- = 1.92 \times 10^{-9}$ at $u_0 \sim 13.0877781$. Fine-tuning u_0 such that T_- is precisely zero is hard and this is the best we could attain. However, the trend is clear from Figure 5.6 and Figure 5.7.

suitable cut-off on u. As we have already discussed, the cut-off is in any case required to fulfill the condition (5.25) so that the asymptotic solutions (5.17), (5.19) may apply.

5.8 Behaviour of the asymptotic brane-antibrane separation

Another interesting feature of the classical solution is the variation of asymptotic brane-antibrane separation, h_0, as a function of u_0. This has been plotted in Figure 5.9. We see that h_0 steadily

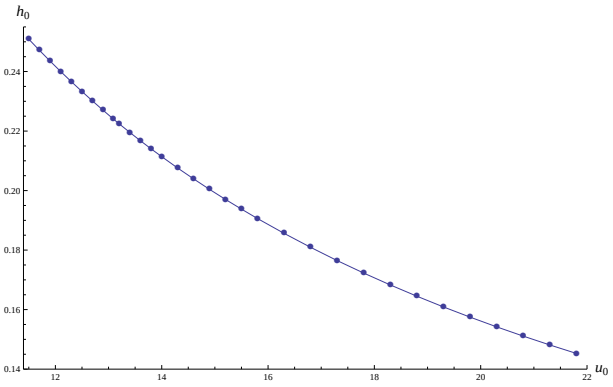

Figure 5.9: h_0 as a function of u_0.

decreases through the special value $u_0 \sim 13.0878$. Although we do not have an analytical formula for the dependence of h_0 on u_0 for large values of the latter, the trend in Figure 5.9 seems to indicate that it decreases to zero as u_0 becomes large. Presumably the brane-antibrane pair overlap and disappear as u_0 goes to infinity. This is consistent with the trend of increasing T_- for increasing values of u_0 (far beyond $u_0 \sim 13.0878$) which we have seen in Figure 5.8, provided this parameter is interpreted as the bare quark mass, since in that case the disappearance of the brane-antibrane pair for $u_0 = \infty$ can be understood as the infinite bare quark mass limit. Within the SS model there is no explanation for this phenomenon. It should be clear from the above discussion that the limit $h_0 \to 0$ does not reduce to the case of overlapping $D8$ branes and $\overline{D8}$ branes considered in [85]. For this case, one must begin afresh with $x_i^4 = 0,\ l = 0$ in the action (5.6).

5.9 Comparison with the Sakai-Sugimoto solution

Finally, we must ensure that the solution with the tachyon has lower energy compared to the SS model. The energy density in the modified model is given by

$$\begin{aligned} E_{\rm T} &= 2V_4R^9\, V(0)\int_{u_0}^{u_{\rm max}} du\, E_{\rm T}(u), \\ E_{\rm T}(u) &= u^{13/4}\,\frac{V(T)}{V(0)}\sqrt{u^{-3/2}+\frac{1}{4}u^{3/2}h'(u)^2+T'(u)^2+T(u)^2h(u)^2}, \end{aligned} \tag{5.26}$$

while for the SS model it is given by

$$\begin{aligned} E_{\rm SS} &= 2V_4R^9\, V(0)\int_{u_0}^{u_{\rm max}} du\, E_{\rm SS}(u), \\ E_{\rm SS}(u) &= u^{13/4}\sqrt{u^{-3/2}+\frac{1}{4}u^{3/2}h'_{\rm SS}(u)^2}. \end{aligned} \tag{5.27}$$

To get these expressions for energy density, we have set $f(u)$ to unity, which is a good approximation for large u_0. Also, in the SS model one must use the solution of the tachyon free equation, $h'_{\rm SS}(u) = 2u_0^4u^{-3/2}(u^8-u_0^8)^{-1/2}$.

Close to u_0, in the IR, the exponentially vanishing tachyon potential suppresses contribution to $E_{\rm T}$ compared to $E_{\rm SS}$. Since the UV solutions for the two models are almost identical [2], one might argue that the energy for the modified model must be lower than that for the SS model. However, for $u \gtrsim u_0$ there is a competition between the exponentially vanishing tachyon potential and the power law increase of the square-root factor coming from $|T'|$ in the integrand $E_{\rm T}(u)$ in (5.26). This results in a local maximum in $E_{\rm T}(u)$ at some value of u, which can be easily estimated analytically. The relevant quantity,

$$e^{-\frac{\pi}{4}u_0^{3/2}(u-u_0)^{-2}}(u-u_0)^{-3},$$

has a maximum at $u = u_0 + (\frac{\pi}{6})^{1/2}u_0^{3/4}$. For small u_0, the position of the maximum is close to u_0, so in this case the argument about the IR behaviour of the integrand in (5.26) is not very clean, except in the very deep IR. But since the position of the maximum grows with increasing u_0 as $u_0^{3/4}$, our argument should hold for large values of u_0, which is precisely where the action for the modified model can be trusted. However, the expression used for estimating the position of the local maximum breaks down if it is too far away from u_0. So, in practice we need to do a numerical calculation to see what the real story is. As we will see in the numerical plots given below, what really happens is that for relatively

[2] There is a caveat here. Strictly speaking this is true only when the coefficient of the non-normalizable term, T_-, in the asymptotic tachyon solution (5.17) vanishes. As we have discussed, when T_- is nonzero, one must introduce a cut-off, $u_{\rm max}$, chosen carefully such that the asymptotic solution is satisfied. In particular, one must ensure T is positive in the region below $u_{\rm max}$. In the calculations reported here and earlier in this section, this is what we have done.

large values of u_0 the integrand $E_T(u)$ increases rapidly at first, then slows down almost to a constant and finally settles into an asymptotic power law increase similar to that of the integrand $E_{SS}(u)$ for the SS model. Moreover, the place where the rapid increase begins shifts to larger values of u as u_0 increases, in accordance with the above expectation.

We have numerically evaluated the integrals in (5.26) and (5.27). Because the relation between u_0 and the asymptotic brane-antibrane separation is different in the two models, a given value of u_0 corresponds to two different values of the latter and vice versa. We have chosen to do the comparison for the same value of the asymptotic brane-antibrane separation in the two models, but the conclusions are similar with the other choice as well. In Figure 5.10 we have plotted numerical solutions for $h(u)$

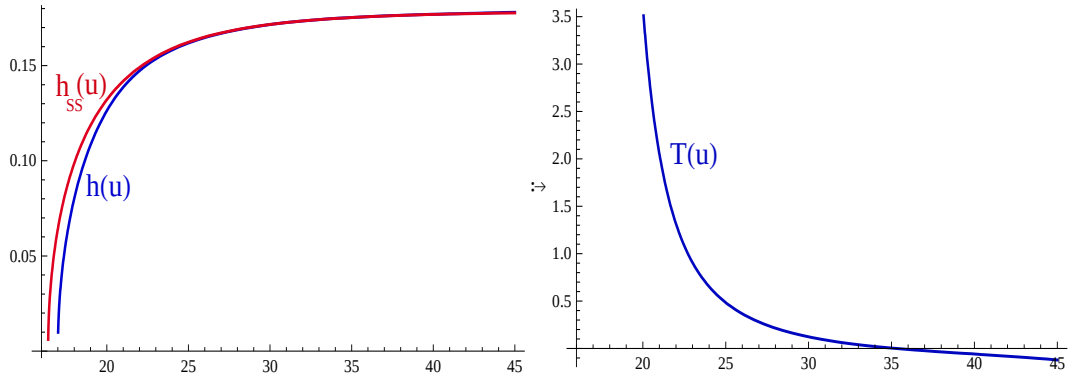

Figure 5.10: $h(u)$ and $T(u)$ profiles for $u_0 = 17$. For comparison, h_{SS} profile has also been plotted after adjusting the value of u_0 to 16.4 for it since this value of u_0 produces the same asymptotic brane-antibrane separation.

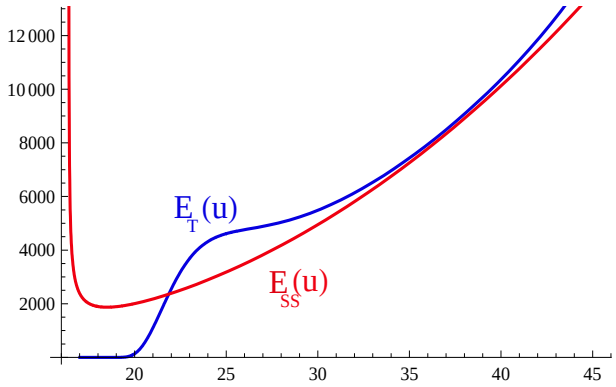

Figure 5.11: The energy density integrands $E_{SS}(u)$ and $E_T(u)$. The rapid rise of the latter in the IR is clearly seen. The divergence between the two curves in the asymptotic region, $u \gtrsim u_{max}$, is due to a nonzero T_-.

and $T(u)$ for $u_0 = 17$. For comparison with the SS model, we have also plotted h_{SS} after adjusting the value of u_0 for it to produce the same value of the asymptotic brane-antibrane separation. The required value turns out to be $u_0 = 16.4$. The corresponding energy density integrands, $E_T(u)$ and

$E_{SS}(u)$, have been plotted in Figure 5.11. We can clearly see the rapid rise of $E(u)$ in the IR, the subsequent flattening out and finally the power-law rise in the asymptotic region. Using $u_{max} = 35.32$ [3], numerical evaluation of the integrals gives $(E_T - E_{SS}) = -300.3$. Therefore, the solution with the tachyon taken into account corresponds to a lower energy state. Similar behaviour is seen for values of $u_0 \gtrsim 14$. Below $u_0 \sim 14$, however, the energy difference becomes very small and even reverses sign. This may be connected with the breakdown of the approximate action in this region, similar to the observation of a zero quark mass at $u_0 \sim 13.01$.

5.10 The chiral condensate

By the standard dictionary of AdS/CFT [55, 50, 94, 95], once we have identified T_- with the quark mass parameter, we should identify T_+ with the chiral condensate. However, it is not clear that the standard rules apply to the present case of a boundary theory which is not a CFT and has a scale. Moreover, the fact that there is no known lift of $D8$ brane to 11-dimensions forces an essential cut-off in the theory with flavours. In fact, for a non-zero value of T_-, the real cut-off is much lower, as we have seen from numerical computations in the last section. Despite these difficulties, we will assume that the identification of sources in the boundary theory with boundary values of bulk fields holds in the theory with cut-off.

To derive an expression for the condensate, we calculate the variation of the action in (5.11) under a general variation of T and use the equations of motion to reduce it to a boundary term:

$$\delta S = -\frac{2V_4}{R^9}\int d^4x \frac{V(T)u^{13/4}}{\sqrt{d_T}} T'(u)\delta T(u)|_{u=u_{max}}. \tag{5.28}$$

Only the UV boundary contributes to the on-shell action; there is no IR contribution because the tachyon potential vanishes exponentially for the diverging tachyon in the IR. For calculation of the chiral condensate, we are only interested in retaining the variation δT_-, so we set δT_+ to zero. Doing this and using (5.17) in (5.28), we get the leading contribution for large u_{max},

$$\delta S \approx \frac{2h_0 V_4 V(0)}{R^9}(T_+ - T_- e^{2h_0 u_{max}})\int d^4x\, \delta T_-. \tag{5.29}$$

On-shell brane actions have UV divergences which need to be removed by the holographic renormalization procedure to get finite answers for physical quantities. One adds boundary counter terms to the brane action to remove the divergences, following a procedure described in [130]. Our

[3] This is the value at which $T(u)$ vanishes. The asymptotic form, (5.17), fits the numerically computed $T(u)$ in the range $33 \le u \le u_{max}$ to better than a percent with the parameter values $h_0 = 0.179$, $T_+ = 28904$, $T_- = -0.0937$. In appendix B, we also study the robustness of the parameters with changes in u_{max}.

on-shell action (5.29) diverges as the cut-off is removed. This is because, as discussed in section 5.4, we are keeping T_+ and $T_- e^{h_0 u_{\rm max}}$ fixed as the cut-off is removed and the last term in (5.29) diverges as $e^{h_0 u_{\rm max}}$ in this limit. The holographic renormalization procedure has been developed for examples with CFT boundary theories. Since, with the $D8$ branes present, there is no 11-dimensional description available to us, it is not clear that the procedure described in [130] is applicable to the present case. We will proceed on the assumption that this is the case. Therefore, to subtract the UV divergent term in (5.29), we will add the following counter term to the boundary action,

$$S_{\rm ct} = \frac{V_4 V(0)}{R^9} \int d^4x \ \sqrt{-\gamma}\, h(u) T^2(u)|_{u_{\rm max}}, \tag{5.30}$$

where $\gamma = -u_{\rm max}^8$ is the determinant of the metric on the 8-dimensional boundary orthogonal to the slice at $u = u_{\rm max}$. Note that the counter terms must be even in powers of the tachyon because of gauge symmetry. Using the solution (5.17) and retaining only the parameter T_-, we find that the variation of the counter term action is

$$\delta S_{\rm ct} = \frac{2h_0 V_4 V(0)}{R^9}(T_+ + T_- e^{2h_0 u_{\rm max}}) \int d^4x\, \delta T_-. \tag{5.31}$$

Adding to (5.29), the divergent term drops out and we get the variation of the renormalized action

$$\delta S_{\rm renorm} \approx \frac{4h_0 V_4 V(0)}{R^9} T_+ \int d^4x\, \delta T_-. \tag{5.32}$$

Note that the variation of the renormalized action is twice as large as it would have been if we had simply dropped the divergent term [4] in (5.29).

We are now ready to calculate an expression for the chiral condensate in terms of the parameters of the tachyon solution. The parameters $T_\pm$ are dimensionless. To construct a parameter of dimension mass from T_-, we introduce a scale μ and define $m_q = \mu|T_-|$. Then, identifying the chiral condensate $\chi \equiv < \bar{q_L} q_R >$, with $\delta S_{\rm renorm}/\mu\delta T_-(x)$, we get

$$\chi \approx \frac{4h_0 V_4 V(0)}{\mu R^9} T_+ \tag{5.33}$$

We see that the parameter T_+ determines the condensate. Figure 5.12 shows a plot of T_+ as a function of T_- for $T_- \sim 0$. Also shown is the variation with u_0 which corresponds to a set of values for T_- and T_+. T_+ seems to attain a maximum value at $T_- = 0$ and drops off rapidly, at least for small values of

[4] In (5.29), it is inconsistent to drop the term proportional to T_- in the limit of large cut-off, holding T_+ and $T_- e^{h_0 u_{\rm max}}$ fixed. In fact, it is the T_- term that dominates in the action (5.29) in this limit. Taking a different limit that allows one to simply drop this term creates difficulties in the calculation of the mass of pseudo-Goldstone boson as we will see in section 6.3 in the next chapter. Consistency with the chiral condensate calculation then demands that the term proportional to $T_+ T_-$ be dropped in the mass calculation since it is smaller than the T_+^2 term.

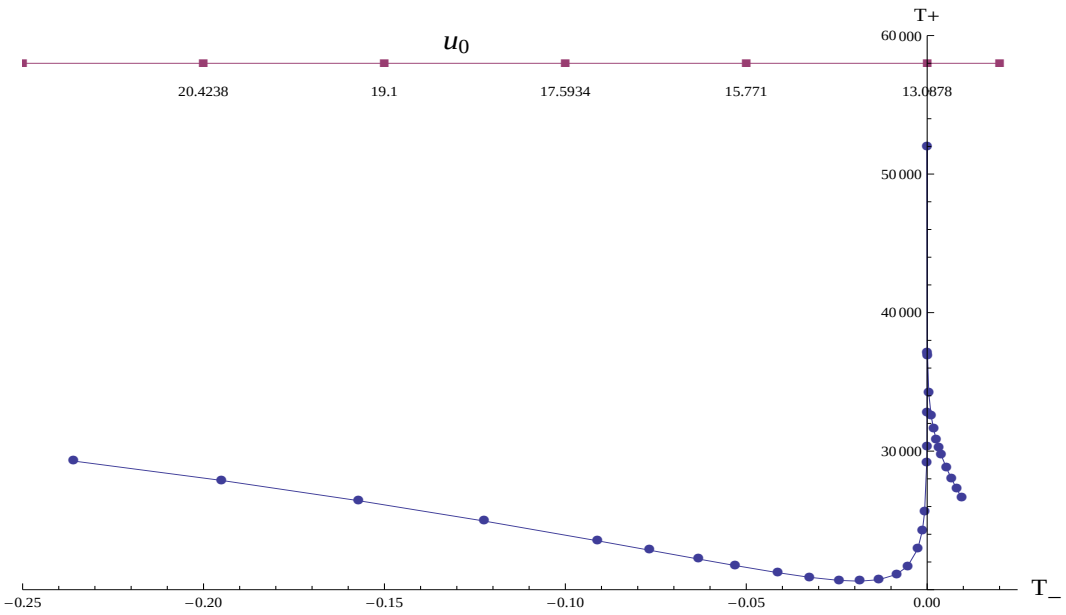

Figure 5.12: T_+ as a function of T_-.

$|T_-|$.

Let us now summarise the discussion in this chapter. In the work presented in this chapter, we have proposed a modification of the SS model that may allow one to consider a non-zero quark mass within the setup. The model also provides an explicit order parameter for χSB. The SS model, on the other hand, is known to lack both of these features. Our model involves a study of the $D8 - \overline{D8}$ open string tachyon dynamics in the $D4 - D8 - \overline{D8}$ system. The open string tachyon, that transforms as a bifundamental under the flavor group, has the right quantum numbers to give rise to an order parameter for χSB. Further, it can couple to a chiral bilinear in such a way that its condensation gives rise to a 'quark' mass term.

In this chapter, we studied the vacuum configuration of the $D8-\overline{D8}$ profile given by the separation, $h(u)$ and the tachyon, $T(u)$. We saw that even in the presence of the tachyon, the geometrical picture of chiral symmetry breaking of the SS model is essentially preserved. Asymptotically separated $D8$ and $\overline{D8}$ branes meet each other in the bulk of the background $D4$ geometry. Further, there is a vacuum solution for the tachyon $T(u)$ which blows up in the bulk at the point in which the branes meet. The UV behaviour is associated with normalisable and non-normalisable parts, T_+ and T_- respectively. Similarly, the UV behaviour of $h(u)$ is associated with two parameters. The IR behaviour of $T(u)$ and $h(u)$, on the other hand, is associated with just a single parameter u_0. Therefore, all the four parameters in the UV are determined by the IR parameter u_0.

Using AdS/CFT correspondence, we expect that the parameter T_- sources the chiral bilinear and is hence the 'quark' mass. We find that increasing u_0 corresponds to tuning the parameter T_- to large values. This implies increasing the parameter T_- removes the flavor branes to infinity. This is found

to be consistent with the expectation that the flavors become non-dynamical in this limit. We also find that the chiral condensate, obtained after differentiating the renormalised action with T_-, is given by a factor of T_+, the parameter associated with normalisable part of the tachyon solution. We find that for a small quark mass, the chiral condensate decreases with an increase in the mass.

Chapter 6

Mesons in the modified SS model

Having introduced the tachyon modified Sakai-Sugimoto model, in this chapter, let us discuss the spectra for various low spin mesons described by the fluctuations of the flavour branes around the classical solution. In the last chapter, we obtained the classical vacuum configuration of a $D8$-$\overline{D8}$ pair, described by $h(u)$ and $T(u)$, with UV behaviour given by equations (5.19) and (5.17) and IR behaviour governed by equations (5.21) and (5.22). In this chapter, our aim is to study the spectrum of fluctuations around this configuration and, in particular, identify the meson spectra. To proceed we first write the complex tachyon τ in terms of its magnitude and phase, $\tau = T(u)e^{i\theta}$. Then, we re-express the brane-antibrane action (5.6) in terms of the gauge field combinations $V = (A_L + A_R)$ and $A = (A_L - A_R - \partial\theta)$. The field V is invariant under the axial transformations of the flavor gauge group U(1) $\times$ U(1) but transforms (as an adjoint) under the vector subgroup. On the other, the field A is a gauge invariant object (for the full flavor gauge group) since the gauge transformations of the combination A_L-A_R is compensated by the change of θ under gauge transformation. We will treat V and A as small fluctuations and expand upto quadratic order in these fields. This gives the following action for the fluctuations:

$$\begin{aligned}\Delta S_{\text{gauge}} &= -\int d^4x\, du\Big[a(u)A_u^2 + b(u)A_\mu^2 + c(u)\left((F^V_{\mu\nu})^2 + (F^A_{\mu\nu})^2\right) + e(u)F^A_{\mu u}A^\mu \\ &\quad + d(u)\left((F^V_{\mu u})^2 + (F^A_{\mu u})^2\right)\Big], \end{aligned} \tag{6.1}$$

where

$$a(u) = R^{-15}V_4V(T)u^{13/4}\frac{T^2}{\sqrt{d_T}}, \tag{6.2}$$

$$b(u) = R^{-3}V_4V(T)u^{7/4}\sqrt{d_T}\frac{T^2}{Q}\left(1 + \frac{f^2T^2h^2h'^2}{4d_T}u^3\right), \tag{6.3}$$

$$c(u) = \frac{R^3}{8} V_4 V(T) u^{1/4} \sqrt{d_T}, \tag{6.4}$$

$$d(u) = R^{-9} V_4 V(T) u^{7/4} \frac{Q}{4\sqrt{d_T}}, \tag{6.5}$$

$$e(u) = R^{-6} V_4 V(T) u^{13/4} \frac{f T^2 h h'}{2\sqrt{d_T}}. \tag{6.6}$$

Here $F^V_{\mu\nu}$ is the usual field strength for the U(1) vector gauge field V and $F^A_{\mu\nu}$ is the field strength for the U(1) axial vector field A. The mixed components are given by

$$F^V_{\mu u} = -F^V_{u\mu} = \partial_\mu V_u - R^3 \partial_u V_\mu, \quad F^A_{\mu u} = -F^A_{u\mu} = \partial_\mu A_u - R^3 \partial_u A_\mu. \tag{6.7}$$

The relative factor of R^3 simply reflects the change of variables (5.10).

As we shall see, the gauge field $V_\mu(x,u)$ gives rise to a tower of vector mesons while the fields $A_\mu(x,u)$ and $A_u(x,u)$, which are gauge invariant, lead to towers of axial-vector and pseudoscalar mesons respectively. Note that the coefficients $a(u)$, $b(u)$ and $e(u)$ vanish if the tachyon is set to zero. In the absence of the tachyon, the vector and axial vector mesons acquire masses because of a nonzero $d(u)$, but there is always a massless pseudoscalar Goldstone boson arising from A_u as can be seen on comparing the action to the strongly coupled Sakai-Sugimoto model discussed before. The presence of the tachyon is thus essential to give a mass to the analog of pion. Also note that with the tachyon present, the masses of the vector and axial vector mesons are in principle different.

6.1 Vector mesons

The vector field ($V_\mu(x,u)$, $V_u(x,u)$) is not gauge invariant. We will choose the gauge in which $V_u(x,u) = 0$. Note that this still allows the freedom to make u-independent gauge transformations. We will discuss this further in the following. Expanding in modes, we have

$$V_\mu(x,u) = \sum_m V^{(m)}_\mu(x) W_m(u), \tag{6.8}$$

where $\{W_m(u)\}$ form a complete set of basis functions. These satisfy orthonormality conditions which will be determined presently. The fields $\{V^{(m)}_\mu(x)\}$ form a tower of vector mesons in the physical $(3+1)$-dimensional space-time. In terms of these fields, the vector part of the action (6.1) takes the form,

$$\Delta S^V_{\text{gauge}} = -\int d^4x \sum_{m,n} \Big[Q^V_{mn} F^{V(m)}_{\mu\nu} F^{V(n)\mu\nu} + L^V_{mn} V^{(m)}_\mu V^{(n)\mu} \Big], \tag{6.9}$$

where $F^{V(m)}_{\mu\nu}$ are the usual (3 + 1)-dimensional U(1)-invariant field strengths for the vector potentials $\{V^{(m)}_\mu\}$. Also, we have defined

$$Q^V_{mn} = \int du\, c(u) W_m(u) W_n(u), \quad L^V_{mn} = R^6 \int du\, d(u) W'_m(u) W'_n(u). \tag{6.10}$$

Let us now choose the basis functions $\{W_m(u)\}$ to satisfy the eigenvalue equation

$$-R^6 \left(d(u) W'_m(u)\right)' = 2\lambda^V_m c(u) W_m. \tag{6.11}$$

With this, we get

$$\begin{aligned} L^V_{mn} &= R^6 \Big(d(u) W'_m(u) W_n(u) \Big)_{\partial u} + 2\lambda^V_m Q^V_{mn} \\ &= \frac{1}{2}\Big[R^6 \Big(d(u) W'_m(u) W_n(u) \Big)_{\partial u} + 2\lambda^V_m Q^V_{mn} \Big] + m \leftrightarrow n, \end{aligned} \tag{6.12}$$

where, ∂u refers to boundaries in the u-direction. The second line follows from the symmetry of L^V_{mn} and Q^V_{mn} under the interchange of indices m and n.

Let us now come back to the residual symmetry of making u-independent gauge transformations which is still available after fixing the gauge $V_u = 0$. We can use this freedom, together with the requirement of finiteness of the action, (6.9), to gauge away the zero mode in the expansion (6.8) that corresponds to zero eigenvalue $\lambda^V_m = 0$. Let this mode correspond to $m = 0$. According to (6.11), $W_0(u)$ goes to a constant at $u \to \infty$. Since $c(u) \sim u^{-1/2}$ at large u, Q^V_{00} diverges. Then, finiteness of the action (6.9) requires that we set $F^{V(0)}_{\mu\nu} = 0$. Therefore, $V^{(0)}_\mu$ is a pure gauge which can be gauged away using the residual gauge freedom.

For the nonzero modes we may, without loss of generality, choose

$$Q^V_{mn} = \frac{1}{4}\delta_{mn}. \tag{6.13}$$

Then, using the requirement of finiteness of L^V_{mn} in (6.12), gives

$$L^V_{mn} = \frac{1}{2}\lambda^V_m \delta_{mn}. \tag{6.14}$$

Finally, using (6.13) and (6.14) in (6.9), we get

$$\Delta S^V_{\text{gauge}} = -\int d^4x \sum_m \Big[\frac{1}{4} F^{V(m)}_{\mu\nu} F^{V(m)\mu\nu} + \frac{1}{2}\lambda^V_m V^{(m)}_\mu V^{(m)\mu} \Big]. \tag{6.15}$$

This is the expected infinite tower of massive vector mesons.

6.2 Axial vector and pseudoscalar mesons

As we have already noted, A_μ and A_u are gauge invariant. There is no gauge freedom that can put any of these to zero and both provide physical fields. Expanding in modes, we have

$$A_\mu(x,u) = \sum_m A_\mu^{(m)}(x)P_m(u), \quad A_u(x,u) = \sum_i \phi^{(i)}(x)S_i(u), \tag{6.16}$$

where $\{P_m(u)\}$ and $\{S_i(u)\}$ form complete sets of basis functions. These satisfy orthonormality conditions which will be determined presently. The fields $\{A_\mu^{(m)}(x)\}$ and $\{\phi^{(i)}(x)\}$ form towers of axial vector and pseudoscalar mesons in the physical (3 + 1)-dimensional space-time. In terms of these fields, the axial-vector and pseudoscalar part of the action (6.1) takes the form,

$$\begin{aligned}\Delta S^A_{\text{gauge}} &= -\int d^4x \Big[Q^A_{mn}F^{A(m)}_{\mu\nu}F^{A(n)\mu\nu} + L^A_{mn}A^{(m)}_\mu A^{(n)\mu} + T_{ij}\phi^{(i)}\phi^{(j)} \\ &\quad + K_{ij}\partial_\mu\phi^{(i)}\partial^\mu\phi^{(j)} + J_{mi}A^{(m)\mu}\partial_\mu\phi^{(i)}\Big],\end{aligned} \tag{6.17}$$

where the repeated indices m, n, i and j are summed over. $F^{A(m)}_{\mu\nu}$ are the usual (3 + 1)-dimensional U(1)-invariant field strengths for the axial-vector fields $\{A^{(m)}_\mu\}$. Also, we have defined

$$\begin{aligned}Q^A_{mn} &= \int du\, c(u)P_m(u)P_n(u), \\ L^A_{mn} &= \int du \left(R^6 d(u)P'_m(u)P'_n(u) + (b(u) + \frac{1}{2}R^3 e'(u))P_m(u)P_n(u)\right), \\ J_{mi} &= \int du \left(e(u)P_m(u) - 2R^3 d(u)P'_m(u)\right)S_i(u), \\ K_{ij} &= \int du\, d(u)S_i(u)S_j(u), \\ T_{ij} &= \int du\, a(u)S_i(u)S_j(u).\end{aligned} \tag{6.18}$$

We note that because of the last term in (6.17), the longitudinal component of $A^{(m)}_\mu$ and $\phi^{(i)}$ mix. So we need to define new field variables in terms of which the action (6.17) is diagonal. Before we do that, let us first note that the axial vector potential $A_\mu(x,u)$ has a possible zero mode provided the corresponding (3 + 1)-dimensional field strength vanishes, for reasons explained in the previous subsection. Hence the zero mode, which we shall denote by $A^{(0)}_\mu$, can only have a longitudinal component. The zero mode is gauge-invariant and, because of its mixing with the pseudoscalars, plays a special role. Let us see this in some detail.

Let us choose the basis functions $\{P_m(u)\}$ to satisfy the eigenvalue equation

$$-R^6\Big(d(u)P'_m(u)\Big)' + \Big(b(u) + \frac{1}{2}R^3 e'(u)\Big)P_m(u) = 2\lambda^A_m c(u)P_m(u). \tag{6.19}$$

Using this we see that

$$\begin{aligned} L^A_{mn} &= R^6\Big(d(u)P'_m(u)P_n(u)\Big)_{\partial u} + 2\lambda^A_m Q^A_{mn} \\ &= \frac{1}{2}\Big[R^6\Big(d(u)P'_m(u)P_n(u)\Big)_{\partial u} + 2\lambda^A_m Q^A_{mn}\Big] + m \leftrightarrow n, \end{aligned} \tag{6.20}$$

where, as before, ∂u refers to boundaries in the u-direction and the second line follows from the symmetry of L^A_{mn} and Q^A_{mn}. The zero mode $A^{(0)}_\mu$ is conjugate to the eigenfunction $P_0(u)$ which satisfies the equation

$$-R^6\Big(d(u)P'_0(u)\Big)' + \Big(b(u) + \frac{1}{2}R^3 e'(u)\Big)P_0(u) = 0. \tag{6.21}$$

If there is no solution to this equation, then the zero mode does not exist and we should proceed directly to diagonalize the action (6.17). If, however, a solution $P_0(u)$ to this equation exists and is such that it goes to a constant at infinity, then the zero mode $A^{(0)}_\mu$ exists. Since Q^A_{00} blows up for this, $A^{(0)}_\mu$ must be purely longitudinal, for a reason identical to that discussed in the vector case. We make this explicit by writing it in terms of a pseudoscalar field, $A^{(0)}_\mu = \partial_\mu \alpha(x)$.

The terms in the action (6.17) which contain $\alpha(x)$ can be separated out. Let us first see if there is any mixing between the zero mode and non-zero modes of the axial-vector fields. Since the field strength vanishes for the zero mode, the only possible mixing can arise from the L^A_{0n} term for $n \neq 0$. It can be seen from the first line of equation (6.20) that L^A_{0n} can get any contribution only from the boundary term. The contribution at $u = u_0$ vanishes as the tachyon potential vanishes. As we will see later, the zero mode exists when T_- is zero for the background tachyon solution. The solution is such that $d(u)P'_0(u)$ goes to a constant as $u \to \infty$. Further, $P_n(u)$ for $n \neq 0$ vanishes at $u \to \infty$ so that $L^A_{0n} = 0$. Therefore, the only terms containing $\alpha(x)$ are:

$$L^A_{00}\partial_\mu\alpha\partial^\mu\alpha + \sum_i J_{0i}\partial_\mu\alpha\partial^\mu\phi^{(i)}.$$

Without loss of generality, we may choose $L^A_{00} = 1/2$ (to get the normalization of the kinetic term of $\phi^{(0)}$ right). Then, we can rewrite the above as

$$\frac{1}{2}\partial_\mu\pi\partial^\mu\pi - \frac{1}{2}\sum_{i,j} J_{0i}J_{0j}\partial_\mu\phi^{(i)}\partial^\mu\phi^{(j)}, \tag{6.22}$$

where $\pi \equiv (\alpha + \sum_i J_{0i}\phi^{(i)})$.

With the zero modes explicitly separated out in this way, for the nonzero modes we may, without loss of generality, choose

$$Q^A_{\bar{m}\bar{n}} = \frac{1}{4}\delta_{\bar{m}\bar{n}}. \tag{6.23}$$

Note that $c(u) \sim u^{-1/2}$ as $u \to \infty$ so that normalizability of the kinetic term requires that $P_{\bar{m}}(u)$ should fall faster than $u^{-1/4}$ at large u. Equation (6.19) furher implies that $d(u)P'_{\bar{m}}(u) \lesssim u^{1/2}P_{\bar{m}}(u)$ so that the boundary term in $L^A_{\bar{m}\bar{n}}$ vanishes. (The contribution from boundary at u_0 anyway vanishes because of the tachyon potential.) Therefore, on using (6.23) in (6.20), we get

$$L^A_{\bar{m}\bar{n}} = \frac{1}{2}\lambda^A_{\bar{m}}\delta_{\bar{m}\bar{n}}. \tag{6.24}$$

Putting (6.22), (6.23) and (6.24) in the action (6.17), we get

$$\begin{aligned}\Delta S^A_{\text{gauge}} &= -\int d^4x \left[\left(T_{ij}\phi^{(i)}\phi^{(j)} + \frac{1}{4}F^{A(\bar{m})}_{\mu\nu}F^{A(\bar{m})\mu\nu} + \frac{1}{2}\lambda^A_{\bar{m}}A^{(\bar{m})}_\mu A^{(\bar{m})\mu}\right)\right. \\ &\left. + \frac{1}{2}\partial_\mu\pi\partial^\mu\pi + \left(\tilde{K}_{ij}\partial_\mu\phi^{(i)}\partial^\mu\phi^{(j)} + J_{\bar{m}i}A^{(\bar{m})\mu}\partial_\mu\phi^{(i)}\right)\right],\end{aligned} \tag{6.25}$$

where $\tilde{K}_{ij} = (K_{ij} - \frac{1}{2}J_{0i}J_{0j})$. The above action describes a massless particle, π, besides other massive particles. The existence of this massless particle depends on the existence of a solution to the equation (6.21), and reproduction of the canonical kinetic term for it through the normalization condition

$$R^6\Big(d(u)P_0(u)P'_0(u)\Big)_{\partial u} = \frac{1}{2}. \tag{6.26}$$

Later we will see that the existence of the desired solution $P_0(u)$ depends on the absence of a non-normalizable part in $T(u)$.

To diagonalize the action (6.25) for the massive modes, we define the new variables

$$A^{(\bar{m})}_\mu = \tilde{A}^{(\bar{m})}_\mu - \sum_i (\lambda^A_{\bar{m}})^{-1}J_{\bar{m}i}\partial_\mu\phi^{(i)}. \tag{6.27}$$

Putting in (6.25), we get

$$\begin{aligned}\Delta S^A_{\text{gauge}} &= -\int d^4x \left[\left(T_{ij}\phi^{(i)}\phi^{(j)} + \frac{1}{4}F^{\tilde{A}(\bar{m})}_{\mu\nu}F^{\tilde{A}(\bar{m})\mu\nu} + \frac{1}{2}\lambda^A_{\bar{m}}\tilde{A}^{(\bar{m})}_\mu\tilde{A}^{(\bar{m})\mu}\right)\right. \\ &\left. + \frac{1}{2}\partial_\mu\pi\partial^\mu\pi + K'_{ij}\partial_\mu\phi^{(i)}\partial^\mu\phi^{(j)}\right],\end{aligned} \tag{6.28}$$

where $K'_{ij} = (\tilde{K}_{ij} - \frac{1}{2}\sum_{\bar{m}}(\lambda^A_{\bar{m}})^{-1}J_{\bar{m}i}J_{\bar{m}j})$. The modes have now been decoupled. To get the standard

action for massive pseudoscalars we may, without loss of generality, set

$$T_{ij} = \frac{1}{2}\lambda_i^{\phi}\delta_{ij}, \tag{6.29}$$

and

$$K'_{ij} = \frac{1}{2}\delta_{ij} = K_{ij} - \frac{1}{2}J_{0i}J_{0j} - \frac{1}{2}\sum_{\bar{m}}(\lambda_{\bar{m}}^{A})^{-1}J_{\bar{m}i}J_{\bar{m}j} \tag{6.30}$$

Equation (6.30) can be rewritten in a more conventional form as follows. We define

$$\psi_i(u) \equiv \sum_{\bar{m}}(\lambda_{\bar{m}}^{A})^{-1}P_{\bar{m}}(u)J_{\bar{m}i} + P_0(u)J_{0i}, \tag{6.31}$$

and using (6.19) note that it satisfies the equation

$$-R^6\Big(d(u)\psi_i'(u)\Big)' + \Big(b(u) + \frac{1}{2}R^3e'(u)\Big)\psi_i(u) = \frac{1}{2}e(u)S_i(u) + R^3\Big(d(u)S_i(u)\Big)'. \tag{6.32}$$

Using (6.31) in (6.30), we get

$$\delta_{ij} = \int du\Big(d(u)S_i(u)(S_j(u) + R^3\psi_j'(u)) - \frac{1}{2}e(u)S_i(u)\psi_j(u)\Big) + i \leftrightarrow j. \tag{6.33}$$

In terms of new variables defined by

$$S_i(u) \equiv R^3\eta_i'(u), \qquad \theta_i(u) \equiv \psi_i(u) + \eta_i(u), \tag{6.34}$$

(6.33) can be written as

$$\int du\ \eta_i'(u)\Big(R^6d(u)\theta_j'(u) - \frac{1}{2}R^3e(u)(\theta_j(u) - \eta_j(u))\Big) + i \leftrightarrow j = \delta_{ij}. \tag{6.35}$$

Moreover, in terms of these variables the differential equation (6.32) reads

$$-R^6\Big(d(u)\theta_i'(u)\Big)' + \Big(b(u) + \frac{1}{2}R^3e'(u)\Big)\Big(\theta_i(u) - \eta_i(u)\Big) - \frac{1}{2}R^3e(u)\eta_i'(u) = 0, \tag{6.36}$$

From these two equations one can obtain the orthonormality condition

$$\begin{aligned}\int du\Big(&R^6d(u)\theta_i'(u)\theta_j'(u) + (b(u) + \frac{1}{2}R^3e'(u))(\theta_i(u) - \eta_i(u))(\theta_j(u) - \eta_j(u))\\ &-\frac{1}{2}R^3e(u)\eta_i'(u)(\theta_j(u) - \eta_j(u)) - \frac{1}{2}R^3e(u)\eta_j'(u)(\theta_i(u) - \eta_i(u))\Big) = \frac{1}{2}\delta_{ij}.\end{aligned} \tag{6.37}$$

Also, rewriting (6.29) in terms of the new variables, we have

$$R^6 \int du\, a(u)\eta_i'(u)\eta_j'(u) = \frac{1}{2}\lambda_i^\phi \delta_{ij}. \tag{6.38}$$

Finally, (6.35) and (6.38) give

$$R^6 a(u)\eta_j'(u) = \lambda_j^\phi\Big(R^6 d(u)\theta_j'(u) - \frac{1}{2}R^3 e(u)(\theta_j(u) - \eta_j(u))\Big). \tag{6.39}$$

Equations (6.36) and (6.39) are the final form of the eigenvalue equations and (6.37) and (6.38) are the orthonormality conditions in the pseudoscalar sector.

It is interesting to note from (6.36) that if η is constant, then the variable $(\theta - \eta)$ satisfies a differential equation that is identical to the equation (6.21) satisfied by the zero mode P_0. Also, using (6.36) and (6.37) one can show that for constant η, $(\theta - \eta)$ satisfies the normalization condition (6.26). From (6.39) it follows that if η is constant, the eigenvalue λ^ϕ vanishes. Thus, the presence of a massless pseudoscalar can be naturally considered to be identical to the question of the existence of a solution to the equations (6.36)-(6.39) with zero eigenvalue, and so it becomes a part of the spectrum in the pseudoscalar tower of states. Hence, the action in this sector can be written in the form

$$\begin{aligned} \Delta S^{A}_{\text{gauge}} \;=\; -\int d^4x \Big[&\frac{1}{4}F^{\tilde{A}(\bar{m})}_{\mu\nu}F^{\tilde{A}(\bar{m})\mu\nu} + \frac{1}{2}\lambda^{A}_{\bar{m}}\tilde{A}^{(\bar{m})}_{\mu}\tilde{A}^{(\bar{m})\mu} \\ &+\frac{1}{2}\partial_\mu\phi^{(i)}\partial^\mu\phi^{(i)} + \frac{1}{2}\lambda_i^\phi\phi^{(i)}\phi^{(i)}\Big], \end{aligned} \tag{6.40}$$

where the repeated indices are summed over. Note that we have dropped the field $\pi(x)$, but extended the sum over i to cover a zero mode as well. If there is a solution to the equations (6.36)-(6.39) with constant η_0 and $\lambda_0^\phi = 0$, then a massless pseudoscalar Goldstone boson will reappear as the zero mode $\phi^{(0)}$ in the pseudoscalar tower. Otherwise, the lowest mode in this sector will be massive, whose mass can be computed as in the following section.

6.3 Relation between mass of pseudo-Goldstone boson and non-normalizable part of tachyon

In this section we will derive a relation between the mass of pseudo-Goldstone boson and the non-normalizable part of tachyon parametrized by T_-. This will give us further evidence for identifying the parameters T_+ and T_- with the chiral condensate and quark mass respectively. We first note that for $T(u) = 0$, $a(u)$ vanishes and hence λ_i^ϕ also vanishes by (6.39). However, as we will see from the following calculations, $T(u) = 0$ is a sufficient condition, but not necessary to guarantee the presence

of a massless Goldstone boson. The necessary condition is that the non-normalizable piece in $T(u)$ should be absent, i.e. $T_- = 0$.

Let us assume that $T(u) \neq 0$ so that $a(u) \neq 0$. Then, (6.39) can be used to solve for $\eta_i(u)$ in terms of $\psi_i(u)$, which is related to $\theta_i(u)$ and $\eta_i(u)$ by (6.34). We get,

$$\eta_i'(u) = \frac{\lambda_i^\phi}{a(u) - \lambda_i^\phi d(u)}\left(d(u)\psi_i'(u) - \frac{e(u)}{2R^3}\psi_i(u)\right) \tag{6.41}$$

Let us now denote by λ_0^ϕ the lowest mass eigenvalue. The corresponding eigenfunctions are $\psi_0(u)$ and $\eta_0(u)$. Assuming $\lambda_0^\phi \ll a(u)/d(u)$ [1], we can approximate the above equation for $\eta_0(u)$:

$$\eta_0'(u) \approx \frac{\lambda_0^\phi}{a(u)}\left(d(u)\psi_0'(u) - \frac{e(u)}{2R^3}\psi_0(u)\right) \tag{6.42}$$

If we know $\psi_0(u)$, then using the above in (6.38) we can compute the mass. Now, $\psi_0(u)$ satisfies the following differential equation, which can be obtained from (6.36) using (6.42) and the approximation $\lambda_0^\phi \ll a(u)/d(u)$:

$$-R^6\left(d(u)\psi_0'(u)\right)' + \left(b(u) + \frac{1}{2}R^3 e'(u)\right)\psi_0(u) \approx 0. \tag{6.43}$$

Also, using (6.43) and the approximation under which it was obtained, the normalization condition on $\psi_0(u)$ given by (6.37) can be approximated as

$$R^6 d(u)\psi_0'(u)\psi_0(u)|_{u=u_{\max}} \approx \frac{1}{2}. \tag{6.44}$$

These equations cannot be solved analytically in general. However, analytic solutions can be obtained in the IR and UV regimes. In the UV regime, for $u \lesssim u_{\max}$, we use (5.17) and (5.19) to approximate the coefficients in (6.43); we get

$$b(u) \approx \frac{V_4 V(0)}{R^3} u T^2(u), \quad d(u) \approx \frac{V_4 V(0)}{4R^9} u^{5/2}, \quad e(u) \approx \frac{9V_4 V(0)}{4R^6} h_0 h_1 u^{-3/2} T^2(u). \tag{6.45}$$

In writing these, we have used $f(u) \approx 1$, which is a good approximation for large u. We see that we can clearly neglect $e(u)$ compared to $b(u)$ in (6.43), while $b(u)$ is itself negligible compared to $d(u)$. Using these approximations in (6.43) and (6.44) then gives

$$-\left(u^{\frac{5}{2}}\psi_0'(u)\right)' \approx 0, \quad \frac{V_4 V(0)}{4R^3} u^{\frac{5}{2}}\psi_0'(u)\psi_0(u)|_{u=u_{\max}} \approx \frac{1}{2}, \tag{6.46}$$

[1] This approximation can be justified a posteriori by the solution because the eigenvalue λ_0^ϕ turns out to be parametrically much smaller by a factor of $1/R^3$, see (6.57), compared to the ratio $a(u)/d(u)$.

which are solved by

$$\psi_0(u) \approx c_0 - \frac{1}{3c_0}\frac{4R^3}{V_4 V(0)}u^{-3/2}. \tag{6.47}$$

In the above expression c_0 is a parameter which is related to the decay constant of the analog of pion. This can be argued as follows. The decay constant f_π is related to a two-point correlator of the axial-vector current as

$$\int d^4x\, e^{ik.x}\langle 0|j_A^{a\mu}(x)j_A^{b\mu}(0)|0\rangle = f_\pi^2\, k^\mu k^\nu\, \delta^{ab}. \tag{6.48}$$

Using the AdS/CFT dictionary, one can use duality of the axial vector current in the boundary theory to the axial vector bulk field. The axial current correlator can then be computed from the action (6.17), evaluated on-shell, by differentiating twice with respect to the transverse part of the axial vector field on the UV boundary. This is the source which couples to the axial current on the boundary. The source arises from the same zero mode solution, $P_0(u)$, which we discussed in connection with a possible zero mode (the pseudo-Goldstone boson analogous to pion) in the longitudinal component of the axial gauge field. $P_0(u)$ satisfies the equation (6.21), which is identical to that satisfied by $\psi_0(u)$, (6.43). However, the boundary condition now is different; it is the boundary condition for a source, $P_0(u_{\rm max}) = 1$. In addition, one imposes the condition

$$R^6 d(u)P_0'(u)P_0(u)|_{u=u_{\rm max}} \approx \frac{f_\pi^2}{2}, \tag{6.49}$$

which is required to reproduce the correct zero momentum axial current correlator. This follows from the action (6.17). Now, $P_0(u)$ satisfies (6.21) and the condition (6.49) if we set $P_0(u) = f_\pi\psi_0(u)$. Then, requiring $P_0(u_{\rm max}) = 1$ gives $c_0 = 1/f_\pi$.

In the IR regime, $u \gtrsim u_0$, we use (5.21) and (5.22) to approximate the coefficients in (6.43); we get

$$b(u) \approx \frac{\pi^{3/2}V_4 u_0^{17/4}}{26R^3}\frac{V(T)}{(u-u_0)^4}, \quad d(u) \approx \frac{13V_4 u_0^{9/4}}{32\sqrt{\pi}R^9}V(T), \quad e(u) \approx \frac{13V_4 u_0^{9/4}}{16\sqrt{\pi}R^6}\frac{V(T)}{(u-u_0)}. \tag{6.50}$$

In writing these, we have used $f(u_0) \approx 1$, which is a good approximation for large u_0. Using $dV(T)/du = T'(u)V'(T)$, we see that $b(u)$ and $R^3e'(u)$ both go as $(u-u_0)^{-4}$ in this regime. However, the coefficient of the latter is suppressed by a relative factor of $u_0^{-1/2}$, so for large u_0 we may neglect it compared to $b(u)$. But, unlike in the UV regime, $b(u)$ cannot be neglected compared to $d(u)$. In fact, this term is crucial for getting a nontrivial solution. In this regime, then, the leading terms in equation (6.43) give

$$\psi_0'(u) \approx \frac{32\pi R^6 u_0^{1/2}}{169}\frac{\psi_0(u)}{(u-u_0)}, \tag{6.51}$$

which has the solution

$$\psi_0(u) \approx \tilde{c_0}(u-u_0)^{\frac{32\pi R^6 u_0^{1/2}}{169}}, \tag{6.52}$$

where $\tilde{c_0}$ is an integration constant. Note that the normalization condition remains unchanged and cannot be used here because it receives contribution only from the UV end due to the exponentially vanishing tachyon potential for large $T(u)$ at the IR end.

Let us now consider the formula, (6.38), for the lowest mode, using which one can compute the eigenvalue λ_0^ϕ:

$$R^6 \int_{u_0}^{u_{\rm max}} du\, a(u)(\eta_0'(u))^2 = \frac{1}{2}\lambda_0^\phi. \tag{6.53}$$

Using $a(u) \approx \frac{\sqrt{\pi}V_4 u_0^{19/4}}{8R^{15}}\frac{V(T)}{(u-u_0)}$ in the IR and (6.52) in (6.42), we see that $\eta_0'(u) \propto \psi_0(u)$ vanishes very rapidly as $u \to u_0$, with a power which grows as $u_0^{1/2}$ for large u_0. Moreover, since $V(T)$ vanishes exponentially for large T, the IR region makes a negligible contribution to the integral. Therefore, it is reasonable to calculate the integral by substituting the UV estimate of the integrand in it. In the UV region, $a(u) \approx \frac{V_4 V(0)}{R^{15}}u^4 T^2(u)$. Moreover, in this region the second term on the right hand side of (6.42) can be neglected. So, we get

$$\begin{aligned}\frac{1}{2}\lambda_0^\phi = R^6 \int_{u_0}^{u_{\rm max}} du\, a(u)(\eta_0'(u))^2 &\approx R^6(\lambda_0^\phi)^2 \int_{\tilde{u}_0}^{u_{\rm max}} du\, \frac{d^2(u)}{a(u)}(\psi_0'(u))^2 \\ &\approx (\lambda_0^\phi)^2\kappa \int_{\tilde{u}_0}^{u_{\rm max}} \frac{h_0\, du}{(T_+e^{-h_0u}+T_-e^{h_0u})^2},\end{aligned}$$

where $\tilde{u}_0 > u_0$ avoids the IR region in the integral and we have defined

$$\kappa \equiv \frac{f_\pi^2 R^9}{4h_0 V_4 V(0)}. \tag{6.54}$$

The integral is easily done, giving

$$\lambda_0^\phi \approx \frac{1}{\kappa}\frac{(T_+e^{-h_0\tilde{u}_0}+T_-e^{h_0\tilde{u}_0})(T_+e^{-h_0u_{\rm max}}+T_-e^{h_0u_{\rm max}})}{e^{h_0(u_{\rm max}-\tilde{u}_0)}-e^{-h_0(u_{\rm max}-\tilde{u}_0)}}. \tag{6.55}$$

From our numerical solutions we see that it is possible to choose $\tilde{u}_0$ to be relatively large and also satisfy the conditions $|T_+|e^{-h_0\tilde{u}_0} \gg |T_-|e^{h_0\tilde{u}_0}$ and $e^{h_0(u_{\rm max}-\tilde{u}_0)} \gg e^{-h_0(u_{\rm max}-\tilde{u}_0)}$. For such values of the parameters, then, to a good approximation (6.55) gives

$$\lambda_0^\phi \approx \frac{1}{\kappa}(T_+T_- + T_+^2 e^{-2h_0u_{\rm max}}). \tag{6.56}$$

Now, let us tune $u_{\rm max}$ to large values. We will do this in a manner consistent with the inequality (5.25). As explained in section 5.4, one way of maintaining this inequality is to keep $|T_+|$ and $|T_-|e^{h_0u_{\rm max}}$

fixed as $u_{\rm max}$ becomes large. In that case, the second term on the right hand side of (6.56) becomes exponentially smaller than the first term as the cut-off is increased beyond some value. We may then neglect this term compared with the first term. This gives

$$\lambda_0^\phi \approx \frac{1}{\kappa} T_+ T_-. \tag{6.57}$$

Finally, using $\lambda_0^\phi = m_\pi^2$ and (5.33) in this relation, we get

$$m_\pi^2 \approx \frac{m_q \chi}{f_\pi^2}, \tag{6.58}$$

This is the well-known Gell-Mann−Oakes−Renner formula, up to a factor of 2.

Let us now summarize our discussion in this chapter. We have studied in detail the fluctuations of flavour gauge fields on the brane-antibrane system. These give rise to vector, axial vector and pseudoscalar towers of mesons, which become massive through a kind of Higgs mechanism, except for the Goldstone boson. These arise from a gauge-invariant combination of the tachyon phase and the longitudinal zero mode of the axial vector field. We have shown that the Goldstone boson, the analog of pion, remains massless, unless a quark mass (non-normalizable part of the tachyon solution) is switched on. For small quark mass, we have derived an expression for the mass of the lowest pseudoscalar meson in terms of the chiral condensate and shown that it satisfies the Gell-Mann−Oakes−Renner relation. The vector and axial vector spectra are expected to be non-degenerate because they arise from eigenvalue equations with different tachyon contributions.

A non-zero quark mass is essential to correctly reproduce phenomenology in the low-energy sector of QCD. Although the model, like Sakai-Sugimoto model, has aspects that make it very different from QCD, it can be the starting point of a more quantitative version of the phenomenology initiated in [67]. The model can be extended to the case with multiple flavors by a non-abelian extension of the action for flavor gauge field fluctuations.

It would be worth noting that since the work presented in this thesis was completed, a few alternate proposals of introducing quark mass in Sakai-Sugimoto model appeared in the literature. In [124], the authors consider a deformation of Sakai-Sugimoto model using additional $D4$ or $D6$ branes. This deformation leads to an introduction of quark mass in the model. In [125] the authors consider long open strings between the flavor branes in Sakai-Sugimoto model and show that it gives rise to a non-zero quark mass. In the work presented in [126] also, the authors study non-local operators to add quark mass to the model. A possible connection among these different models, including ours, deserves further investigation.

Chapter 7

Summary

The central topic of interest in this thesis has been the phenomenon of chiral symmetry breaking which is known to play a significant role in strong interactions. However, it has not been possible till date to provide an exact derivation of the phenomenon in QCD. The scale of chiral symmetry breaking is believed to be of the order of confinement scale and this makes the phenomenon of chiral symmetry breaking inaccessible to perturbative methods. Although it is difficult to study the phenomenon analytically in QCD, it is possible to obtain some general results analytically in the large N_c analog of QCD. An argument for chiral symmetry breaking in such a theory was given by Coleman and Witten. The emergence of AdS/CFT correspondence in string theory has provided a further leap in understanding many of these non-perturbative phenomena in gauge theories using a dual gravity picture. It has been possible to extend many features of this correspondence to QCD-like gauge theories. One such string theory model is due to Sakai and Sugimoto. The model consists of a setup of intersecting branes ($D4$-$D8$-$\overline{D8}$) in which the $D4$ branes are wrapped on a SUSY breaking circle of radius R_k. The $D4$ branes provide the color degrees of freedom and a finite value of R_k leads to confinement in the model. The $D8$ and $\overline{D8}$ branes are the flavor branes and are separated from each other by a distance L along this direction. This system reproduces a QCD-like model at low energies. Using holographic techniques, the authors showed that the model gives rise to a non-abelian chiral symmetry breaking and also identified the meson spectra.

In this thesis, we first carried out a thorough study of the phenomenon in the weak coupling limit (and at energies low compared to string scale and high compared to the confinement scale) of Sakai-Sugimoto model. In this limit, the spectrum consists of left-handed and right-handed fermions at the $D4-D8$ and $D4-\overline{D8}$ intersections interacting through exchange of $D4$ gauge fields. We saw that the parameter L in the model, the separation between the $D8$ and $\overline{D8}$ branes, gives rise to be a one parameter deformation of U(N_c) QCD. Furthermore, we saw that tuning L/R_k, it becomes possible to drive the energy scale associated with chiral symmetry breaking to values which are much larger

than the confinement scale. On doing so, the phenomenon of chiral symmetry breaking becomes accessible to perturbative techniques. This was the motivation behind studying the phenomenon of chiral symmetry breaking in the weakly coupled Sakai-Sugimoto model.

In our study of the model, we restricted to the hierarchy of scales $g_5^2 N_c \ll l_s \ll L \ll \pi R_k$, where g_5 is the $D4$ brane gauge coupling. We saw that $g_5^2 N_c \ll l_s$ ensures that string loop corrections are small, $l_s \ll L$ allows us to neglect non-trivial dilaton and RR ten-form created by $D8$ branes and $L \ll \pi R_k$ allows us to study chiral symmetry breaking perturbatively. We then studied the model by expressing it as a theory in (3+1) dimensions obtained after expanding the $D4$ gauge field in harmonic functions of x^4. This left an infinite tower of KK modes of $D4$ gauge fields interaction with left-handed and right-handed fermions.

In order to study chiral symmetry breaking it was useful to study the effective coupling between the left-handed and right-handed fermions. We saw that at energies higher than the confinement scale, it becomes possible to carry out an exact integration of the $D4$ gauge fields in the large N_c limit. This led to an effective non-local four-fermi interaction which has a finite range determined by the confinement scale, Λ (arising from R_k). The final effective action for fermions was found to be a non-local generalisation of Nambu−Jona-Lasinio model. We then derived the gap equation for a non local chiral condensate of left-handed and right-handed fermions separated by a distance. We also obtained numerical chiral symmetry breaking solutions starting with an ansatz motivated by the fact that the condensate should go to a constant at small separations and vanish beyond a certain length scale l.

One of the notable features of the solutions we obtained is the following. We found that as we decrease the coupling from a large value, the length scale l, characterising the solutions, keeps increasing with an increasing rate. We saw that for $l \gtrsim \Lambda^{-1}$, the profile hits a wall and there is no further decrease in the coupling. This indicates a critical value of the coupling below which there is no chiral symmetry breaking. To understand this, we note that for $l \gg \Lambda^{-1}$, the non-local NJL model essentially approximates to a usual local NJL model. Such a model, on the other hand, is well known to have a critical value of coupling for chiral symmetry breaking. Another important feature of the solutions obtained is the following. We found that there are no solutions with $l \lesssim L$. Therefore, as L/R_k is tuned in such a way that $L\Lambda$ becomes smaller and smaller, it becomes possible to get a wider range of solutions for which $l\Lambda \ll 1$, that is, the energy scale of chiral symmetry breaking is far above the confinement scale. This was considered as an a posteriori justification for the application of perturbative techniques to study the solutions.

We also tried to study the non-compact limit of the model in the weak coupling limit. We considered two different approaches of taking the non-compact limit while maintaining the hierarchy $L \ll \pi R_k \ll \Lambda^{-1}$. However, we were unable to find any consistent chiral symmetry breaking solutions

in both the approaches. This may indicate that the weakly coupled non-compact Sakai Sugimoto model does not show chiral symmetry breaking.

Like the weakly coupled model, the strongly coupled model also displays various features of chiral symmetry breaking. In this limit, Sakai and Sugimoto studied the model by considering the flavor branes $D8$ and $\overline{D8}$ as probes in the near horizon geometry of $D4$ branes. The model leads to a geometrical picture for chiral symmetry breaking in which asymptotically separated $D8$ and $\overline{D8}$ branes meet each other in the bulk. The model, however, does not have any parameter that allows us to turn on a quark mass term. Further, it does not have any explicit order parameter for chiral symmetry breaking. A major part of the work done in this thesis consists of a modification of the strongly coupled SS model that we proposed to resolve these two issues.

We studied the dynamics of the $D8$-$\overline{D8}$ system in $D4$ background taking into account the brane-antibrane open string tachyon. The motivation it was that the tachyon transforms like a bifundamental under the flavor group transformations and couples to a chiral bilinear of left-handed and right-handed fermions. Thus, condensation of tachyon can lead to a mass term for the fermions. In order to carry out an extensive investigation we needed to have an action for the system. Proposals for effective action for such brane-antibrane systems in curved background are available in the literature. However, these proposals exist for non-compact space-time directions only. On the other hand, our model involved a compact direction along which the $D8$ and $\overline{D8}$ branes are separated. We, therefore, applied these results to our model with the supposition that the $D8 - \overline{D8}$ separation is much smaller than the size, $2\pi R_k$ of the compact direction.

To proceed, we first obtained the classical vacuum configuration for the profiles of the $D8$-$\overline{D8}$ separation and the magnitude of the tachyon field. Since the equations of motion are non-linear, it is difficult to find exact analytical solutions to them. However, we obtained analytical results for the behaviour of the solution in the IR and UV regions which were then verified using numerical solutions. We found that the geometrical picture of chiral symmetry breaking in SS model, where asymptotically separated brane and anti-brane meet in bulk, is still preserved in this model. In addition, there is a vacuum expectation value acquired by the tachyon that blows up at the point where the $D8$ and $\overline{D8}$ meet. In the UV region of the holographic coordinate, it is associated with a 'normalisable' and a 'non-normalisable' components. This UV behaviour was, however, obtained under the assumption that the tachyon becomes small in this region. It cannot, therefore, be extended to a region where the non-normalisable component becomes very large. This forced us to use an upper cutoff on the holographic coordinate in the model. Although, the choice of this cutoff involved some degree of arbitrariness, we found that the parameters associated with the solutions obtained are sufficiently robust under small changes in the cutoff.

Since the tachyon couples to a chiral bilinear of fermions, AdS/CFT correspondence says that the

non-normalisable component sources the chiral bilinear in the boundary field theory. Therefore, we identified this mode with the quark mass parameter. After carrying out a holographic renormalisation, we also showed that the normalisable component of the background tachyon solution gives the vacuum expectation value of chiral condensate, an order parameter for chiral symmetry breaking. The fact that the the tachyon blows up at the point in bulk where the $D8$ and $\overline{D8}$ meet, played an important role in this. This ensured that the tachyon potential vanishes at this point and there is no contribution from the IR boundary to the calculation of chiral condensate.

After finding the classical vacuum configuration, we also carried out a fluctuations analysis of the flavor brane gauge fields A_L and A_R and the phase of the tachyon field θ. We observed that the action for these fluctuations can be written in terms of a vector combination $V = (A_L + A_R)$ and an axial-vector combination $A = (A_L - A_R - \partial\theta)$. The field V is invariant under the axial transformations of the flavor gauge group U(1)×U(1) but transforms as an adjoint under the vector subgroup. The field A, on the other hand, is invariant under the full flavor gauge group. We showed that, after fixing a gauge, the field V gives rise to a tower of vector meson in (3 + 1) dimensions. The field, A, on the other hand gives rise to a tower of axial-vector and pseudo-scalar mesons in (3 + 1) dimensions. In particular, when the non-normalisable component of the tachyon solution is zero, we found that the field A has a zero mode that gives rise to a massless pseudo-Goldstone boson, the analog of a massless pion. When the non-normalisable component does not vanish, the zero mode ceases to exist and the lightest pseudo-scalar is also massive. Further, the mass squared is proportional to this component and satisfies the GOR relation. This was, therefore, identified as the analog of a massive pion in phenomenology.

Since the work presented in this thesis was completed, some alternate proposals of introducing quark mass in Sakai-Sugimoto model have also appeared in the literature. In [124], a model involving a deformation of Sakai-Sugimoto model using additional $D4$ or $D6$ branes was proposed. The authors showed that this deformation leads to an introduction of quark mass in the model. In [125] the authors incorporated quark mass in Sakai-Sugimoto model using long open strings between the flavor branes. In yet another work carried out in [126], the authors studied non-local operators to add quark mass to the model. The possibility of a connection among these different models and ours deserves further investigation.

Appendix A

Alternate Green's function for $D4 - D8 - \overline{D8}$ at weak coupling

In this appendix we tabulate the data for solutions to the gap equation we obtained using Green's function (3.31). In the tables below, we have tabulated the values of parameters of solutions viz. l_Λ, σ, and ϕ_{00} corresponding to each value of the coupling λ for three sets of values of $\left\{R_\Lambda, L_\Lambda\right\}$. The value of the parameter c turns out to be given by l_Λ/L_Λ in each case. We have also plotted the variation of l_Λ with λ corresponding to each of the three sets. We see that the qualitative behaviour of the variation remains the same as obtained with Green's function (3.32).

R_Λ=1/5		L_Λ=1/100	
l_λ	σ	λ	ϕ_{00}
0.02	0.380	0.0949	5.60×10^{-9}
0.04	0.626	0.0831	1.32×10^{-6}
0.06	0.700	0.0784	3.08×10^{-5}
0.08	0.745	0.0751	2.34×10^{-4}
0.1	0.779	0.0721	1.86×10^{-3}
0.25	0.825	0.0712	2.27
0.6	0.865	0.0700	2.55×10^{3}
1	0.884	0.0693	1.60×10^{5}
1.5	0.8963	0.0689	4.31×10^{6}
2.5	0.903	0.0738	2.60×10^{8}
3	0.903	0.0738	1.11×10^{9}
3.5	0.904	0.0752	3.80×10^{9}

Table A.1: Table of parameters for the solution to gap equation with the set $R_\Lambda = 1/5$ and $L_\Lambda = 1/100$.

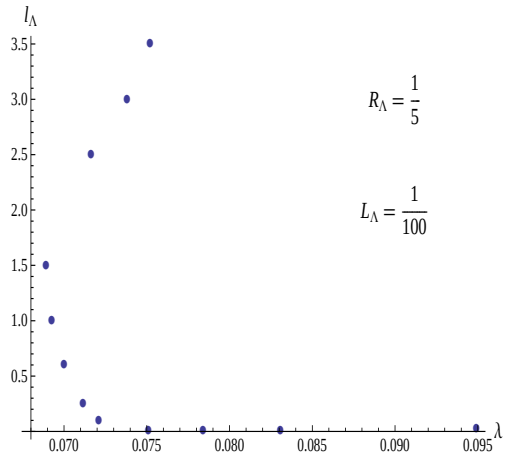

Figure A.1: Variation of l_Λ with λ for the set R_Λ=1/5, L_Λ=1/100 corresponding to the data in Table A.1.

R_Λ=1/5		L_Λ=1/200	
l_λ	σ	λ	ϕ_{00}
0.015	0.540	0.0439	2.10×10^{-9}
0.03	0.700	0.0392	4.81×10^{-7}
0.05	0.755	0.0376	2.48×10^{-5}
0.10	0.825	0.03469	6.60×10^{-3}
0.25	0.870	0.03345	10.08
0.50	0.888	0.03392	2.58×10^{3}
0.75	0.894	0.03486	6.58×10^{4}
1.00	0.898	0.03569	6.57×10^{5}

Table A.2: Table of parameters for the solution to gap equation with the set $R_\Lambda = 1/5$ and $L_\Lambda = 1/200$.

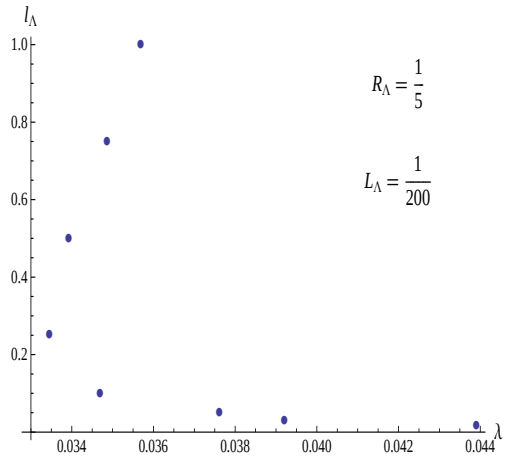

Figure A.2: Variation of l_Λ with λ for the set R_Λ=1/5, L_Λ=1/200 corresponding to the data in Table A.2.

R_Λ=1/20		L_Λ=1/300	
l_λ	σ	λ	ϕ_{00}
0.01	0.545	0.1167	3.02×10^{-9}
0.02	0.700	0.1045	6.76×10^{-7}
1/30	0.780	0.0959	4.10×10^{-5}
1/15	0.820	0.0935	4.16×10^{-4}
1/6	0.860	0.0920	12.84
7/30	0.865	0.0944	1.80×10^{2}
8/30	0.868	0.09494	5.20×10^{2}
0.30	0.870	0.09569	1.32×10^{3}
1/3	0.870	0.0972	3.00×10^{3}

Table A.3: Table of parameters for the solution to gap equation with the set $R_\Lambda = 1/20$ and $L_\Lambda = 1/300$.

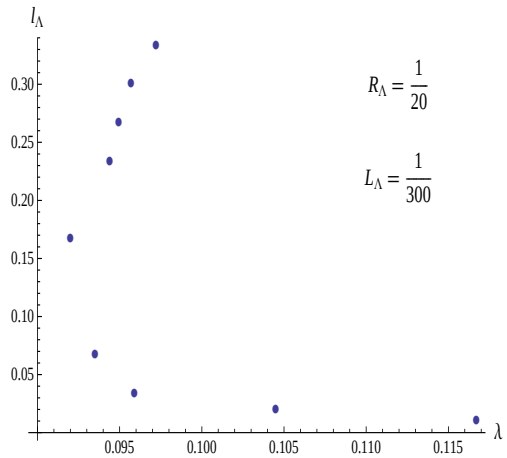

Figure A.3: Variation of l_Λ with λ for the set R_Λ=1/20, L_Λ=1/300 corresponding to the data in Table A.3.

Appendix B

Robustness of quark mass and chiral condensate

We have seen that the equations of motion derived from the DBI action of the $D8-\overline{D8}$ in the modified Sakai-Sugimoto model admit a solution where the tachyon profile has a quadratically diverging IR behaviour given by equation (5.22) and a UV behaviour has a double exponential factor divided by square of the holographic coordinate given by equation (5.17). The solutions can have two different forms namely, one in which the tachyon amplitude is positive everywhere and the other in which it crosses to negative values at some value of u as seen for the solutions with $u_0 > 13.0877781$. Physically speaking, the profile being the amplitude of tachyon should be positive everywhere since any change in the sign of the tachyon field should be taken care of by the phase of the field. Hence, for the second kind of solution, one needs to truncate it at some point u_{max} restricting it to only positive values. Moreover, u_{max} should be such that the solution has a double exponential fit near it. Satisfying these two criteria does not, however, lead to a specific value of u_{max} but only suggests a possible range. In the following, we show that this freedom of choice of u_{max} does not impact the robustness of the parameters T_- and T_+ we have reported.

B.1 Method to study robustness

In this sub-section we introduce a method to study the robustness of the parameters T_- and T_+ under small changes in the cut-off u_{max}. We choose a range of values of u_0 and truncate all of the corresponding tachyon profiles at a common u_{max} such that it lies in the region where the tachyon values are positive and asymptotic behaviour (5.17) is satisfied. Then we change the value of u_{max} for a fixed u_0, still maintaining the asymptotic conditions. This changes the values of the parameters T_-

and T_+. The fractional change in T_- for a given value of u_0 is

$$\delta_2 T_- = \frac{T_-(u^{(2)}_{max}) - T_-(u^{(1)}_{max})}{T_-}|_{u_0}, \tag{B.1}$$

where the value of u_{max} is changed from $u^{(1)}_{max}$ to $u^{(2)}_{max}$. Similarly we define $\delta_2 T_+$.

These are then compared to the changes occurring in the parameters T_- and T_+ for an equal shift in u_0 keeping u_{max} the same. The fractional change in T_-, in this case, is given by

$$\delta_1 T_- = \frac{T_-(u^{(2)}_0) - T_-(u^{(1)}_0)}{T_-}|_{u_{max}}, \tag{B.2}$$

where $u^{(2)}_0 - u^{(1)}_0 = u^{(2)}_{max} - u^{(1)}_{max}$. $\delta_1 T_+$ is defined in a similar way. The changes in the parameters T_- and T_+ caused by the variation of u_0 are understood as physical changes due to considering configurations with different values of bare quark mass. As we will show numerically, it turns out that $\delta_2 T_- \ll \delta_1 T_-$ and $\delta_2 T_+ \ll \delta_1 T_+$. Thus, the change due to ambiguity in the choice of u_{max} is small compared to the physical change. Hence, it demonstrates that the parameters are robust under small changes in the cutoff u_{max}.

In order to numerically demonstrate the above statements, a range of values of u_0 is chosen from 15 to 15.7 in steps of 0.1. We have plotted the corresponding figures for tachyon profile in Figure B.1. Then we choose two values of the cutoff given by $u_{max} = 33$ and $u_{max} = 32.9$. For each of these

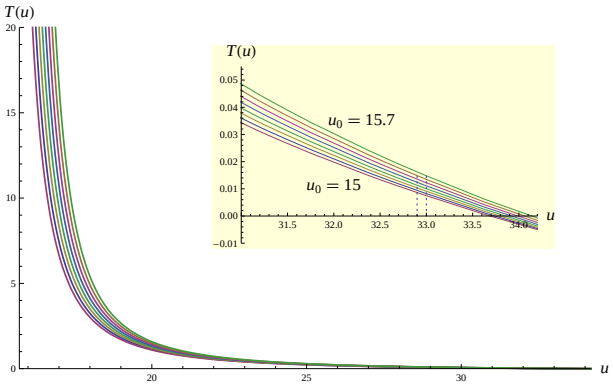

Figure B.1: The tachyon profiles corresponding to u_0 from 15.0 to 15.7 in steps of 0.1. The inset figure shows the asymptotic behaviour. The dotted lines show the two values of u_{max} used in studying the robust

tachyon profiles we carry out an asymptotic fitting for each of the two values of u_{max}. In order to track the quality of fit we use the quantity

$$\delta T = \frac{|T(u_{max}) - T_f(u_{max})| + |T(u_i) - T_f(u_i)|}{T(\frac{u_{max}+u_1}{2})} \tag{B.3}$$

where u_1 and u_{max} are the two ends of the fitted region and T_f gives the fitted value of the tachyon at the corresponding point. Figures B.2-B.4 show some of the fits we have done. In fitting the data we have ensured that $\delta T \leq 0.01$ (varies from 0.0095 to 0.01 in our set) and the value of $k \equiv 2h_0^2 u_i^{-2.5}(T_+^2 e^{-2h_0 u_i} + T_-^2 e^{2h_0 u_i}) \leq 0.07$ (kept between 0.045 to 0.07 in our set) for the validity of double exponential asymptotic form. Notice that in the figures we have indicated the ranges of values of u over which the fitting is done with the above criterion although we have shown the profile over a larger region. Using these, we compute $\delta_1 T_-$, $\delta_2 T_-$, $\delta_1 T_+$ and $\delta_2 T_+$.

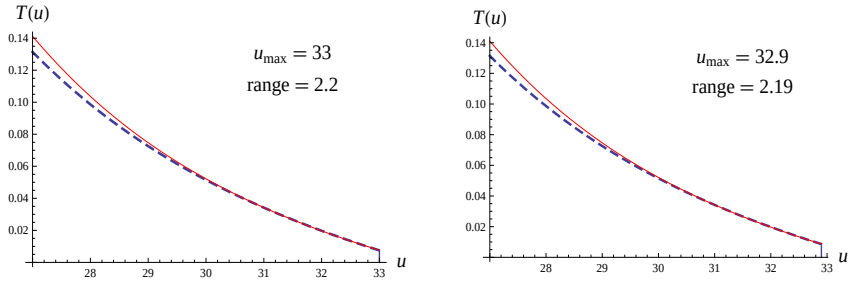

Figure B.2: Fits for u_0=15 with the asymptotic behaviour.

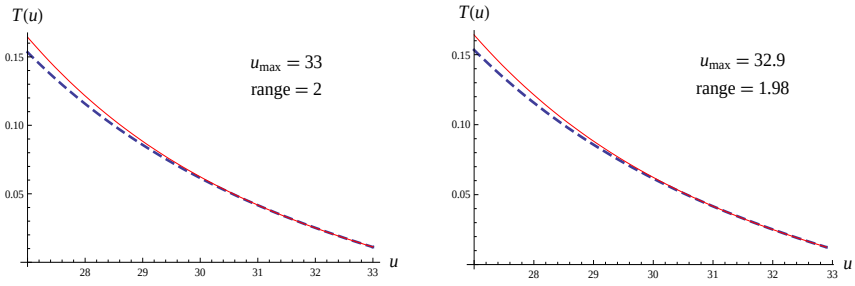

Figure B.3: Fits for u_0=15.4 with the asymptotic behaviour.

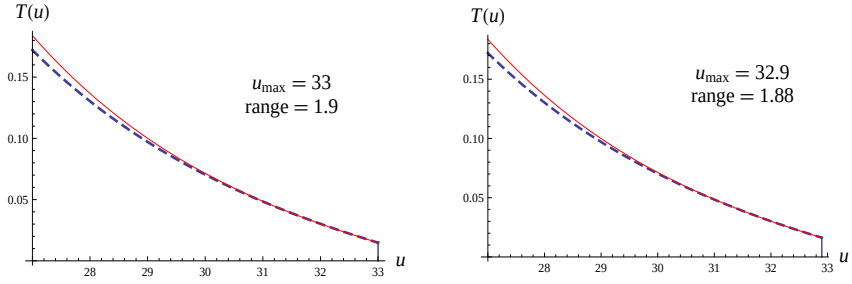

Figure B.4: Fits for u_0=15.7 with the asymptotic behaviour.

In the left panel of Figure B.5 we have plotted $\delta_2 T_-$ in red and $\delta_1 T_-$ in blue for various values of u_0. In the right panel, the same thing is done for T_+ instead of T_-. This example shows that $\delta_2 T_\pm \ll \delta_1 T_\pm$, indicating that the parameters are quite robust with respect to small variations in u_{max}. We verified

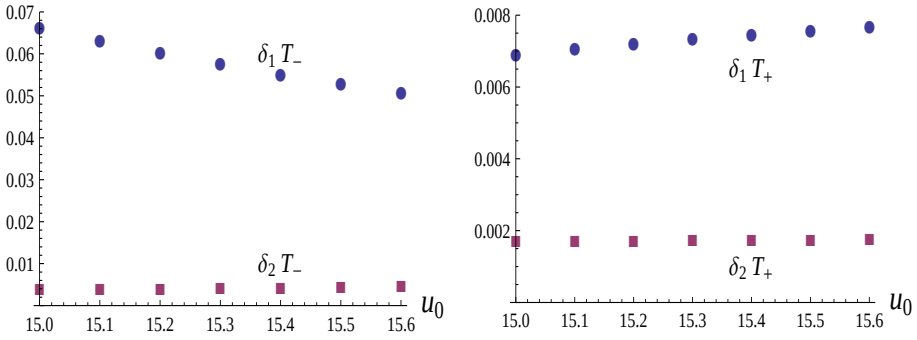

Figure B.5: Fractional changes in T_- and T_+ for change in u_{max} from 33 to 32.9

this over a larger range of values of u_{max}. In the set of figures given by Figure B.6 we have shown the asymptotic fitting of the tachyon profile where u_0 is fixed to 15.2 and the cutoff u_{max} is varied from 33 to 32.3 in steps of 0.1. In each part of the figure the fitting range is suitably changed such that δT varies only from 0.0089 to 0.01 and k varies from 0.029 to 0.05. We calculate the fractional changes in T_- and T_+ using equation (B.1) and the corresponding one for T_+, as we change u_{max} from 33 to the values indicated in the figures. Figure B.7 shows them as a function of u_{max}. We can easily see that these values are much smaller than the values of $\delta_1 T_\pm$ for u_0=15.2 displayed in Figure B.5. This demonstrates the robustness of $T_\pm$ with respect to small changes in u_{max}.

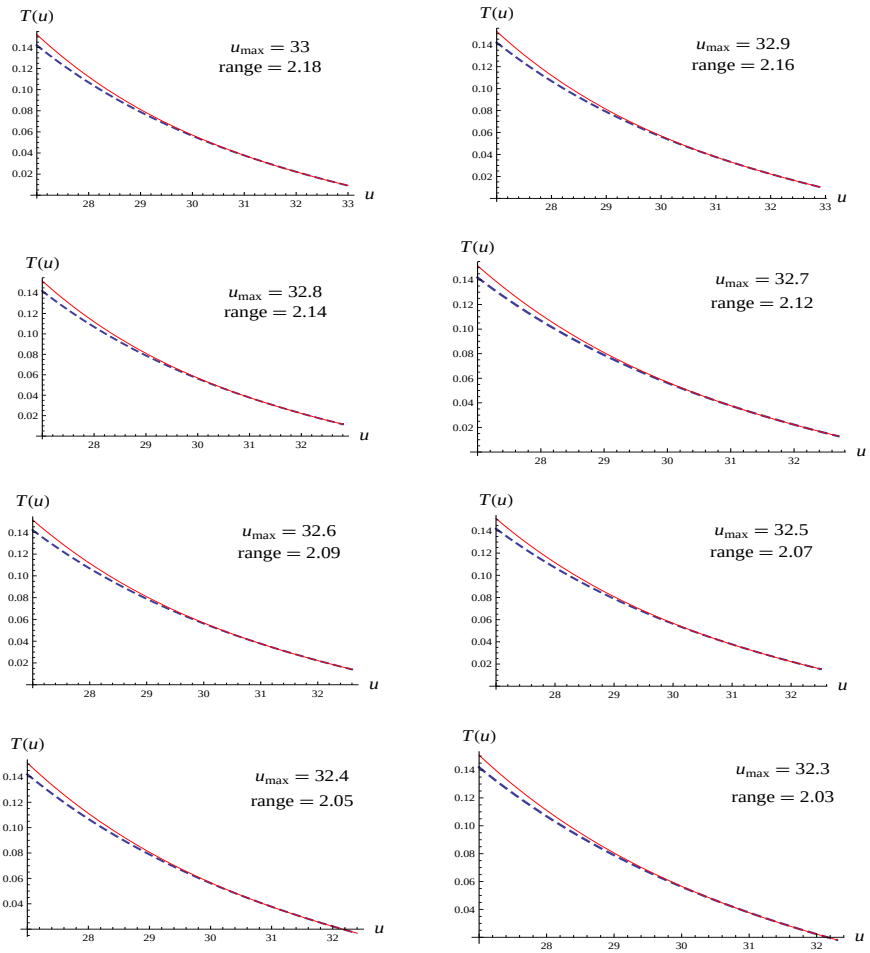

Figure B.6: Fits for varying u_{max} with u_0=15.2

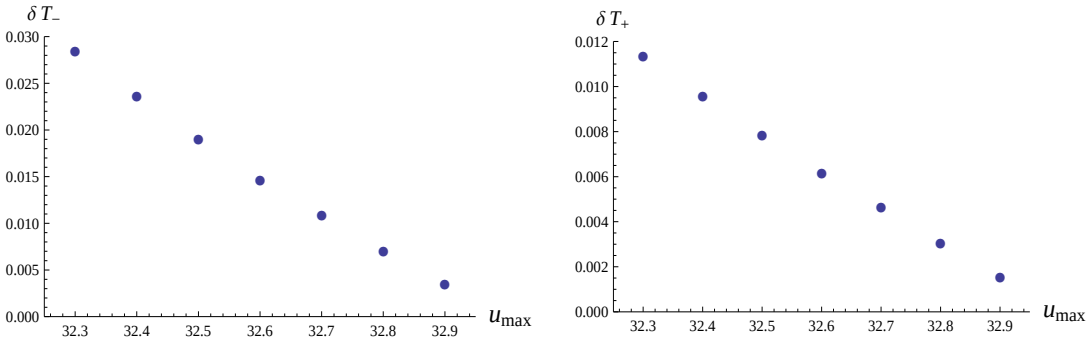

Figure B.7: The behaviour of fractional changes in values of T_- and T_+ for Δu_{max}=0.1 with u_{max} corresponding to $u_0 = 15.2$

Bibliography

[1] M. Gell-Mann, “A Schematic Model of Baryons and Mesons,” Phys. Lett. **8**, 214 (1964).

[2] G. Zweig, “An SU(3) model for strong interaction symmetry and its breaking,” In *Lichtenberg, D. B. (Ed.), Rosen, S. P. (Ed.): Developments In The Quark Theory Of Hadrons, Vol. 1*, 22-101 and CERN Geneva - TH. 401 (REC.JAN. 64) 24p.

[3] O. W. Greenberg, “Spin And Unitary Spin Independence In A Paraquark Model Of Baryons And Mesons,” Phys. Rev. Lett. **13**, 598 (1964).

[4] M. Gell-Mann, “The Symmetry group of vector and axial vector currents,” Physics **1**, 63 (1964).

[5] M. Y. Han and Y. Nambu, “Three-triplet model with double SU(3) symmetry,” Phys. Rev. **139**, B1006 (1965).

[6] J. D. Bjorken, “Asymptotic Sum Rules at Infinite Momentum,” Phys. Rev. **179**, 1547 (1969).

[7] D. J. Gross and F. Wilczek, “ULTRAVIOLET BEHAVIOR OF NON-ABELIAN GAUGE THEORIES,” Phys. Rev. Lett. **30**, 1343 (1973).

[8] H.D. Politzer, “RELIABLE PERTURBATIVE RESULTS FOR STRONG INTERACTIONS?,” Phys. Rev. Lett. **30**, 1346 (1973).

[9] H. Fritzsch, M. Gell-Mann and H. Leutwyler, “Advantages of the Color Octet Gluon Picture,” Phys. Lett. B **47**, 365 (1973).

[10] M. E. Peskin and D. V. Schroeder, *An Introduction to quantum field theory*, Addison-Wesley (1995).

[11] W. Greiner and A. Schafer, *Quantum chromodynamics*, Springer-verlag (1994).

[12] A. G. Grozin, *Lectures on QED and QCD*, World Scientific (2007).

[13] G. Altarelli, *The development of perturbative QCD*, World Scientific (1994).

[14] S. Narrison, *QCD as a theory of hadrons: from partons to confinement*, Cambridge University Press (2004).

[15] R. K. Ellis, W. J. Stirling, B. R. Webber, "QCD and collider physics," Camb. Monogr. Part. Phys. Nucl. Phys. Cosmol. **8**, 1-435 (1996).

[16] S. Donnachie, H. G. Dosch, O. Nachtmann, P. Landshoff, "Pomeron physics and QCD," Camb. Monogr. Part. Phys. Nucl. Phys. Cosmol. **19**, 1-347 (2002).

[17] V. L. Chernyak and A. R. Zhitnitsky, "Asymptotic Behavior of Exclusive Processes in QCD," Phys. Rept. **112**, 173 (1984).

[18] T. Hatsuda and T. Kunihiro, "QCD phenomenology based on a chiral effective Lagrangian," Phys. Rept. **247**, 221 (1994) [arXiv:hep-ph/9401310].

[19] T. Schafer and E. V. Shuryak, "Instantons in QCD," Rev. Mod. Phys. **70**, 323 (1998) [arXiv:hep-ph/9610451].

[20] U. D'Alesio, (ed.), N. Brambilla, (ed.), A. Devoto, (ed.), K. Muang, (ed.), G. M. Prosperi, (ed.) and S. Serci, (ed.), "Quark confinement and the hadron spectrum. Proceedings, 6th Conference, QCHS 2004, Villasimius, Italy, September 21-25, 2004,"

[21] Y. L. Dokshitzer, D. Diakonov and S. I. Troian, "Hard Processes in Quantum Chromodynamics," Phys. Rept. **58**, 269 (1980).

[22] G. Altarelli, "Partons in Quantum Chromodynamics," Phys. Rept. **81**, 1 (1982).

[23] K. G. Wilson, "Confinement of Quarks," Phys. Rev. D **10**, 2445 (1974).

[24] C. Aubin *et al.* [MILC Collaboration], "Light pseudoscalar decay constants, quark masses, and low energy constants from three-flavor lattice QCD," Phys. Rev. **D70**, 114501 (2004). [hep-lat/0407028].

[25] Q. Mason, talk at Lattice 2004.

[26] F. J. Yndurain, "The theory of quark and gluon interactions," *Berlin, Germany: Springer (1999) 413 p*

[27] J. S. Poucher *et al.*, "High-Energy Single-Arm Inelastic e - p and e - d Scattering at 6-Degrees Phys. Rev. Lett. **32**, 118 (1974).

[28] M. I. Buchoff, "Topics in Lattice QCD and Effective Field Theory," arXiv:1005.1908 [hep-lat].

[29] T. DeGrand and C. E. Detar, "Lattice methods for quantum chromodynamics," {http://www.slac.stanford.edu/spires/find/hep/www?irn=7352689}{SPIRES entry}, *New Jersey, USA: World Scientific (2006) 345 p*

[30] S. Hashimoto, "Recent results from lattice calculations," Int. J. Mod. Phys. A **20**, 5133 (2005) [arXiv:hep-ph/0411126].

[31] S. Aoki *et al.* [JLQCD Collaboration], "Kaon B parameter from quenched lattice QCD," Phys. Rev. Lett. **80**, 5271-5274 (1998). [hep-lat/9710073].

[32] Y. Aoki, G. Endrodi, Z. Fodor, S. D. Katz, K. K. Szabo, "The Order of the quantum chromodynamics transition predicted by the standard model of particle physics," Nature **443**, 675-678 (2006). [hep-lat/0611014].

[33] Y. Aoki, Z. Fodor, S. D. Katz, K. K. Szabo, "The QCD transition temperature: Results with physical masses in the continuum limit," Phys. Lett. **B643**, 46-54 (2006). [hep-lat/0609068].

[34] M. Cheng, N. H. Christ, S. Datta, J. van der Heide, C. Jung, F. Karsch, O. Kaczmarek, E. Laermann *et al.*, "The QCD equation of state with almost physical quark masses," Phys. Rev. **D77** (2008) 014511. [arXiv:0710.0354 [hep-lat]].

[35] P. Petreczky, "Heavy quark potentials and quarkonia binding," Eur. Phys. J. **C43** (2005) 51-57. [hep-lat/0502008].

[36] N. Seiberg and E. Witten, "Monopole Condensation, And Confinement In N=2 Supersymmetric Yang-Mills Theory," Nucl. Phys. B **426**, 19 (1994) [Erratum-ibid. B **430**, 485 (1994)] [arXiv:hep-th/9407087].

[37] N. Seiberg and E. Witten, "Monopoles, duality and chiral symmetry breaking in N=2 supersymmetric QCD," Nucl. Phys. B **431**, 484 (1994) [arXiv:hep-th/9408099].

[38] R. Gupta, "Introduction to lattice QCD: Course," hep-lat/9807028.

[39] K. Nakamura et al. (Particle Data Group), J. Phys. G 37, 075021 (2010)

[40] D. Ebert, H. Reinhardt and M. K. Volkov, "Effective Hadron Theory Of QCD," Prog. Part. Nucl. Phys. **33**, 1 (1994).

[41] Y. Nambu and G. Jona-Lasinio, "Dynamical model of elementary particles based on an analogy with superconductivity. I," Phys. Rev. **122**, 345 (1961).

[42] Y. Nambu and G. Jona-Lasinio, "DYNAMICAL MODEL OF ELEMENTARY PARTICLES BASED ON AN ANALOGY WITH SUPERCONDUCTIVITY. II," Phys. Rev. **124**, 246 (1961).

[43] A. Dhar and S. R. Wadia, "The Nambu-Jona-Lasinio Model: An Effective Lagrangian For Quantum Chromodynamics At Intermediate Length Scales," Phys. Rev. Lett. **52**, 959 (1984).

[44] A. Dhar, R. Shankar and S. R. Wadia, "Nambu-Jona-Lasinio Type Effective Lagrangian. 2. Anomalies And Nonlinear Lagrangian Of Low-Energy, Large N QCD," Phys. Rev. D **31**, 3256 (1985).

[45] G. 't Hooft, "A PLANAR DIAGRAM THEORY FOR STRONG INTERACTIONS," Nucl. Phys. B **72**, 461 (1974).

[46] A. V. Manohar, "Large N QCD," arXiv:hep-ph/9802419.

[47] E. E. Scholz, "Light Hadron Masses and Decay Constants," arXiv:0911.2191 [hep-lat].

[48] J. M. Maldacena, "The large N limit of superconformal field theories and supergravity," Adv. Theor. Math. Phys. **2**, 231 (1998) [Int. J. Theor. Phys. **38**, 1113 (1999)] [arXiv:hep-th/9711200].

[49] S. S. Gubser, I. R. Klebanov and A. M. Polyakov, "Gauge theory correlators from non-critical string theory," Phys. Lett. B **428**, 105 (1998) [arXiv:hep-th/9802109].

[50] E. Witten, "Anti-de Sitter space and holography," Adv. Theor. Math. Phys. **2**, 253 (1998) [arXiv:hep-th/9802150].

[51] C. V. Johnson, "D-branes," *Cambridge, USA: Univ. Pr. (2003) 548 p*

[52] M. R. Gaberdiel, R. Gopakumar, T. Hartman and S. Raju, "Partition Functions of Holographic Minimal Models," arXiv:1106.1897 [hep-th].

[53] O. Aharony, "The NonAdS / nonCFT correspondence, or three different paths to QCD,"[hep-th/0212193].

[54] J. Erlich, E. Katz, D. T. Son and M. A. Stephanov, "QCD and a holographic model of hadrons," Phys. Rev. Lett. **95**, 261602 (2005) [arXiv:hep-ph/0501128].

[55] O. Aharony, S. S. Gubser, J. M. Maldacena, H. Ooguri and Y. Oz, "Large N field theories, string theory and gravity," Phys. Rept. **323**, 183 (2000) [arXiv:hep-th/9905111].

[56] I. R. Klebanov, "TASI lectures: Introduction to the AdS / CFT correspondence," arXiv:hep-th/0009139.

[57] K. Skenderis, "Lecture notes on holographic renormalization," Class. Quant. Grav. **19**, 5849 (2002) [arXiv:hep-th/0209067].

[58] D. Weingarten, "MASSES AND DECAY CONSTANTS IN LATTICE QCD," Nucl. Phys. B **215**, 1 (1983).

[59] S. R. Coleman and E. Witten, "Chiral Symmetry Breakdown in Large N Chromodynamics," Phys. Rev. Lett. **45**, 100 (1980).

[60] E. Witten, "Anti-de Sitter space, thermal phase transition, and confinement in gauge theories," Adv. Theor. Math. Phys. **2**, 505 (1998) [arXiv:hep-th/9803131].

[61] N. Itzhaki, J. M. Maldacena, J. Sonnenschein and S. Yankielowicz, "Supergravity and the large N limit of theories with sixteen supercharges," Phys. Rev. D **58**, 046004 (1998) [arXiv:hep-th/9802042].

[62] A. Karch and E. Katz, "Adding flavor to AdS / CFT," JHEP **0206**, 043 (2002) [arXiv:hep-th/0205236].

[63] M. Kruczenski, D. Mateos, R. C. Myers and D. J. Winters, "Towards a holographic dual of large N(c) QCD," JHEP **0405**, 041 (2004) [arXiv:hep-th/0311270].

[64] D. J. Gross and H. Ooguri, "Aspects of large N gauge theory dynamics as seen by string theory," Phys. Rev. D **58**, 106002 (1998) [arXiv:hep-th/9805129].

[65] A. Karch and A. Katz, "Adding flavor to AdS/CFT," Fortsch. Phys. **51**, 759 (2003).

[66] J. Polchinski, "String theory. Vol. 2: Superstring theory and beyond," Cambridge, UK: Univ. Pr. (1998) 531 p.

[67] T. Sakai and S. Sugimoto, "Low energy hadron physics in holographic QCD," Prog. Theor. Phys. **113**, 843 (2005) [arXiv:hep-th/0412141].

[68] E. Witten, "Baryons and branes in anti-de Sitter space," JHEP **9807**, 006 (1998). [hep-th/9805112].

[69] O. Bergman, G. Lifschytz and M. Lippert, "Holographic Nuclear Physics," JHEP **0711**, 056 (2007) [arXiv:0708.0326 [hep-th]].

[70] A. Dhar and P. Nag, "Intersecting branes and Nambu−Jona-Lasinio model," Phys. Rev. D **79**, 125013 (2009) [arXiv:0901.4942 [hep-th]].

[71] M. Gell-Mann, R. J. Oakes and B. Renner, "Behavior of current divergences under SU(3) x SU(3)," Phys. Rev. **175**, 2195 (1968).

[72] E. Antonyan, J. A. Harvey, S. Jensen and D. Kutasov, "NJL and QCD from string theory," arXiv:hep-th/0604017.

[73] O. Aharony, J. Sonnenschein and S. Yankielowicz, "A holographic model of deconfinement and chiral symmetry restoration," Annals Phys. **322**, 1420 (2007) [arXiv:hep-th/0604161].

[74] A. Dhar, *Chiral symmetry, large-N limit and effective lagrangians in strong interactions*, Invited lecture delivered at the University of Delhi Workshop in Physics (Jan. 1984), TIFR report TIFR/TH/84-25. Unpublished.

[75] T. Hatsuda and T. Kunihiro, *QCD phenomenology based on a chiral effective Lagrangian*, Phys. Rept. **247** (1994) 221, hep-ph/9401310.

[76] E. Antonyan, J. A. Harvey and D. Kutasov, *Chiral symmetry breaking from intersecting D-branes*, Nucl. Phys. **B784** (2007) 1, hep-th/0608177.

[77] J. Babington, J. Erdmenger, N. J. Evans, Z. Guralnik and I. Kirsch, *Chiral symmetry breaking and pions in non-supersymmetric gauge/gravity duals*, Phys. Rev. D **69** (2004) 066007, hep-th/0306018.

[78] T. Sakai and S. Sugimoto, *More on a holographic dual of QCD,* Prog. Theor. Phys. **114**, 1083 (2006), hep-th/0507073.

[79] K. Nawa, H. Suganuma and T. Kojo, *Baryons in holographic QCD*, Phys. Rev. **D75** (2007) 086003, hep-th/0612187.

[80] K. Nawa, H. Suganuma and T. Kojo, *Brane-induced Skyrmions: Baryons in holographic QCD*, Prog. Theor. Phys. Suppl. **168** (2007) 231, hep-th/0701007.

[81] D. K. Hong, M. Rho, H. U. Yee and P. Yi, *Chiral dynamics of baryons from string theory*, hep-th/0701276.

[82] H. Hata, T. Sakai and S. Sugimoto, *Baryons from instantons in holographic QCD*, hep-th/0701280.

[83] D. Yamada, *Sakai-Sugimoto model at high density*, arXiv:0707.0101.

[84] A. Parnachev and D. A. Sahakyan, *Chiral phase transition from string theory*, Phys. Rev. Lett. **97** (2006) 111601, hep-th/0604173.

[85] R. Casero, E. Kiritsis and A. Paredes, *Chiral symmetry breaking as open string tachyon condensation*, Nucl. Phys. **B787** (2007) 98, hep-th/0702155.

[86] K. Hashimoto, T. Sakai and S. Sugimoto, *Holographic Baryons: Static Properties and Form Factors from Gauge/String Duality*, Prog. Theor. Phys. **120** (2008) 1093, arXiv:0806.3122.

[87] M. Edalati, R. G. Leigh and N. Nguyen, *Transversely-intersecting D-branes at finite temperature and chiral phase transition*, arXiv:0803.1277.

[88] P. C. Argyres, M. Edalati, R. G. Leigh and J. F. Vazquez-Poritz, *Open Wilson Lines and Chiral Condensates in Thermal Holographic QCD*, arXiv:0811.4617.

[89] D. Bak and H. U. Yee, *Separation of spontaneous chiral symmetry breaking and confinement via AdS/CFT correspondence*, Phys. Rev. **D71** (2005) 046003, hep-th/0412170.

[90] I. S. Gradshteyn and I. M. Ryzhik, *Table of Integrals, Series, and Products*, Fifth Edition, Ed. A. Jeffrey, Academic Press (1993).

[91] T. Sakai and J. Sonnenschein, *Probing flavoured mesons of confining gauge theories by supergravity*, JHEP **0309** (2003) 047, hep-th/0305049.

[92] J. L. F. Barbon, C. Hoyos, D. Mateos and R. C. Myers, *The holographic life of the eta'*, JHEP **0410**, 029 (2004), hep-th/0404260.

[93] H. Nastase, *On Dp-Dp+4 systems, QCD dual and phenomenology*, hep-th/0305069.

[94] V. Balasubramanian, P. Kraus and A. E. Lawrence *Bulk versus boundary dynamics in anti-de Sitter space-time*, Phys. Rev. **D59** (1999) 046003, hep-th/9805171.

[95] V. Balasubramanian, P. Kraus, A. E. Lawrence and S. P. Trivedi, *Holographic probes of anti-de Sitter space-times*, Phys. Rev. **D59** (1999) 104021, hep-th/9808017.

[96] S. Sugimoto and K. Takahashi, *QED and String Theory*, Adv. Theor. Math. Phys. **3** (1999) 281, hep-th/0403247.

[97] N. Itzhaki, J. M. Maldacena, J. Sonnenschein and S. Yankielowicz, *Supergravity and the large N limit of theories with sixteen supercharges*, Phys. Rev. D **58** (1998) 046004, hep-th/9802042.

[98] A. A. Tseytlin, *On non-abelian generalization of the Born-Infeld action in string theory*, Nucl. Phys. B **501** (1997) 41, hep-th/9701125.

[99] A. Sen, "Tachyon condensation on the brane antibrane system," JHEP **9808**, 012 (1998) [arXiv:hep-th/9805170].

[100] A. Sen, "Supersymmetric world-volume action for non-BPS D-branes," JHEP **9910**, 008 (1999) [arXiv:hep-th/9909062].

[101] M. R. Garousi, "Tachyon couplings on non-BPS D-branes and Dirac-Born-Infeld action," Nucl. Phys. B **584**, 284 (2000) [arXiv:hep-th/0003122].

[102] M. R. Garousi, "On-shell S-matrix and tachyonic effective actions," Nucl. Phys. B **647**, 117 (2002) [arXiv:hep-th/0209068].

[103] E. A. Bergshoeff, M. de Roo, T. C. de Wit, E. Eyras and S. Panda, "T-duality and actions for non-BPS D-branes," JHEP **0005**, 009 (2000) [arXiv:hep-th/0003221].

[104] J. Kluson, "Proposal for non-BPS D-brane action," Phys. Rev. D **62**, 126003 (2000) [arXiv:hep-th/0004106].

[105] A. Sen, "Field theory of tachyon matter," Mod. Phys. Lett. A **17**, 1797 (2002) [arXiv:hep-th/0204143].

[106] A. Sen, "Time and tachyon," arXiv:hep-th/0209122.

[107] A. Sen, "Tachyon dynamics in open string theory," Int. J. Mod. Phys. A **20** (2005) 5513 [arXiv:hep-th/0410103].

[108] A. Sen, *Dirac-Born-Infeld action on the tachyon kink and vortex*, Phys. Rev. D **68** (2003) 066008, hep-th/0303057.

[109] A. Sen, "NonBPS states and Branes in string theory," hep-th/9904207.

[110] M. R. Garousi, *D-brane anti-D-brane effective action and brane interaction in open string channel*, JHEP **0501** (2005) 029, hep-th/0411222.

[111] K. B. Fadafan and M. R. Garousi, *Non-abelian expansion of S-matrix elements and non-abelian tachyon DBI action*, hep-th/0607249; M. R. Garousi, *On the effective action of D-brane-anti-D-brane system*, arXiv:0710.5469; M. R. Garousi and H. Golchin, *On higher derivative corrections of the tachyon action*, arXiv:0801.3358; M. R. Garousi and E. Hatefi, *On Wess-Zumino terms of Brane-Antibrane systems*, arXiv:0710.5875. M. R. Garousi, *Higher derivative corrections to Wess-Zumino action of Brane-Antibrane systems*, arXiv:0712.1954.

[112] V. Niarchos, "Hairpin-Branes and Tachyon-Paperclips in Holographic Backgrounds," Nucl. Phys. B **841**, 268 (2010) [arXiv:1005.1650 [hep-th]].

[113] D. Erkal, D. Kutasov and O. Lunin, "Brane-Antibrane Dynamics From the Tachyon DBI Action," arXiv:0901.4368 [hep-th].

[114] C. j. Kim, H. B. Kim, Y. b. Kim and O. K. Kwon, "Electromagnetic string fluid in rolling tachyon," JHEP **0303**, 008 (2003) [arXiv:hep-th/0301076].

[115] F. Leblond and A. W. Peet, "SD-brane gravity fields and rolling tachyons," JHEP **0304**, 048 (2003) [arXiv:hep-th/0303035].

[116] N. D. Lambert, H. Liu and J. M. Maldacena, "Closed strings from decaying D-branes," JHEP **0703**, 014 (2007) [arXiv:hep-th/0303139].

[117] J. A. Minahan and B. Zwiebach, *Effective tachyon dynamics in superstring theory*, JHEP **0103** (2001) 038, hep-th/0009246.

[118] D. Kutasov, M. Marino and G. W. Moore, *Remarks on tachyon condensation in superstring field theory*, hep-th/0010108.

[119] P. Kraus and F. Larsen, *Boundary string field theory of the DD-bar system*, Phys. Rev. **D63** (2001) 106004, hep-th/0012198.

[120] T. Takayanagi, S. Terashima and T. Uesugi, *Brane-antibrane action from boundary string field theory*, JHEP **0103** (2001) 019, hep-th/0012210.

[121] A. Dhar and P. Nag, "Sakai-Sugimoto model, Tachyon Condensation and Chiral symmetry Breaking," JHEP **0801**, 055 (2008) [arXiv:0708.3233 [hep-th]].

[122] A. Dhar and P. Nag, "Tachyon condensation and quark mass in modified Sakai-Sugimoto model," Phys. Rev. D **78**, 066021 (2008) [arXiv:0804.4807 [hep-th]].

[123] O. Bergmann, S. Seki and J. Sonnenschein, *Quark mass and condensate in HQCD*, JHEP **0712** (2007) 037, arXiv:0708.2839.

[124] K. Hashimoto, T. Hirayama, F. L. Lin and H. U. Yee, "Quark Mass Deformation of Holographic Massless QCD," JHEP **0807**, 089 (2008) [arXiv:0803.4192 [hep-th]].

[125] O. Aharony and D. Kutasov, "Holographic Duals of Long Open Strings," Phys. Rev. D **78**, 026005 (2008) [arXiv:0803.3547 [hep-th]].

[126] R. McNees, R. C. Myers and A. Sinha, "On quark masses in holographic QCD," JHEP **0811**, 056 (2008) [arXiv:0807.5127 [hep-th]].

[127] K. Hashimoto, T. Hirayama and D. K. Hong, "Quark Mass Dependence of Hadron Spectrum in Holographic QCD," Phys. Rev. D **81**, 045016 (2010) [arXiv:0906.0402 [hep-th]].

[128] M. Bianchi, D. Z. Freedman and K. Skenderis, *Holographic renormalization*, Nucl. Phys. **B631** (2002) 159, hep-th/0112119.

[129] K. Skenderis, *Lecture Notes on Holographic Renormalization*, Class. Quant. Grav. **19** (2002) 5849, hep-th/0209067.

[130] A. Karch, A. O'Bannon and K. Skenderis, *Holographic Renormalization of Probe D-Branes in AdS/CFT*, JHEP **0604** (2006) 015, hep-th/0512125.

[131] J. Erdmenger, N. Evans, I. Kirsch and E. Threlfall, *Mesons in Gauge/Gravity Duals - A Review*, arXiv:0711.4467.